

Phosphorescent Semiconductor Nanocrystals and Proteins for Biological Oxygen Sensing

Emily J. McLaurin

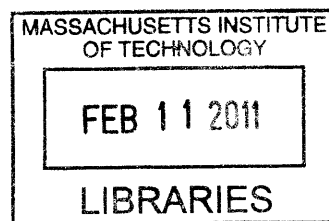
B. S. Chemistry
University of California, San Diego (2005)

Submitted to the Department of Chemistry
in Partial Fulfillment of the Requirements
for the Degree of

DOCTOR OF PHILOSOPHY IN INORGANIC CHEMISTRY
at the
MASSACHUSETTS INSTITUTE OF TECHNOLOGY

February 2011

© 2011 Massachusetts Institute of Technology
All Rights Reserved




ARCHIVES

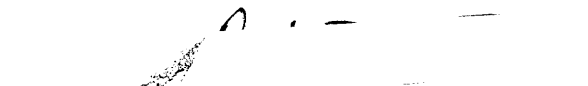
Signature of Author


Department of Chemistry
December 6, 2010

Certified by:


Daniel G. Nocera
Henry Dreyfus Professor of Energy and Professor of Chemistry
Thesis Supervisor

Accepted by:


Robert W. Field
Haslam and Dewey Professor of Chemistry
Chairman, Departmental Committee on Graduate Studies

This doctoral thesis has been examined by a Committee of the Department of Chemistry as follows:

Professor Mounji G. Bawendi _____

Lester Wolfe Professor in Chemistry
Chairman

Professor Daniel G. Nocera _____

Henry Dreyfus Professor of Energy and Professor of Chemistry
Thesis Supervisor

Professor Stephen J. Lippard _____

Arthur Amos Noyes Professor of Chemistry

To Mary and Keith,
who taught me to love science and learning,
while supporting me in all my endeavors

Phosphorescent Semiconductor Nanocrystals and Proteins for Biological Oxygen Sensing

by

Emily J. McLaurin

Submitted to the Department of Chemistry on December 6, 2010
In Partial Fulfillment of the Requirements for the Degree of Doctor of Philosophy

Abstract

Oxygen is required for cellular respiration by all complex life making it a key metabolic profiling factor in biological systems. Tumors are defined by hypoxia (low pO_2), which has been shown to influence response to radiation therapy and chemotherapy. However, very little is known about spatio-temporal changes in pO_2 during tumor progression and therapy. To fully characterize and probe the tumor microenvironment, new tools are needed to quantitatively assess the microanatomical and physiological changes occurring during tumor growth and treatment.

This thesis explores the design and construction of new oxygen sensors as tools for monitoring the tumor microenvironment in real-time. Semiconductor nanocrystals or quantum dots (QDs) are the basis of these tools. Previously, most imaging applications of QDs have used them as indicators of position; they have lacked a response to their local environment. Tethering a phosphorescent complex to a QD enables fluorescence resonance energy transfer to be exploited as a signal transduction mechanism, sensitizing the QD to oxygen.

The mechanism for oxygen sensing involves kinetic quenching of the emission of the energy accepting phosphor in the presence of oxygen, while the emission of the energy donating QD remains stable. This mechanism was chosen owing to the unique ability of oxygen to quench emission from a phosphorescent compound, but not fluorescence from a QD. Phosphors such as osmium polypyridines (Chapter 2), Pd or Pt porphyrins (Chapters 3 and 4), or phosphorescent proteins (Chapters 5 and 6) may all be employed. An additional benefit of FRET excitation includes very large one- and two-photon excitation cross-sections of QDs. Together, these properties make the probes ideal candidates for O_2 sensing applications in biological microenvironments, where probe concentrations may vary, and where the use of multiphoton excitation in microscopy presents significant advantages in imaging thick samples and in limiting extraneous tissue damage.

Thesis Supervisor: Daniel G. Nocera
Henry Dreyfus Professor of Energy & Professor of Chemistry

Table of Contents

Table of Contents.....	7
List of Figures.....	12
List of Schemes.....	20
List of Tables.....	22
List of Abbreviations.....	23
Chapter 1. Introduction.....	29
1.1 Sensing on the Nanoscale.....	30
1.2 Photophysics of Sensing Mechanisms.....	30
1.3 Methods for O ₂ Sensing in Biology.....	32
1.4 Förster or Fluorescence Resonance Energy Transfer (FRET) Sensing.....	33
1.5 Metabolic Profiling of Tumors.....	36
1.6 Multiphoton Spectroscopy and Microscopy.....	37
1.7 Quantum Dots (QDs) as Energy Transfer Donors.....	41
1.8 QD FRET O ₂ Sensing.....	43
1.9 Oxygen Sensing Proteins.....	45
1.10 Scope of Thesis.....	46
1.11 References.....	48
Chapter 2. Osmium Polypyridine O₂ Sensors.....	55
2.1 Motivation.....	56
2.2 Background.....	56

2.3	Results	57
2.4	Synthesis and Characterization of Osmium Polypyridines	57
2.5	Synthesis of QD-Osmium Sensors	58
2.6	Spectroscopic Properties of 1 and 2 and QD-1 and QD-2	61
2.7	Energy Transfer Analysis.....	63
2.8	Two-photon Emission Studies of QD, 2, and QD-2.....	67
2.9	Oxygen Quenching of Phosphorescence	68
2.10	Discussion	70
2.11	Conclusions	74
2.12	Experimental Section	74
2.13	References	83
Chapter 3. Pd(II) <i>meso</i>-Tetra(4-carboxyphenyl) porphyrin O₂ Sensors.....		87
3.1	Motivation	88
3.2	Background	88
3.3	Results and Discussion.....	89
3.4	R ₀ as an Oxygen Sensor	89
3.5	Synthesis of QD-R ₀ Sensors.....	91
3.6	Purification of R ₀ -QD Sensors	93
3.7	Spectroscopic Properties of QD-R ₀ : an Energy Transfer Study.....	97
3.8	Oxygen Quenching of Phosphorescence	103

3.9	Conclusions	106
3.10	Experimental Section	106
3.11	References	115
Chapter 4. Synthesis of Phosphorescent A₃B Porphyrins for O₂ Sensing.....		117
4.1	Motivation	118
4.2	Nitration of Tetraphenyl Porphyrin.....	118
4.2.1	Background.....	118
4.2.2	Results and Discussion	119
4.2.3	Synthesis.....	119
4.2.4	Spectroscopic Properties.....	122
4.3	Statistical Synthesis of M ^{II} 5-(4-carboxyphenyl)-10,15,20-triphenylporphyrin	123
4.3.1	Background.....	123
4.3.2	Results and Discussion	123
4.3.3	Synthesis Pt ^{II} 5-(4-carboxyphenyl)-10,15,20-triphenylporphyrin.....	123
4.3.4	Spectroscopic Properties of Compounds Pt ³ and Pd ³	125
4.3.5	Synthesis and Purification of a Phosphorescent Imidazole Polymer	126
4.3.6	Spectroscopic Properties of PolyPt ³ (Polymer Bound Pt ³)	129
4.4	Conclusions	130
4.5	Experimental Section	130
4.6	References	136

Chapter 5. Luminescent Ruthenium Protein Scaffolds.....139

5.1	Motivation	140
5.2	Background	140
5.3	Results	141
5.3.1	Ru Tt H-NOX	141
5.3.2	Ru Mb.....	144
5.4	Discussion	145
5.5	Conclusions	147
5.6	Experimental Section	147
5.7	References	155

Chapter 6. Conclusions and Future Directions.....159

6.1	Preliminary Work on Pd <i>Tt</i> H-NOX.....	160
6.1.1	Motivation	160
6.1.2	Background.....	161
6.1.3	Results and Discussion	162
6.1.4	Pd <i>Tt</i> H-NOX.....	162
6.1.5	QD-Pd <i>Tt</i> H-NOX.....	163
6.1.6	Conclusions	166
6.2	Comparison of Selected Oxygen Sensors	166
6.3	Future Work	169

6.4	Experimental Section	170
6.5	References	179
	Acknowledgements.....	181
	Curriculum Vitae	192

List of Figures

- Figure 1.1** Jablonski diagram showing the various radiative and nonradiative pathways available for a molecule upon excitation. The quenching of the triplet excited state by molecular oxygen is also shown..... 31
- Figure 1.2** Plot of the emission of a QD donor (green) and absorption of a porphyrin acceptor (orange). The area where the two overlap characterizes the overlap integral, J 35
- Figure 1.3** Normal tissue vessels distribute nutrients and waste efficiently. Abnormal tissue vessels are tortuous and leaky, leading to poor distribution of nutrients and waste. Anti-angiogenic therapy prohibits the growth of the tumor blood vessels, leading to inadequacy, where the vessels can no longer distribute drugs throughout the tumor. A hypothesized period of normalization between abnormal and inadequate vessels would be the ideal time for efficient delivery of drugs and therapy. See reference 53.. 37
- Figure 1.4** Jablonski diagram of single-photon absorption (left) and fluorescence and two-photon absorption and fluorescence (right). 38
- Figure 1.5** Samples excited by single-photon light at 488 nm (left) and two-photon light at 960 nm (right). Taken from reference 62. 39

Figure 1.6	Absorption spectra of various biological substances presented as a function of wavelength to show the window present between 700 and 1100 nm (pink), where there is minimal absorption in biological samples. Reproduced from reference 31..... 39
Figure 1.7	Six sizes of CdSe QDs showing the change in the emission wavelength with respect to the QD diameter. The emission can be tuned from blue to red as the size of the QDs is increased. Photography by Felice Frankel. . 42
Figure 1.8	Oxygen sensing system in which the phosphor (Pt porphyrin) is sensitized to two-photon excitation using energy transfer from coumarin donors. Taken from reference 49..... 44
Figure 2.1	A GFC trace of the conjugates QD-1 and QD-2 and the mixtures of the QD with 1 and QD with 2 . The GFC peaks recorded with a detection wavelength of 280 nm are shown in (top) QD-1 (—) and a mixture of the QD and 1 (—) and (bottom) QD-2 (—) and a mixture of the QD and 2 (—). The peak at 14.5 min is the elution peak for the single QDs. 60
Figure 2.2	Electronic spectra of complexes 1 and 2 in the steady state. The absorption of 1 (—) was not altered upon conjugation. The emission of 1 (—) blue-shifts upon conjugation. Similar changes, or lack thereof, were observed for the absorption (—) and emission (—) of 2 62

Figure 2.3	(Top) absorbance of the QD (—), 1 (—) and the QD-1 (—) conjugate. (Bottom) absorbance of the QD (—), 2 (—) and the QD-2 (—) conjugate. 63
Figure 2.4	Steady-state emission spectra ($\lambda_{exc} = 450$ nm) of the conjugates and their individual components in aqueous solution. Spectra were adjusted for concentration. (a) Spectra of the QD (—) and the QD-1 conjugate (—) with the same QD peak intensity. (b) Spectra of 1 (—) and QD-1 (—) with the same Os(II)PP emission peak intensity. (c) Spectra of the QD (—) and QD-2 (—) (1:135 QD:2 ratio) with the same QD peak intensity. (d) Spectra of 2 (—) and QD-2 (—) with the same Os(II)PP emission peak intensity..... 64
Figure 2.5	Time-resolved emission decay of the QD (—), QD-1 (—), and QD-2 (—). The quenching of the QD excited state is obvious from the accelerated decay. 65
Figure 2.6	Two-photon emission of 2 (—) and the QD-2 (—) conjugate with the same Os(II)PP concentration. 67
Figure 2.7	Energy dependence plots for the QD alone (slope = 1.75, top), QD in QD-2 (center, slope = 1.92), and 2 in QD-2 (slope = 1.82, bottom). The power listed was measured using a 20% beam pick-off..... 66

Figure 2.8	Emission profiles of QD-1 (—) and QD-2 (—) under vacuum and QD-1 (—) and QD-2 (—) under 1 atm of oxygen.....	68
Figure 2.9	The excited state lifetime decay curves of 1 (—) and 2 (—) when conjugated to QD. The lifetimes of both 1 (—) and 2 (—) decrease upon transferring QD-1 and QD-2 from vacuum to oxygen.	69
Figure 2.10	Emission from the Os(II)PP center of the QD-2 conjugate in the presence of 0 (—), 133 (—), 233 (—), 382 (—), 551 (—), and 760 (—) mmHg O ₂ (left). Stern-Volmer plot of the excited state lifetime of the Os(II)PP center in the QD-2 conjugate vs. pO ₂ (right). The Stern-Volmer slope yields a quenching rate constant, $k_q = 1.8 \times 10^9 \text{ s}^{-1} \text{ M}^{-1}$ ($3000 \text{ s}^{-1} \text{ torr}^{-1}$).....	70
Figure 3.1	Pd <i>meso</i> -tetra(4-carboxyphenyl) porphyrin.	90
Figure 3.2	Absorption spectrum of R ₀ . The incorporation of the Pd metal leads to a single Q-band with a small shoulder.....	90
Figure 3.3	R ₀ Steady-state emission with varying oxygen levels (left). R ₀ Stern-Volmer plot using time-resolved emission lifetimes (right). A k_q value of $380 \text{ torr}^{-1} \text{ s}^{-1}$ was calculated. Samples were bubbled with Argon gas and the oxygen levels (%) were monitored using an Ocean Optics fiber optic oxygen sensor.....	91

Figure 3.4	GFC trace of QDs with 50% amino-PEG ligands and 50% hydroxyl-PEG ligands. Aggregation can be seen in the purified QD sample (blue) indicating likely aggregation over time.	94
Figure 3.5	Coupling of R_0 to 50% amino-PEG QDs in ratios (R_0 to QD) of 1:1 (left) and 2:1 (right).	95
Figure 3.6	GFC traces of 20% amino-PEG QDs alone (left) and coupled with R_0 (right).	96
Figure 3.7	GFC traces of three reactions where the amount of R_0 is varied. Sample A is a control sample and thus contained no R_0 . The elution rate was 1 mL per minute so the x-axis may be read as minutes as well as mL.	97
Figure 3.8	Absorption profile of R_0 and emission profiles of green emitting QDs (QD1) showing significant overlap for high energy transfer efficiency (J in eq 4).	99
Figure 3.9	Emission spectra of green QD- R_0 samples with varying QD: R_0 ratios (see Table 2.2). All spectra were taken in the absence of oxygen.	100
Figure 3.10	Emission enhancement of R_0 in Samples QD1-B (orange) and QD1-C (green) vs. R_0 alone (blue) through energy transfer from the QD. The emission of R_0 in QD1-B and QD1-C is enhanced about 15 times and 8 times respectively.....	101

Figure 3.11	Absorption of R ₀ (orange) and red QD emission (red) showing the lack of overlap, preventing FRET.....	102
Figure 3.12	Emission spectra of red QD-R ₀ samples with QD:R ₀ ratios of 1:0 (red), 1:5 (orange) and 1:9 (green). The emissions of the samples are normalized to the QD concentration and the R ₀ alone (blue) emission is normalized to its concentration. The spectra were taken in the absence of oxygen with 350 nm excitation.....	103
Figure 3.13	Emission spectra of samples QD1-A (red), QD1-B (orange), QD1-C (green), and R ₀ (blue) in the absence of oxygen as well as in the presence of oxygen (black).	104
Figure 3.14	Stern-Volmer plot of the oxygen response of a QD-R ₀ Sensor. An approximate k _q value of 750 ± 40 torr ⁻¹ s ⁻¹ was calculated. The oxygen level didn't reach 0 before sample decomposition, so the plot is τ ⁻¹ vs. pO ₂	106
Figure 3.15	Ocean Optics oxygen sensing system. A bifurcated fiber optic cable sends an optical excitation to the phosphor-based probe tip. The excited state lifetime of the phosphor is monitored by the spectrometer and converted to an oxygen level using software.....	113
Figure 3.16	Method for controlling and monitoring oxygen levels using nitrogen or argon gas flow. A gas inlet and outlet are accompanied by a fiber optic	

	oxygen probe within the cell. Oxygen levels are monitored and correlated with the sensor emission profile for calibration.....	114
Figure 4.1	Absorption spectra of TPPNH ₂ COCH ₂ CH ₂ COOH (purple, top), PdTPPNH ₂ (orange, bottom left), and PtTPPNH ₂ (right, red). Incorporation of the metal dramatically changes the lower energy absorption of the porphyrin.....	122
Figure 4.2	Absorption (left) and emission (right) spectra of Pt3 (red) and Pd3 (orange). The emission spectra are shown under vacuum (colored) and in air (black). The emissions of both phosphors are almost completely quenched in the presence of air. All spectra were taken in THF.	126
Figure 4.3	HPLC traces of during the purification of polyPt3 . The absorbances at 280 (blue), 410 (orange), and 510 (red) are shown with respect to elution time.	128
Figure 4.4	Full absorption spectra (right) of the fractions collected at 5 minutes (red) and 1 minute (dark red).....	129
Figure 5.1	Chemical structure of M mesoporphyrin IX, where M is Ru in the unnatural porphyrin and Fe in the natural heme.	141
Figure 5.2	Structure of Ru <i>Tt</i> H-NOX showing the position of the RuMP IX.	142
Figure 5.3	Absorption and emission spectra of Ru <i>Tt</i> H-NOX (left). The emission spectra are shown in the presence (orange) and absence (red) of oxygen.	

	Stern-Volmer plot of Ru <i>Tt</i> H-NOX yielding a k_q of $1350 \text{ s}^{-1} \text{ torr}^{-1}$ (right).	143
Figure 5.4	Absorption and emission spectra of Ru Mb (left). Emission spectra are shown in the absence (red) and the presence (orange) of oxygen. Stern Volmer plot of the oxygen sensitivity of Ru Mb.	144
Figure 5.5	Absorption spectrum of Ru Mb before (blue) and after (red) laser excitation over a period of 8 hours.	145
Figure 5.6	Overall alignment showing secondary structural elements of Ru <i>Tt</i> H-NOX () and heme-bound <i>Tt</i> H-NOX (molecule B, PDB 1U55) ¹ () (~90° rotation shown).	145
Figure 6.1	Absorption and emission spectra of Pd <i>Tt</i> H-NOX (left). Emission spectra are shown in the absence (red) and the presence (orange) of oxygen. Stern Volmer plot of the oxygen sensitivity of Pd <i>Tt</i> H-NOX.....	162
Figure 6.2	Structure of <i>Tt</i> H-NOX (left) and a close up of the distance from the heme to the terminal asparagine residue (right).	164
Figure 6.3	Absorption of the QD (blue) with the emission of the Pd <i>Tt</i> H-NOX in the absence (red) and presence (orange) of oxygen.....	165
Figure 6.4	Emission spectra of a mixture of DHLA-QDs and Pd <i>Tt</i> H-NOX from 0 to 60 minutes (left) and from 60 to 150 minutes (right).	166

List of Schemes

Scheme 1.1	Left: the donor (D) emits (green lightening bolt) upon excitation (red lightening bolts) and no FRET occurs to the acceptor (A). Right: upon interaction with an analyte (circle), FRET occurs between the donor and acceptor. 34
Scheme 1.2	Signal transduction mechanism for oxygen sensing. Multiphoton excitation of the QD donor leads to energy transfer to the phosphor, followed by phosphorescence. In the presence of oxygen, the QD emission and energy transfer efficiency remain unchanged, while the phosphorescence of the acceptor is quenched by oxygen..... 43
Scheme 1.3	Mechanism of oxygen sensing by an unnatural porphyrin containing protein scaffold. Excitation of the porphyrin is reversibly quenched in the presence of oxygen. 46
Scheme 2.1	Synthesis of Bis(NN))(N-(6-aminohexyl)-4'-methyl-2,2'bipyridine-4-carboxamide)-osmium(II) bis(hexafluorophosphate) [OsII(NN) ₂ (Nbpy)](PF ₆) ₂ through lower temperature methods, preserving the diamine linker. 57
Scheme 2.2	Formation of water soluble QDs through mixing of amphiphilic polymer with the QDs in CHCl ₃ followed by solvent removal and dissolution of the polymer-QD solution in sodium bicarbonate buffer (pH ~8.5). 59

Scheme 2.3	Conjugation of the osmium polypyridine phosphor to polymer encapsulated QDs.....	59
Scheme 3.1	Cap exchange of TOPO-QDs with hydroxy and amine terminated PEG dithiol ligands yielding water soluble QDs. The percent of amino-PEG used may be varied to allow more sites for coupling of phosphors.....	92
Scheme 3.2	Coupling of R ₀ to the amino-PEG ligands on the QDs yields phosphorescent QDs.	93
Scheme 4.1	Synthesis of an A ₃ B porphyrin through nitration, metallation, reduction, and amide bond formation with succinic anhydride. An additional step, reaction with <i>tert</i> -butyl 6-aminohexylcarbamate followed by deprotection, could yield a free amine, which is preferable for amide bond formation (as opposed to an aniline).	120
Scheme 4.2	Statistical synthesis of M ^{II} 5-(4-carboxyphenyl)-10,15,20-triphenylporphyrin (MTPPCOOH) where M is palladium or platinum.	124
Scheme 4.3	Attachment of Pt3 to the imidazole polymer through DIC coupling.	127

List of Tables

Table 1.1	Two-photon Absorption Cross-sections for Several Fluorophores. Adapted from References 46, 62, 63, 75-77	41
Table 2.1	Spectroscopic and Photophysical Properties of Os ^{II} polypyridyl Complexes, (Cd _x Zn _{1-x} Se)Cd _y Zn _{1-y} S Core-Shell Nanocrystals, and Os ^{II} Polypyridyl Complexes Conjugated with (Cd _x Zn _{1-x} Se)Cd _y Zn _{1-y} S Core-Shell Nanocrystals in Aqueous Solution at Room Temperature.	61
Table 2.2	Förster Energy Transfer Parameters for QD-1 and QD-2	67
Table 3.1	Spectroscopic and Photophysical Properties of Palladium (II) <i>meso</i> -Tetra(4-Carboxyphenyl) Porphyrin-based Complexes and Their QD-Conjugates.....	98
Table 4.1	Spectroscopic and Photophysical Properties of Porphyrin Complexes ..	127
Table 5.1	Steady-state and Time-resolved Emission Properties of Ru <i>Tt</i> H-NOX and Ru Myoglobin.	143
Table 5.2	Statistics of Crystallographic Data Collection and Refinement for the Ru <i>Tt</i> H-NOX structure.	159
Table 6.1	Steady-state and Time-resolved Emission Properties of Ru <i>Tt</i> H-NOX and Pd <i>Tt</i> H-NOX.	163
Table 6.2	Comparison of Various Optical O ₂ Sensors in Aqueous Solution.....	167

List of Abbreviations

A	Acceptor, Absorption
Å	Ångstrom (1 Å = 10 ⁻¹⁰ m)
Atm	Atmosphere
AU	Arbitrary units
Acac	Acetyl acetate
BOC	<i>t</i> -Butyl carbamate
Bpy	Bipyridine
Ca	Calcium
Cbpy	Mono-carboxylated bipyridine
CCD	Charge-coupled device
CdMe ₂	Dimethylcadmium
CdSe	Cadmium selenide
CdTe	Cadmium telluride
CdZnS	Cadmium zinc sulfide
CHCl ₃	Chloroform
cm ⁻¹	Wavenumber
CO	Carbon monoxide
D	Donor
DCC	Dicyclohexylcarbodiimide
Det	Detection
DHLA	Dihydrolipoic acid

DIEA	Diisopropylethylamine
DMAP	4,4'-Dimethylaminopyridine
DMF	Dimethylformamide
DMSO	Dimethylsulfoxide
DNA	Deoxyribonucleic acid
DPPhen ₂	Diphenyl phenanthroline
ϵ	Molar absorptivity
E	Efficiency
EDC	1-Ethyl-3-(3-dimethylaminopropyl) carbodiimide
Em	Emission
EPR	Electronic paramagnetic resonance
Eq	Equation
Eq.	Equivalent
Exc	Excitation
Eu	Europium
F	Fluorescence, Fluorine
FRET	Fluorescence or Förster resonance energy transfer
FWHM	Full-width at half-maximum
GFC	Gel filtration chromatography
GM	Göppert-Meyer
HDA	Hexadecylamine
H-NOX	Heme nitric oxide / oxygen binding

HOBt	1-Hydroxybenzotriazole
HPA	Hexylphosphonic acid
Hr	Hour
I	Intensity
IR	Infrared
ISC	Inter-system crossing
<i>J</i>	Spectral overlap integral
k	Rate
κ	Relative orientation factor
λ	Wavelength
L, mL, μ L	Liter, Milliliter, Microliter
<i>m</i>	Acceptors per donor
m, mm, nm, fl	Meter, Millimeter, Nanometer, Femtoliter
M, μ M	Molar, Micromolar
MALDI	Matrix assisted laser desorption by ionization
MLCT	Metal-ligand charge transfer
mmHg	Millimeters mercury, Torr
MPLSM	Multi-photon laser scanning microscopy
Min	Minute
Mol	Mole
MW, MWCO	Molecular weight, molecular weight cut-off
Mb	Myoglobin

N	Avogadro's number (6.022×10^{23} u)
n	Refractive index
NC	Nanocrystal
NHS	N-Hydroxysuccinimide
NIR	Near infrared
NMR	Nuclear magnetic resonance
NO	Nitric oxide
nr	Non-radiative
O ₂	Oxygen
OA	Octylamine
Os	Osmium
P	Phosphorescence, Phosphorous
PAA	Poly(acrylic) acid
PBS	Phosphate buffered saline
Pd	Palladium
PdTCPP	Pd(II) <i>meso</i> -tetra(4-carboxyphenyl) porphyrin
PEG	Poly(ethylene glycol)
PET	Positron emission tomography
Ph	Phenyl
Phen	Phenanthroline
PMT	Photomultiplier tube
pO ₂	Partial pressure of molecular oxygen

PP	Polypyridyl
Pt	Platinum
Q	Quencher
QD	Quantum dot
r	Distance, Radiative
R_0	Critical transfer distance, PdTCPP
Ru	Ruthenium
RuMP	Ruthenium mesoporphyrin IX
s, ns, ps, fs	Second, Nanosecond, Picosecond, Femtosecond
σ_2	Two-photon absorption cross-section
S	Signal, Sulfur
S_0	Singlet electronic ground state
Se	Selenium
SV	Stern-Volmer
τ	Lifetime
T	Time
T_1	Triplet electronic excited state
TA	Thioctic acid
TBP	Tributylphosphine
TDPA	Tetradecylphosphonic acid
TFA	Trifluoroacetic acid
THF	Tetrahydrofuran

(TMS) ₂ S	<i>bis</i> (Trimethylsilyl)sulfide
TOP, TOPO	Trioctylphosphine, trioctylphosphine oxide
<i>Tt</i>	<i>Thermoanaerobacter tengcongensis</i>
UV	Ultraviolet
vis	Visible
Φ	Quantum yield
W, mW, nW	Watt, Nanowatt
xs	Excess
ZnEt ₂	Diethylzinc
ZnS	Zinc sulfide
ZnSe	Zinc selenide

Chapter 1

Introduction

1.1 Sensing on the Nanoscale

Chemical and biological sensing (chemo- or bio-sensing) involves sensing of analytes on a molecular scale.¹⁻¹¹ This field of research has grown dramatically due to increased demand for sensors from areas as varied as medicine,¹²⁻¹⁷ national security,¹⁸⁻²⁰ and environmental sciences.²¹⁻²³ Chemosensors provide information on the presence or absence of small analytes through a signal transduction mechanism. As an analyte binds or interacts with the sensor, information on the presence of the analyte is communicated through changes in the sensors physical or chemical properties, such as the excited state lifetime, or changes in the sensor emission energy or intensity. Although other mechanisms of sensing may be employed, such as electron transfer, emission based sensors are highly popular²⁴ due to the advantages they possess. Emission based sensors can have fast response times with reversible signals, allowing dynamic measurements in real-time. They also tend to be minimally invasive, which is especially valuable when sensing within biological environments. These advantages have encouraged our study and exploration the signal transduction mechanisms and analytes that may be employed in emission based sensing.

1.2 Photophysics of Sensing Mechanisms

Use of emission as a signal transduction mechanism for chemical sensing necessitates understanding photophysical processes. The Jablonski diagram in Figure 1.1 depicts the electronic energy levels of a molecule along with the photophysical pathways available to that molecule after excitation. Absorption of a photon (k_A) may be followed by fluorescence (k_F), intersystem crossing (k_{ISC}), or nonradiative decay (k_{nr}). Intersystem crossing populates the triplet

state, from which phosphorescence (k_P) or nonradiative decay may occur. Nonradiative decay, which competes with the radiative decay processes of both fluorescence and phosphorescence, arises from a variety of other decay pathways available to the molecule that do not lead to the release of a photon. Excitation into higher energy vibrations of the molecule, followed by vibrational relaxation of this energy released as heat is one nonradiative mechanism.²⁵⁻²⁷ The presence of electronic trap states may also lead to nonradiative decay.²⁸⁻³⁰

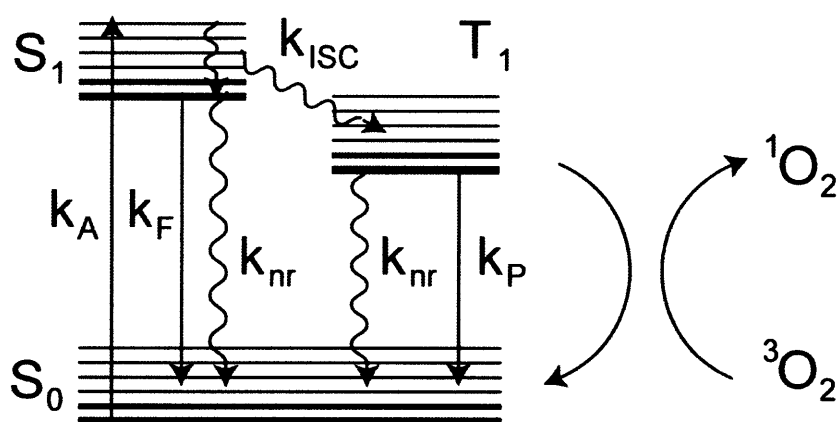


Figure 1.1. Jablonski diagram showing the various radiative and nonradiative pathways available for a molecule upon excitation. The quenching of the triplet excited state by molecular oxygen is also shown.

Aside from the nonradiative decay processes, fluorescence is also decreased by population of the triplet state of the molecule. The triplet excited states of molecules tend to be long lived due to their forbidden nature. As T_1 does not possess the same spin as the electronic ground state (S_0), direct relaxation from T_1 to S_0 is spin-forbidden. Quenching of the long lived triplet excited state by oxygen, which possesses a triplet ground state, is a well-known process. This form of collisional quenching can be described by Stern-Volmer kinetics.³¹ The Stern-Volmer relationship for collisional quenching is given as:

$$\frac{I_0}{I} = \frac{\tau_0}{\tau} = 1 + k_q \tau_0 [Q] = 1 + K[Q] \quad (1)$$

where I_0 and τ_0 are the excited state emission intensity and lifetime, respectively, in the absence of quencher, I and τ are the emission intensity and excited state lifetime in the presence of quencher, k_q is the bimolecular quenching constant, and Q is the quencher. K_{SV} is the Stern-Volmer constant and may be determined by measurement of the excited state emission intensity or lifetime at varying concentrations of quencher, assuming a linear relationship.

1.3 Methods for O₂ Sensing in Biology

A multitude of methods are available for determining oxygen levels, but the criteria for measurement within biological environments places certain limitations on the available methods. Clark electrodes monitor oxygen levels by reducing oxygen to water, leading to changes in electrical current.³² Although they are extremely sensitive and can determine oxygen levels with sub-micromolar resolution,³³ they consume oxygen and even small microelectrodes are invasive.³² Imaging techniques such as nuclear magnetic resonance (NMR), electron paramagnetic resonance (EPR), and positron emission tomography (PET) are less invasive, but suffer from poor spatio-temporal resolution.^{34,35}

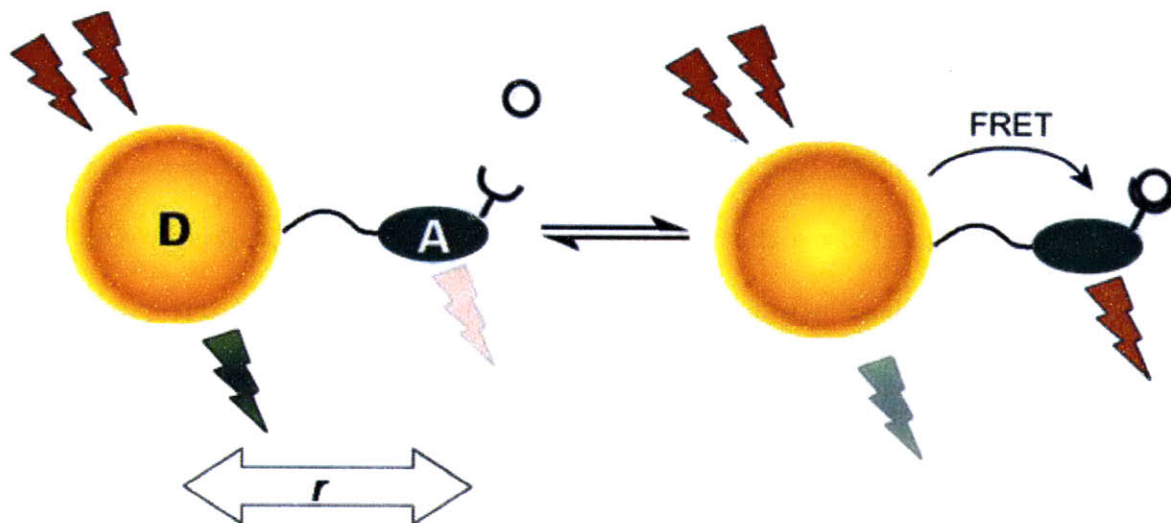
Quenching of small molecule luminescence by O₂ provides a platform for simple, non-invasive imaging of *in vivo* O₂ concentrations.³⁶ The ability of oxygen to quench phosphorescence is well established and has been previously used to quantify oxygen levels.^{37,38} This method provides advantages over other methods for *in-vivo* O₂ sensing as it allows rapid, reversible, oxygen sensing in real-time through measurement of emission intensity or excited state lifetime, as outlined in Section 1.2.

The molecules used for phosphorescence-quenching based O₂ sensing range from polypyridines^{39,40} to porphyrins^{39,41} and even proteins.^{42,43} The synthetic tailorability of these molecules allows the brightness, range of oxygen sensitivity, and wavelengths of absorption and emission to be varied. For example, ruthenium(II) polypyridines possess longer lifetimes than the related osmium(II) complexes, while the Ru complexes wavelengths of absorption and emission are higher in energy than those of the Os complexes.⁴⁴ While Ru(II) (Ph₂phen₃) is the most commonly used fluorophore in oxygen sensors,³¹ platinum(II) and palladium(II) porphyrins and their derivatives have been gaining popularity due to their relatively high phosphorescence quantum yields and long lifetimes.⁴⁵ These organic molecules tend to possess poor water solubility thus limiting their efficacy in biological oxygen sensing. Recent developments in phosphorescent proteins have initiated their use in biological oxygen sensing. However, they, along with the other molecular oxygen sensors, are plagued by low phosphorescence quantum yields. Methods for enhancing the brightness and oxygen sensitivity of these phosphors are current areas of research.⁴⁶ One such method is Förster resonance energy transfer, as described in Section 1.4.

1.4 Förster or Fluorescence Resonance Energy Transfer (FRET) Sensing

FRET involves the transfer of energy, nonradiatively, from a donor fluorophore to an acceptor molecule.⁴⁷ The term fluorescence resonance energy transfer has been coined to describe occurrence of this phenomenon when both the donor and acceptor are fluorescent.³¹ FRET has been frequently employed in optical sensing as satisfaction of the requirements for absorption and emission wavelengths as well as analyte sensitivity are not often present in a single

molecule. One signal transduction mechanism is depicted in Scheme 1.1, where the amount of FRET, or efficiency (E), changes upon the acceptor (A) binding an analyte.



Scheme 1.1. Left: the donor (D) emits (green lightning bolt) upon excitation (red lightning bolts) and no FRET occurs to the acceptor (A). Right: upon interaction with an analyte (circle), FRET occurs between the donor and acceptor.

The efficiency of FRET (E) is described by Förster theory:

$$E = \frac{1}{1 + \left(\frac{r}{R_0}\right)^6} \quad (2)$$

where r is the distance between the donor and acceptor (Scheme 1.1) and R_0 is the Förster transfer distance or the distance between the donor and acceptor at which E is 50%. R_0 is dependent on the relative orientation of the donor and acceptor molecules, κ , the refractive index of the medium, n , Avogadro's number, N , and the overlap between the donor emission and acceptor absorption, the overlap integral, J , as described in equations (3) and (4). Typical values for R_0 fall in the range of 2-9 nm.³¹

$$R_0 = \frac{9000 \ln 10 \kappa^2 \Phi_D J}{128 \pi^5 n^4 N} \quad (3)$$

$$J = \int_0^\infty dv \frac{f_D(v) e_A(v)}{v^4} \quad (4)$$

J depends on the fluorescence intensity of the donor and the extinction coefficient of the acceptor. It is depicted pictorially in Figure 1.2 for an oxygen sensing system further detailed in Chapter 3. The donor emission (green) can be seen to overlap well with the acceptor absorption (orange) near 525 nm.

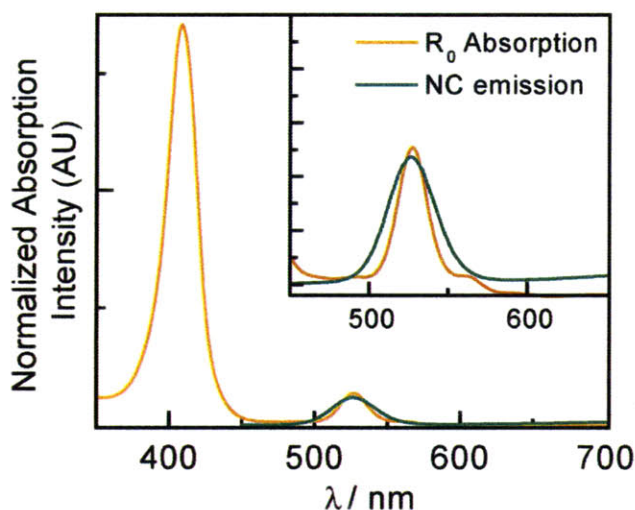


Figure 1.2. Plot of the emission of a QD donor (green) and absorption of a porphyrin acceptor (orange). The area where the two overlap characterizes the overlap integral, J .

E is a measurable quantity through the quenching of the donor excited state emission intensity (I) or lifetime (τ) upon energy transfer to the acceptor through equation (4):

$$E = 1 - \frac{I_{D-A}}{I_D} = 1 - \frac{\tau_{D-A}}{\tau_D} \quad (4)$$

where the D indicates the presence of the donor and $D-A$ indicates the presence of the donor and acceptor. It is important to note that in some cases there may be more than one acceptor present for each donor. This must be taken into account in the energy transfer efficiency through:

$$E = \frac{1}{1 + \left(\frac{r}{R_0}\right)^6} \quad (5)$$

where m is the number of acceptors per donor. Analysis of the efficiency of energy transfer and determination of the distance between the donor and acceptor yields information about donor-acceptor sensing systems that can aid in their characterization and understanding.

1.5 Metabolic Profiling of Tumors

Like any organism, tumors need food (glucose) and oxygen to survive. Tumors recruit blood vessels from the host to supply these nutrients and to remove acidic metabolic byproducts. These parameters are important as they determine tumor growth, metabolism, and response to therapy.⁴⁸ Blood vessels in tumors are inefficient: they are leaky, tortuous, and poorly interconnected. These abnormalities contribute to a tumor environment that is characterized by acidity and hypoxia⁴⁹ due to the poor distribution of nutrients and waste, but also spatial and temporal heterogeneity with respect to each of these metabolic parameters.

In anti-angiogenic therapy, drugs that restrict the growth of blood vessels are administered in an attempt to strangle the tumor. This therapy in combination with other chemotherapies has improved survival in cancer patients, but the way the therapy works is not well understood.⁵⁰ One hypothesis predicts a period of normalized vasculature within the tumor during treatment (Figure 1.3). At such a time, levels of pH, oxygen, and glucose would be similar to those in normal tissue. This would also be an ideal time for combined chemotherapy, as drugs would efficiently reach the tumor, and radiation therapy, as the effectiveness of radiation is mediated by a sufficient concentration of O₂. Past this normalized period of anti-angiogenic therapy lies a period where the tumor vasculature has become inadequate; no nutrients or waste may be

delivered or removed from the tumor. Thus, anti-angiogenic therapy not only restricts nutrients and oxygen from the tumor, but may also limit the effectiveness of cancer therapies. Despite the importance of these metabolic profiling factors, tools for dynamically monitoring them have been lacking.

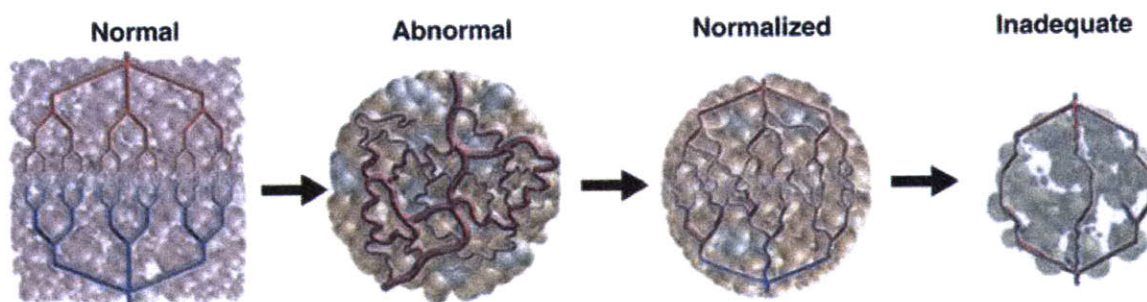


Figure 1.3. Normal tissue vessels distribute nutrients and waste efficiently. Abnormal tissue vessels are tortuous and leaky, leading to poor distribution of nutrients and waste. Anti-angiogenic therapy prohibits the growth of the tumor blood vessels, leading to inadequacy, where the vessels can no longer distribute drugs throughout the tumor. A hypothesized period of normalization between abnormal and inadequate vessels would be the ideal time for efficient delivery of drugs and therapy. See reference 50.

Non-invasive chemosensors with response to these metabolic profiling factors may be used to monitor pH, oxygen, and glucose levels in real time, generating a spatio-temporal map of tumor “health”, essential for further advancing cancer treatment and therapy.

1.6 Multiphoton Spectroscopy and Microscopy

Maria Göppert-Mayer first predicted the possibility of two-photon absorption in 1931.⁵¹ Thirty years later her theory was verified by Kaiser and Garret with the two-photon excitation of $\text{CaF}_2:\text{Eu}^{2+}$.⁵² These multiphoton spectroscopic processes were used to study the structure of molecular excited states^{53,54} and then these non-linear processes were applied to microscopy where Denk *et. al.* took advantage of the two-photon produced fluorescence in a scanning microscope.⁵⁵ Since then, multiphoton processes have become especially important for specific

labeling of biological structures and the study of biochemical processes through the use of fluorescent and phosphorescent dyes. However, many commonly used donors have small two-photon absorption cross-sections limiting their usefulness in two-photon experiments (Table 1.1).

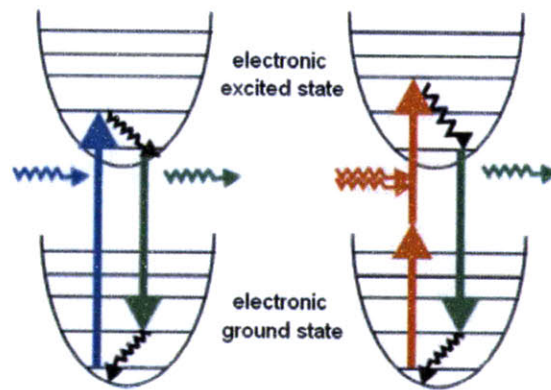


Figure 1.4. Jablonski diagram of single-photon absorption (left) and fluorescence and two-photon absorption and fluorescence (right).

While single-photon spectroscopy involves excitation to the first electronic excited state through absorption of one photon (Figure 1.4), multiphoton spectroscopy involves the absorption of multiple, lower energy photons simultaneously (within ~ 0.5 fs) through intermediate or virtual states.^{56,57} The resulting fluorescence signal (S) is related to the intensity of light (I) through the following equation:

$$S \propto I^n \quad (6)$$

where, n is the number of photons required for excitation to the emissive excited state ($n = 2$ for two-photon excitation). This results in a very specific excitation volume (femtoliter size) that is limited to the focal plane (Figure 1.5, right)^{58,59} providing significant advantages over single-photon excitation in fluorescence microscopy studies. The localization reduces the amount of bleaching and photodamage that occurs, which is especially useful for biological samples, as well as providing extremely high spatial resolution for mapping the heterogeneous tumor

environment.⁶⁰ Absorption of multiple, low energy photons allows excitation through the narrow “biological window” of minimal absorption (Figure 1.6) found in tissues, further decreasing the amount of photodamage.

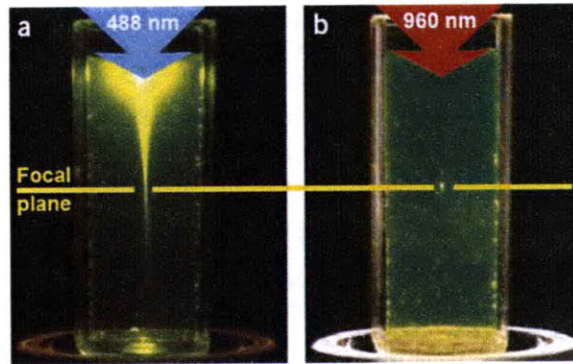


Figure 1.5. Samples excited by single-photon light at 488 nm (left) and two-photon light at 960 nm (right). Taken from reference 59.

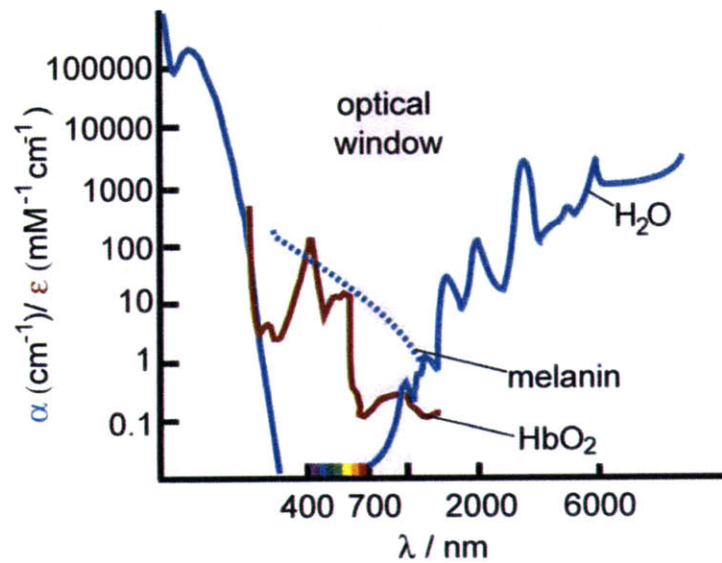


Figure 1.6. Absorption spectra of various biological substances presented as a function of wavelength to show the window present between 700 and 1100 nm (pink), where there is minimal absorption in biological samples. Reproduced from reference 31.

Despite these advantages, the multiphoton absorption cross-sections of many fluorophores remain unknown. This is largely because information regarding the single-photon absorption cross-section does not provide an adequate prediction of the multiphoton ones. A general rule is that the two-photon absorption cross-section will peak at twice the wavelength of the one-photon absorption cross-section, however there are many exceptions, such as rhodamine, which would be expected to have maximum two-photon absorption at 1140 nm, but actually absorbs at 700 nm (see Table 1.1 for more data).⁶¹⁻⁶³ The two-photon absorption cross-section (σ_2) is described by eq (7):

$$\sigma_2 = \sigma_{gi}\sigma_{ie}\tau_i \quad (7)$$

where σ_{gi} and σ_{ie} are the absorption cross-sections of the excitation from the ground to intermediate state and excitation from the intermediate to the excited state, respectively, and τ_i is the lifetime of the intermediate state. This gives absorption in units of $\text{cm}^4 \text{ s/photon}$ and for a typical event the absorption cross-section is about $10^{-50} \text{ cm}^4/\text{photon}$, which is defined to be one Maria Göppert-Mayer unit (GM).^{63,64} The values given in Table 1.1 show σ_2 tends to be quite small for most molecules. Much research has invested in developing donors with large two-photon absorption cross-sections through mechanisms such as intramolecular donor-acceptor charge-transfer interactions or through appending a multiphoton absorbing “antenna” to the desired dye molecule.^{41,65-69} In addition, synthesis of new materials with large σ_2 s such as QDs or metal nanoparticles⁷⁰⁻⁷³ has also been a major thrust. Such materials have been characterized to have two-photon absorption cross-sections of 47,000 GMs, the largest of any label yet used in multiphoton spectroscopy.⁷⁴

Table 1.1. Two-photon Absorption Cross-sections for Several Molecules. Adapted from References 46, 62, 63, and 75-76.

Molecule	λ_{abs}	λ_{em}	2-photon abs cross-section (σ)
Rhodamine B	520	840	210 ± 55
Fluorescein	498	782	38 ± 9.7
GFP wild		~ 800	~ 6
NADH	340	~ 700	~ 0.02
Coumarin 343	450	498	28
H ₂ TPP	515	650	1-6

1.7 Quantum Dots (QDs) as Energy Transfer Donors

Fluorescent semiconductor QDs are characterized by high quantum yields, photostability, narrow emission line-widths, and broad excitation profiles.⁷⁷⁻⁷⁹ They have been used frequently in biological imaging in the past due to these properties. However, their stability leads to a lack of response to their environment. Sensitization of the QD may occur by attachment of an analyte sensitive fluorophore to the QD enabling fluorescence resonance energy transfer (FRET) from the QD to the fluorophore to occur.⁸⁰ This mechanism transfers the valuable properties of the QD such as broad excitation and brightness to the fluorophore. The large multiphoton absorption cross-section found in QDs⁷⁴ is also transferred to the fluorophore.

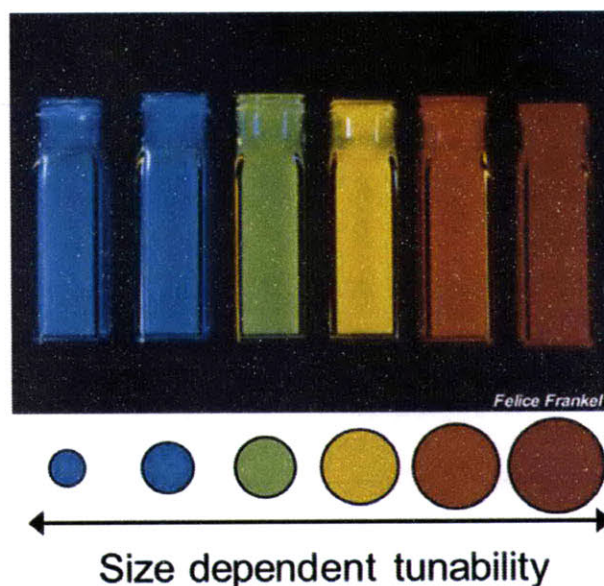
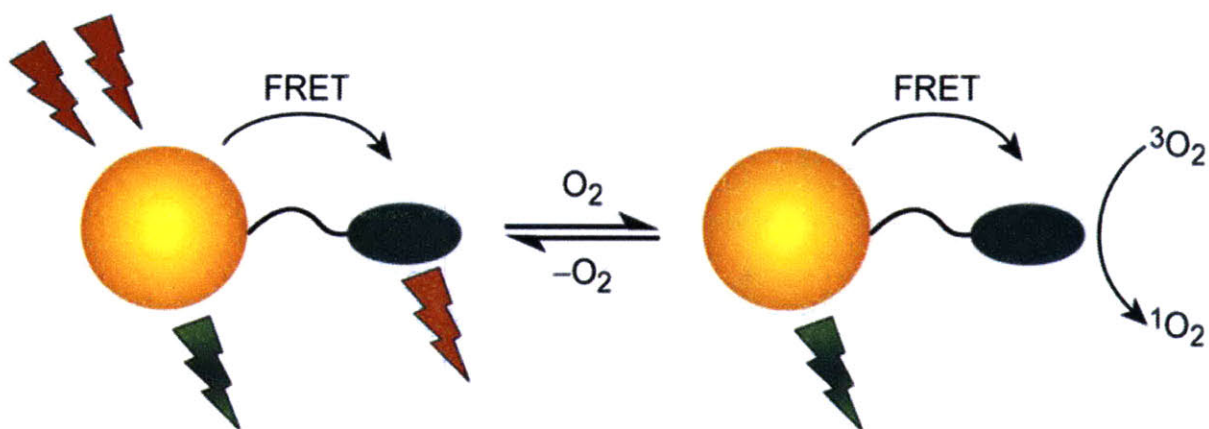


Figure 1.7. Six sizes of CdSe QDs showing the change in the emission wavelength with respect to the QD diameter. The emission can be tuned from blue to red as the size of the QDs is increased. Photography by Felice Frankel.

The FRET requirement of overlap between the donor emission and acceptor absorption is facilitated by using QD donors, as their emission is highly tunable.⁷⁷ As the size of the QD decreases, the effective bandgap of the QD increases, giving rise to an impressive color change (Figure 1.7). Energy transfer from the QD to the analyte sensitive fluorophore also allows establishment of a ratiometric scheme for QD biosensing applications.^{81,82} In this scheme, sensing action results from the engineered overlap of the dye absorption spectrum with an analyte-insensitive QD emission spectrum. Sensing can be quantified by referencing emission peak intensities (QD and dye conjugate) to the intensity of an isosbestic point, which functions as an internal reference. Self-referencing is preserved under a variety of optical conditions, making the method a robust sensing approach within a broad range of biological microenvironments.

1.8 QD FRET O₂ Sensing



Scheme 1.2. Signal transduction mechanism for oxygen sensing. Multiphoton excitation of the QD donor leads to energy transfer to the phosphor, followed by phosphorescence. In the presence of oxygen, the QD emission and energy transfer efficiency remain unchanged, while the phosphorescence of the acceptor is quenched by oxygen.

Our strategy shown in Scheme 1.2 for QD oxygen sensing is based on phosphorescence quenching of an energy accepting phosphor. This mechanism was chosen owing to the unique ability of oxygen to quench phosphorescent emission, but not fluorescence of the QD.⁸³ Using a QD sensor scaffold as a FRET donor and an appended phosphorescent molecule as a FRET acceptor, we can create a system that captures the high excitation rate of the QD under two-photon excitation (increasing brightness vs. phosphor alone) and also achieve an emission-ratiometric detection mode wherein the oxygen-sensitive emission of the phosphor is compared to the oxygen-insensitive emission of the QD. There is also no modulation in FRET efficiency, as the absorption of the phosphor does not change in the presence of oxygen. The QD acts entirely as an internal standard and two-photon antenna for the oxygen sensitive phosphor.

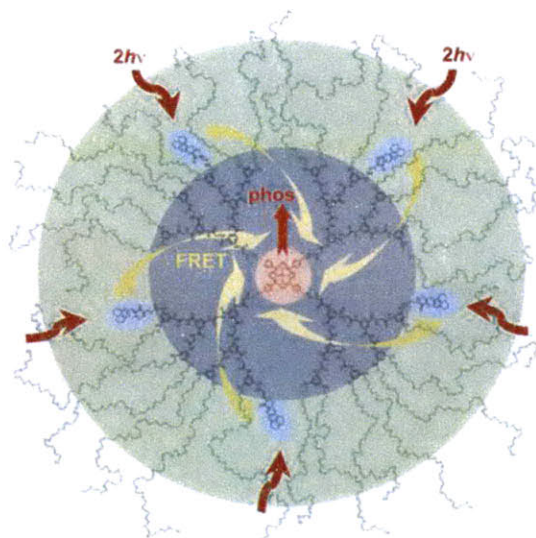


Figure 1.8. Oxygen sensing system in which the phosphor (Pt porphyrin) is sensitized to two-photon excitation using energy transfer from coumarin donors. Taken from reference 46.

Phosphorescent compounds (phosphors) are characterized by long lived excited states and low quantum yields.⁴⁵ While many fluorophores possess small σ_2 s, the signal for two photon emission is proportional to quantum yield (ϕ) as well as σ_2 and excitation intensity (I), as seen in eq (8).

$$S \propto \phi \sigma_2 I^2 \quad (8)$$

Thus, many fluorophores have found utility in multiphoton microscopy despite their small σ_2 s. As phosphors possess much lower quantum yields, they require a sensitizer or antennae to impart enough two-photon brightness for imaging. The oxygen sensing system shown in Figure 1.8 presents one type of two-photon absorbing antennae.⁴⁶ The Pt porphyrin at the center of the sensor is a FRET acceptor. The porphyrin is surrounded by dendrimers into which coumarin molecules are incorporated. Although coumarin has only a moderate σ_2 , it is significantly larger than that of the Pt porphyrin and an enhancement in the two-photon brightness of the oxygen sensor is seen.

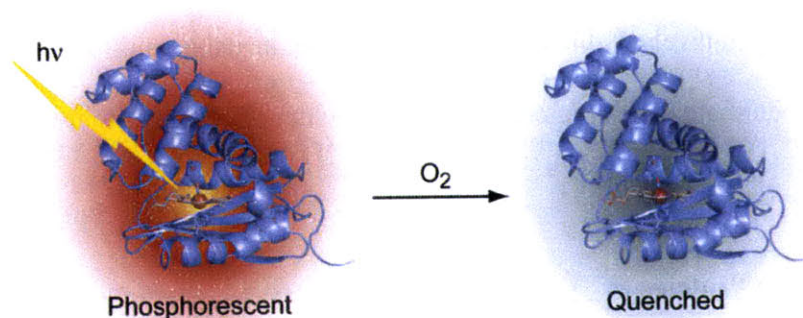
Through FRET from a QD donor to a phosphorescent molecule, an enhanced oxygen sensing system can be developed. An increase in two-photon brightness in conjunction with the ratiometric signal obtained from the combined QD and phosphor emissions facilitates measurement of oxygen levels within biological environments using multiphoton microscopy. Such a sensor can facilitate measurements of tumor growth and response to treatment in real-time.

1.9 Oxygen Sensing Proteins

Proteins that natively bind heme are under-utilized scaffolds for porphyrin-based tools in biology.^{84,85} Traditional methods for unnatural porphyrin incorporation into hemoproteins have limited their utility as biological tools. Harsh, denaturing conditions are typically required to remove native heme from proteins,^{86,87} limiting the number of useful protein constructs. A recently developed method for unnatural porphyrin incorporation into hemoproteins during protein expression⁸⁸ overcomes many of the limitations of traditional methodology. Thus, incorporation of luminescent porphyrins into protein scaffolds can generate a new class of protein-based sensors.

The quenching of small molecule luminescence by O₂ addressed in previous sections provides a platform for simple, non-invasive imaging of *in vivo* O₂ concentrations.³⁶ However, the utility of these small molecule agents is hampered by lack of targetable delivery, non-specific binding, self-aggregation, and limitations in their photophysical properties.^{46,89} Protein-based oxygen sensors utilize the same luminescence quenching mechanism employed by small molecule sensors (Scheme 1.3). However, the protein scaffold can prevent the phosphorescent porphyrin

from interacting with other biological molecules. The protein scaffold can also modulate the range of oxygen sensitivity.



Scheme 1.3. Mechanism of oxygen sensing by an unnatural porphyrin containing protein scaffold. Excitation of the porphyrin is reversibly quenched in the presence of oxygen.

The expression-based method for incorporation of unnatural porphyrins presents a new pathway for obtaining optical oxygen sensors. The stability and tailorability of these protein-based sensors may be further enhanced by incorporation of the sensor into a FRET-based sensing scheme. The advantages of such a scheme, addressed in previous sections as applied to small molecule phosphors such as porphyrin and polypyridine complexes, also apply to a scheme involving protein-based phosphors.

1.10 Scope of Thesis

This thesis investigates and develops optical oxygen sensing molecules and systems for use in biological environments. FRET between the QD and phosphor is examined as a signal transduction mechanism and the prospect of sensor use *in-vivo* is addressed.

Chapter 2 explores two osmium(II) polypyridine phosphors as oxygen sensors and scrutinizes the changes in their photophysical properties when incorporated into a QD FRET sensing system

with special emphasis on enhancement of the two-photon emission of the molecule. Chapter 3 extends the QD FRET studies to a palladium(II) porphyrin phosphor with oxygen sensitivity in the biological range. Chapter 4 details synthetic development of new porphyrin-based phosphors for use as FRET acceptors in a QD-based energy transfer system. Preliminary studies on attachment of one of these porphyrins to a polymer used for QD water solubilization are also mentioned. Chapter 5 introduces new oxygen sensing protein systems based on unnatural ruthenium(II) porphyrins. Chapter 6 extends the protein-based sensing systems to other unnatural porphyrins, namely a palladium(II) porphyrin, and initial prospects for use of the Pd-protein sensor as a QD FRET acceptor are explored with emphasis on future work in this direction.

1.11 References

1. Bell, T. W.; Hext, N. M. *Chem. Soc. Rev.* **2004**, *33*, 589-598.
2. de Silva, A. P.; Gunaratne, H. Q. N.; Gunnlaugsson, T.; Huxley, A. J. M.; McCoy, C. P.; Rademacher, J. T.; Rice, T. E. *Chem. Rev.* **1997**, *97*, 1515-1566.
3. *Chemosensors of Ion and Molecular Recognition*; Kluwer Academic Publishers: Dordrecht, The Netherlands, **1997**; Vol. 492.
4. *Fluorescent Chemosensors for Ion and Molecule Recognition*; American Chemical Society: Washington, D. C., **1993**.
5. Czarnik, A. W. *Acc. Chem. Res.* **1994**, *27*, 302-308.
6. Rudzinski, C. M.; Hartmann, W. K.; Nocera, D. G. *Coord. Chem. Rev.* **1998**, *171*, 115-123.
7. Rudzinski, C. M.; Nocera, D. G. in *Optical Sensors and Switches*, Ramamurthy, V.; Schanze, K.S., Eds.; Marcel Dekker: New York, **2001**, p. 1-91.
8. Rudzinski, C. M.; Young, A. M.; Nocera, D. G. *J. Am. Chem. Soc.* **2002**, *124*, 1723-1727.
9. Swager, T. M. *Acc. Chem. Res.* **1998**, *31*, 201-207.
10. Mohr, G. J. *Chem.-Eur. J.* **2004**, *10*, 1082-1090.
11. de Silva, A. P.; Fox, D. B.; Moody, T. S.; Weir, S. M. *Trends Biotechnol.* **2001**, *19*, 29-34.
12. Arnold, M. A.; Small, G. W. *Anal. Chem.* **2005**, *77*, 5429-5439.
13. Aslan, K.; Zhang, J.; Lakowicz, J. R.; Geddes, C. D. *J. Fluoresc.* **2004**, *14*, 391-400.
14. Ballerstadt, R.; Evans, C.; McNichols, R.; Gowda, A. *Biosens. Bioelectron.* **2006**, *22*, 275-284.
15. Kondepati, V. R.; Heise, H. M. *Anal. Bioanal. Chem.* **2007**, *388*, 545-563.

16. Pickup, J. C.; Hussain, F.; Evans, N. D.; Rolinski, O. J.; Birch, D. J. S. *Biosens. Bioelectron.* **2005**, *20*, 2555-2565.
17. Wang, J. *Chem. Rev.* **2008**, *108*, 814-825.
18. Cable, M. L.; Kirby, J. P.; Sorasaene, K.; Gray, H. B.; Ponce, A. *J. Am. Chem. Soc.* **2007**, *129*, 1474-1475.
19. Yung, P. T.; Lester, E. D.; Bearman, G.; Ponce, A. *Biotechnol. Bioeng.* **2007**, *98*, 864-871.
20. Royo, S.; Martinez-Manez, R.; Sancenon, F.; Costero, A. M.; Parra, M.; Gil, S. *Chem. Commun.* **2007**, 4839-4847.
21. Niessner, R. *Trends Anal. Chem.* **1991**, *10*, 310-316.
22. Scully, P.; Chandy, R.; Edwards, R.; Merchant, D.; Morgan, R. *Environ. Sci. Res.* **2001**, *56*, 175-199.
23. Szmackinski, H.; Lakowicz, J. R. *Sens. Actuators, B* **1995**, *B29*, 16-24.
24. Wolfbeis, O. S. *J. Mater. Chem.* **2005**, *15*, 2657-2669.
25. Jortner, J.; Rice, S. A.; Hochstrasser, R. M. *Adv. Photochem.* **1969**, *7*, 149-309.
26. Freed, K. F. *Acc. Chem. Res.* **1978**, *11*, 74-80.
27. Lin, S. H. *Radiationless Transitions*; Academic Press: New York, **1980**.
28. Califano, M.; Franceschetti, A.; Zunger, A. *Nano Lett.* **2005**, *5*, 2360-2364.
29. Kippeny, T. C.; Bowers, M. J., II; Dukes, A. D., III; McBride, J. R.; Orndorff, R. L.; Garrett, M. D.; Rosenthal, S. J. *J. Chem. Phys.* **2008**, *128*, 084713/1-084713/7.
30. Petrov, E. P.; Cichos, F.; von Borczyskowski, C. *J. Lumin.* **2006**, *119-120*, 412-417.

31. Lakowicz, J. R. *Principles of Fluorescence Spectroscopy*, 2nd ed.; Kluwar Academic/Plenium Publishing: New York, **1999**.
32. Clark, L. C., Jr.; Wolf, R.; Granger, D.; Taylor, Z. *J. Appl. Physiol.* **1953**, *6*, 189-193.
33. Swartz, H. M.; Dunn, J.F. *Adv. Exp. Med. Biol.* **2003**, *530*, 1-12.
34. Mason, R. P.; Rodbumrung, W.; Antich, P. P. *NMR Biomed.* **1996**, *9*, 125-134.
35. Ogawa, S.; Lee, T. M.; Kay, A. R.; Tank, D. W. *Proc. Natl. Acad. Sci. U. S. A.* **1990**, *87*, 9868-9872.
36. Vanderkooi, J. M.; Maniara, G.; Green, T. J.; Wilson, D. F. *J. Biol. Chem.* **1987**, *262*, 5476-5482.
37. Kautsky, H.; Hirsch, A. *Berichte der deutschen chemischen Gesellschaft (A and B Series)* **1931**, *64*, 2677-2683.
38. Kautsky, H.; Muller, G. O. *Zeitschrift fur Naturforschung A (Astrophysik, Physik und Physikalische Chemie)* **1947**, *2a*, 167-172.
39. Papkovsky, D.B. *Methods. Enzymol.* **2004**, *381*, 715-735.
40. Sacksteder, L.; lee, M.; Demas, J. N.; DeGraff, B. A. *J. Am. Chem. Soc.* **1993**, *115*, 8230-8238.
41. Briñas, R.P.; Troxler, T.; Hochstrasser, R.M.; Vinogradov, S.A. *J. Am. Chem. Soc.* **2005**, *127*, 11851-11862.
42. Vanderkooi, J. M.; Wright, W. W.; Erecinska, M. *Biochim. Biophys. Acta* **1994**, *1207*, 249-254.
43. Vanderkooi, J. M.; Maniara, G.; Green, T. J.; Wilson, D. F. *J. Biol. Chem.* **1987**, *262*, 5476-5482.

44. Kober, E. M.; Caspar, J. V.; Lumpkin, R. S.; Meyer, T. J. *J. Phys. Chem.* **1986**, *90*, 3722-3734.
45. Kalyansundaram, K. *Photochemistry of Polypyridine and Porphyrin Complexes*. Academic Press: San Diego, CA, **1992**.
46. Finikova, O.S.; Lebedev, A.Y.; Aprelev, A.; Troxler, T.; Gao, F.; Garnacho, C.; Muro, S.; Hochstrasser, R.M.; Vinogradov, S.A. *Chem. Phys. Chem.* **2008**, *9*, 1673-1679.
47. Förster, T. *Ann. Phys.* **1948**, *2*, 55-75.
48. Helmlinger, G.; Yuan, F.; Dellian, M.; Jain, R. K. *Nat. Med.* **1997**, *3*, 177-182.
49. Vaupel, P.; Kallinowski, F.; Okunieff, P. *Cancer Res.* **1989**, *49*, 6449-6465.
50. Jain, R. K. *Science* **2005**, *307*, 58-62.
51. Göppert-Mayer, M. *Ann. Phys.* **1931**, *9*, 273-294.
52. Kaiser, W.; Garrett, C. G. B. *Phys. Rev. Lett.* **1961**, *7*, 229-231.
53. Friedrich, D. M. *J. Chem. Educ.* **1980**, *59*, 472.
54. Birge, R. R. *Acc. Chem. Res.* **1986**, *19*, 138-146.
55. Denk, W.; Strickler, J. H.; Webb, W. W. *Science* **1990**, *248*, 73-76.
56. Helmchen, F.; Denk, W. *Nature Methods* **2005**, *2*, 932-940.
57. So, P. T. C.; Dong, C. Y.; Masters, B. R.; Berland, K. M. *Annu. Rev. Biomed. Eng.* **2000**, *2*, 399-429.
58. Zipfel, W.R.; Williams, R. M.; Webb, W. W. *Nat. Biotech.* **2003**, *21*, 1369-1377.
59. König, K. *Journal of Microscopy*, **2000**, *200*, 83-104.

60. Squirrell, J. M.; Wokosin, D. L.; White, J. G.; Bavister, B. D. *Nat. Biotechnol.* **1999**, *17*, 763-767.
61. Williams, R. M.; Zipfel, W. R.; Webb, W. W. *Curr. Op. Chem. Bio.* **2001**, *5*, 603-608.
62. Xu, C.; Webb, W. W. *J. Opt. Soc. Am. B* **1996**, *13*, 481-491.
63. Xu, C. *Confocal and Two-Photon Microscopy: Foundations, Applications and Advances*, ed. Diaspro, A. New York, Wiley-Liss, Inc. **2002**.
64. McClain, W.M. *Acc. Chem. Res.* **1974**, *7*, 129-135.
65. Wang, Y.; He, G. S.; Prasad, P. N.; Goodson, III, T. *J. Am. Chem. Soc.* **2005**, *127*, 10128-10129.
66. Zhao, L.; Yang, G.; Su, Z.; Qin, C.; Yang, S. *Synth. Metals* **2006**, *156*, 1218-1224.
67. Ray, P.C.; Sainudeen, Z. *J. Phys. Chem. A* **2006**, *110*, 12342-12347.
68. Morone, M.; Beverina, L.; Abbotto, A.; Silvestri, F.; Collini, E.; Ferrante, C.; Bozio, R.; Pagani, G. A. *Org. Lett.* **2006**, *8*, 2719-2722.
69. Humphrey, J.L.; Kuciauskas, D. *J. Am. Chem. Soc.* **2006**, 3902-3903.
70. Wang, H.; Huff, T. B.; Zweifel, D. A.; He, W.; Low, P. S.; Wei, A.; Cheng, J. -X. *Proc. Natl. Acad. Sci.* **2005**, *102*, 15752-15756.
71. Fu, Y.; Han, T. -T.; Luo, Y.; Agren, H. *J. Phys. Cond. Mat.* **2006**, *18*, 9071-9082.
72. Fedorov, A.V.; Baranov, A. V. *Phys. Rev. B* **1996**, *54*, 8627-8632.
73. Blanton, S.A.; Hines, M. A.; Schmidt, M. E.; Guyot-Sionnest, P. *J. Lumin.* **1996**, *70*, 253-268.

74. Larson, D.R.; Zipfel, W. R.; Williams, R. M.; Clark, S. W.; Bruchez, M. P.; Wise, F. W.; Webb, W. W. *Science* **2003**, *300*, 1434-1436.
75. Chen, Z.P.; Kaplan, D. L.; Yang, K.; Kumar, J.; Marx, K. A.; Tripathy, S. K. *Appl. Opt.* **1997**, *36*, 1655-1659.
76. Kruk, M.; Karotki, A.; Drobizhev, M.; Kuzmitsky, V.; Gael, V.; Rebane, A. *J. Lumines.* **2003**, *105*, 45-55.
77. Murray, C. B.; Norris, D. J.; Bawendi, M. G. *J. Am. Chem. Soc.* **1993**, *115*, 8706-8715.
78. Chan, W. C.; Maxwell, D. J.; Gao, X.; Bailey, R. E.; Han, M.; Nie, S. *Curr. Opin. Biotech.* **2002**, *13*, 40-46.
79. Wu, X. Y.; Liu, H. J.; Liu, J. Q.; Haley, K. N.; Treadway, J. A.; Larson, J. P.; Ge, N. F.; Peale, F.; Bruchez, M. P. *Nat. Biotech.* **2003**, *21*, 41-46.
80. Somers, R. C.; Bawendi, M. G. and Nocera D. G. *Chem. Soc. Rev.* **2007**, *36*, 579-591.
81. Goldman, E. R.; Medintz, I. L.; Whitley, J. L.; Hayhurst, A.; Clapp, A. R.; Uyeda, H. T.; Deschamps, J. R.; Lassman, M. E.; Mattoussi, H. *J. Am. Chem. Soc.* **2005**, *127*, 6744-6751.
82. Michalet, X.; Pinaud, F. F.; Bentolila, L. A.; Tsay, J. M.; Doose, S.; Li, J. J.; Sundaresan, G.; Wu, A. M.; Gambhir, S. S.; Weiss, S. *Science* **2005**, *307*, 538-544.
83. Walker, G. W.; Sundar, V. C.; Rudzinski, C. M.; Wun, A. W.; Bawendi, M. G.; Nocera, D. G. *Appl. Phys. Lett.* **2003**, *83*, 3555-3557.
84. Dou, Y.; Maillett, D. H.; Eich, R. F.; Olson, J. S. *Biophys. Chem.* **2002**, *98*, 127-148.
85. Gillam, E. M. J. *Chem. Res. Toxicol.* **2008**, *21*, 220-231.
86. Teale, F. W. *Biochim. Biophys. Acta* **1959**, *35*, 543.

87. Schmidt, P.; Schramm, M.; Schröder, H.; Stasch, J. P. *Protein Expr. Purif.* **2003**, *31*, 42-46.
88. Woodward, J. J.; Martin, N. I.; Marletta, M. A. *Nat. Methods* **2007**, *4*, 43-45.
89. Berg, K.; Selbo, P. K.; Weyergang, A.; Dietze, A.; Prasmickaite, L.; Bonsted, A.; Engesaeter, B. Ø.; Angell-Petersen, E.; Warloe, T.; Frandsen, N.; Høgset, A. *J. Microsc.* **2005**, *218*, 133-147.

Chapter 2

Osmium Polypyridine O₂ Sensors

Parts of this Chapter have been published:

Mclaurin, E. J.; Greytak, A. B.; Bawendi, M. G.; Nocera, D. G. "Two-Photon Absorbing Nanocrystal Sensors for Ratiometric Detection of Oxygen" *J. Am. Chem. Soc.* **2009**, *131*, 12994-13001.

2.1 Motivation

As outlined in Chapter 1, our interest in signal transduction mechanisms for QD-based sensing led us to explore a novel mechanism in which the amount of energy transfer from the QD donor to the acceptor remains constant, and our handle on oxygen pressure is provided by the quenching of phosphorescence of the acceptor, with no change in the emission of the QD. Investigations of two osmium polypyridine complexes and their propensity for oxygen sensing are presented in this chapter. The advantages of using the QD in these systems are explored. The resulting increase in oxygen sensitivity and two-photon emission indicate the ability of the QDs to act as two-photon sensitizers for polypyridine complexes as well as engendering oxygen sensing abilities to the QD.

2.2 Background

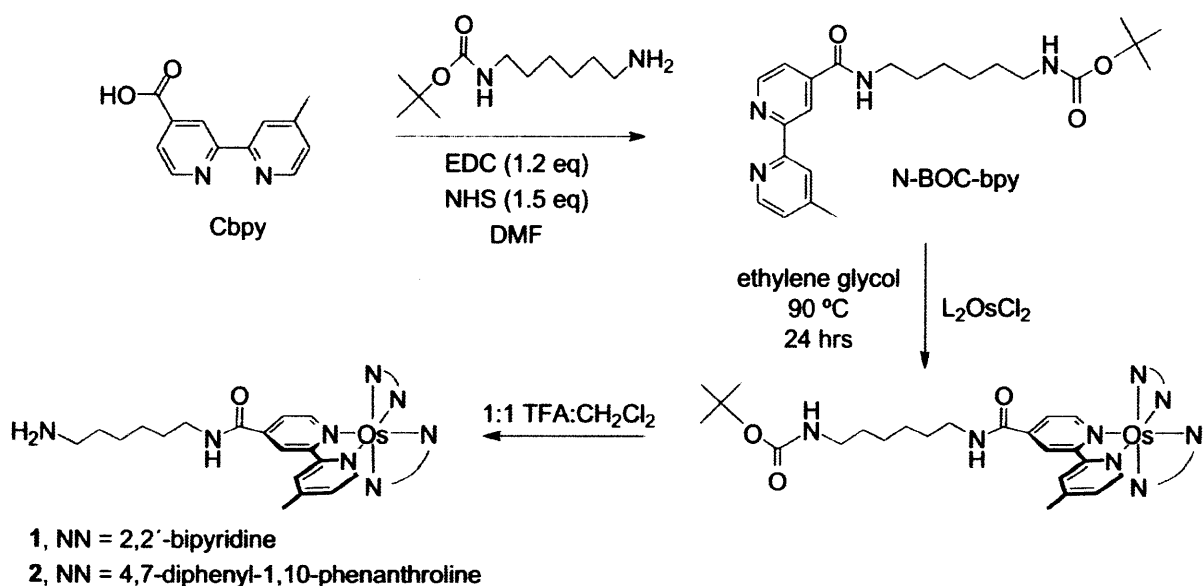
Although there have been studies on both nanoparticle-based ratiometric oxygen sensors and enhancement of two-photon induced phosphorescence through FRET, so far they have been limited mostly to studies using small molecules^{1,2} as the two-photon absorbing energy donor and fluorescent intensity standard, employing a polymer-based nanoparticle as a scaffold³⁻⁵ or having a late transition metal-based porphyrin as the phosphorescent energy acceptor.⁶ The construction of a ratiometric QD-based pO₂ sensor according to the design illustrated in Scheme 1.2 permits sensing to be achieved through the two-photon excitation of the osmium(II) polypyridyl (Os(II)PP) phosphor. Though multiphoton processes in inorganic polypyridine complexes have been established,⁷ exploitation of metal polypyridyls for two-photon sensing has yet to be achieved owing to relatively low two-photon absorption cross-section of the native complexes.⁸ This obstacle is overcome with the approach illustrated in Scheme 1.2 because the large two-

photon excitation profile of the QD may be conferred upon Os(II)PP by utilizing FRET.

Phosphorescence emission from the Os(II)PP complex is reversibly quenched in the presence of O₂ whereas the QD emission is unaffected because the FRET efficiency (QD→Os(II)PP) and the QD emission is unresponsive to O₂.⁹ The QD emission thus affords an easily-resolved internal reference, allowing the Os(II)PP sensor to be used not only in the more typical lifetime detection mode,¹⁰ but also in a ratiometric detection mode, thus offering the advantage of simple signal detection.

2.3 Results

2.4 Synthesis and Characterization of Osmium Polypyridines



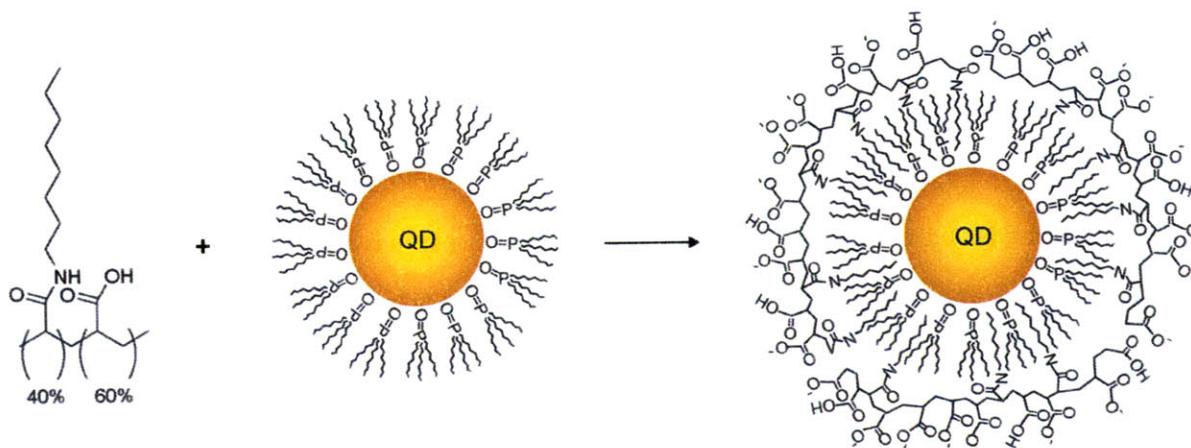
Scheme 2.1. Synthesis of Bis(NN))(N-(6-aminohexyl)-4'-methyl-2,2'-bipyridine-4-carboxamide)-osmium(II) bis(hexafluorophosphate) [OsII(NN)₂(Nbpy)](PF₆)₂ through lower temperature methods, preserving the diamine linker.

Scheme 2.1 presents the synthetic method employed to furnish mono-amine-functionalized Os(II)PP compounds. The single amine embodies a design element that precludes cross-coupling

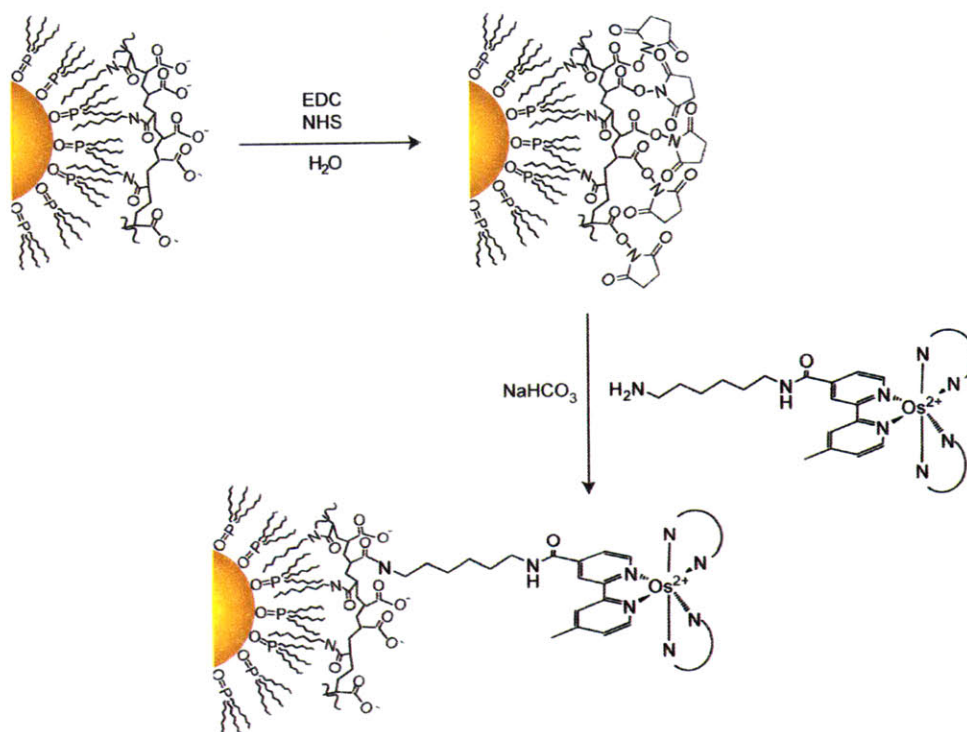
between the osmium complexes and QDs. This asymmetric ligand modification works best when the reactants are heated at low temperature for long periods of time. The more frequently employed conditions of higher refluxing temperatures over shorter periods of time¹¹ produces the tris-substituted complexes as well as undesirable products, especially for the case of **2**. Initial attempts to form the mono-amine-functionalized osmium compound followed by attachment of a protected diamine were largely unsuccessful. Instead, the mono-carboxylated bpy ligand was first coupled to an amine so that it was suitable for facile carbodiimide coupling to a carboxylic acid. Carboxy-bpy was coupled to *tert*-butyl 6-aminohexylcarbamate by carbodiimide coupling to generate N-BOC-bpy. The osmium-dichloride synthons were heated with the N-BOC-bpy ligand in ethylene glycol to afford the protected Os(II)PP complexes. Purification by alumina chromatography, deprotection of the BOC group with TFA, and precipitation of the complex yielded the water soluble, mono-aminated osmium complexes **1** and **2**, as established by ¹H NMR, UV-vis, and emission spectroscopy and MALDI-TOF mass spectrometry.

2.5 Synthesis of QD-Osmium Sensors

Known synthetic methods of water-soluble QDs were employed to ensure a bright and stable scaffold. Water-soluble QDs were synthesized from Cd_xZn_{1-x}Se cores overcoated with Cd_yZn_{1-y}S shells and their surfaces were modified with *n*-octylamine functionalized poly(acrylic) acid (**PAA-OA**), as shown in Scheme 2.2. The polymer is modified by amide bond formation through EDC coupling of *n*-octylamine to the polyacrylic acid. Combination of the QDs and polymer in chloroform allows integration of the alkyl chains from the polymer and QD surface. Removal of chloroform and addition of sodium bicarbonate buffer (pH ~8.5) followed by purification by dialysis with 50,000 MWCO filters yields QDs in aqueous solution.



Scheme 2.2. Formation of water soluble QDs through mixing of amphiphilic polymer with the QDs in CHCl_3 followed by solvent removal and dissolution of the polymer-QD solution in sodium bicarbonate buffer (pH ~ 8.5).



Scheme 2.3. Conjugation of the osmium polypyridine phosphor to polymer encapsulated QDs.

Conjugates were synthesized by using the carbodiimide coupling method shown in Scheme 2.3. Single QDs were appended with either **1** or **2** through the mono-amine functionality. GFC

was used to separate and validate the purity of these conjugates. Characterization of these products is shown in Figure 2.1 along with that of mixtures in the absence of the coupling agent. The large absorption at 14.5 min is characteristic of the QDs. The fractions containing single, unaggregated QDs were collected and used in further analysis. Further analysis of these samples using GFC indicated they were unimodal peaks.

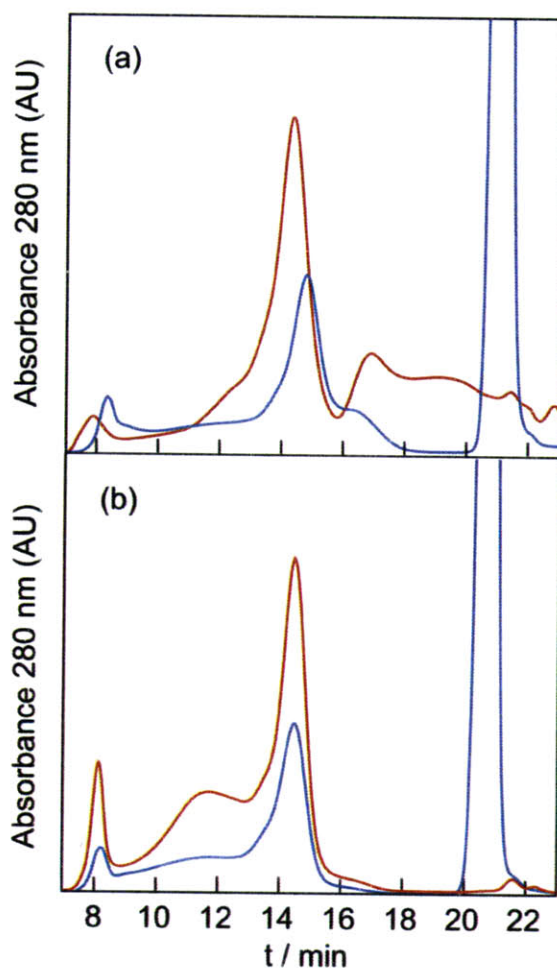


Figure 2.1. A GFC trace of the conjugates QD-1 and QD-2 and the mixtures of the QD with 1 and QD with 2. The GFC peaks recorded with a detection wavelength of 280 nm are shown in (top) QD-1 (—) and a mixture of the QD and 1 (—) and (bottom) QD-2 (—) and a mixture of the QD and 2 (—). The peak at 14.5 min is the elution peak for the single QDs.

2.6 Spectroscopic Properties of **1** and **2** and QD-1 and QD-2

Purified QD conjugates were analyzed with UV-vis absorption spectroscopy, steady-state, and time-resolved emission spectroscopies. The spectroscopic properties for the Os(II)PP complexes and the QD are summarized in Table 2.1. The absorption spectra of the Os(II)PP complexes are dominated by metal-ligand charge transfer (MLCT) transitions that are typical of metal polypyridyl complexes (Figure 2.2). The MLCT absorption band appears in the higher energy region accompanied by a shoulder to the lower energy side of the band. As has been observed previously, the MLCT absorption band of **2** is broader and more intense than that of its bpy relative, **1**.¹²

Table 2.1. Spectroscopic and Photophysical Properties of Os^{II} Polypyridyl Complexes, (Cd_xZn_{1-x}Se)Cd_yZn_{1-y}S Core-Shell Nanocrystals, and Os^{II} Polypyridyl Complexes Conjugated with (Cd_xZn_{1-x}Se)Cd_yZn_{1-y}S Core-Shell Nanocrystals in Aqueous Solution at Room Temperature.

Complex	$\lambda_{\text{abs}} / \text{nm}$	$\lambda_{\text{em}} / \text{nm}$	Φ_{em}	$\tau_{\text{em}} / \text{ns}$
Os(bpy) ₂ (Nbpy) (1) ^a	490, ~650 ^c	800	0.0096	12
Os(DPPhen) ₂ (Nbpy) (2) ^a	450, ~625 ^c	795	0.013	15
QD ^b	525 ^d	549 ^b	0.40	18 ^e
QD-Os(bpy) ₂ (Nbpy) (QD-1) ^f	435, 507, ~650 ^c	549, 765	0.018, ^g 0.85 ^h	6 ^c , 111 ⁱ
QD-Os(DPPhen) ₂ (Nbpy) (QD-2) ^f	445, 507, ~625 ^c	549, 746	0.23, ^g 19.46 ^h	9 ^c , 163 ⁱ

^a $\lambda_{\text{exc}} = 450 \text{ nm}$, $\lambda_{\text{det}} = 700 \text{ nm}$. ^b $\lambda_{\text{exc}} = 355 \text{ nm}$, $\lambda_{\text{det}} = 550 \text{ nm}$. ^c Shoulder. ^d Lowest energy exciton peak ^e $\lambda_{\text{exc}} = 400 \text{ nm}$, $\lambda_{\text{det}} = 550 \text{ nm}$. ^f $\lambda_{\text{exc}} = 355 \text{ nm}$, $\lambda_{\text{det}} = 750 \text{ nm}$. ^g Estimated from the enhancement factor (Figure 3). ^h Increase in the Os(II)PP emission, normalized by Os(II)PP concentration, upon going from the molecule alone to the conjugated molecule. ⁱ $\lambda_{\text{exc}} = 355 \text{ nm}$, $\lambda_{\text{det}} = 750 \text{ nm}$ and in the absence of O₂. Lifetimes were determined from the longer component of the bi-exponential emission fit.

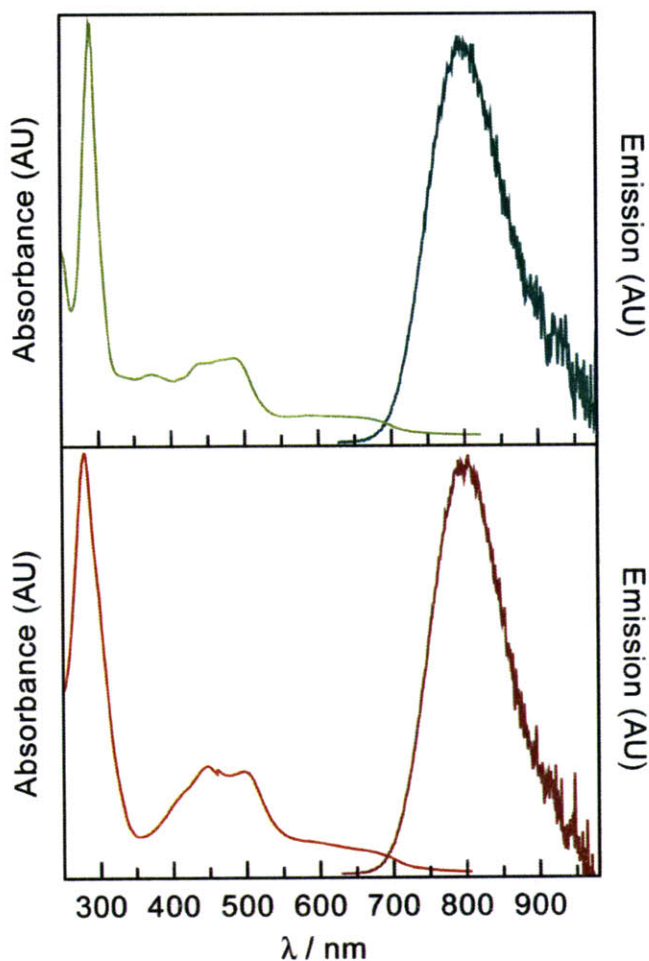


Figure 2.2. Electronic spectra of complexes **1** and **2** in the steady state. The absorption of **1** (—) was not altered upon conjugation. The emission of **1** (—) blue-shifts upon conjugation. Similar changes, or lack thereof, were observed for the absorption (—) and emission (—) of **2**.

Excitation into the MLCT absorption manifold produces broad, featureless emission bands centered in the near infrared (Figure 2.2) corresponding to excited states characterized by mono-exponential decays. The emission maximum of **2** lies to higher energy than that of **1**. This is paralleled by a more intense emission and longer lifetime (τ_{em}). The QD absorption spectrum exhibits a band at 525 nm and the emission spectrum exhibits a Gaussian band centered at 549 nm (FWHM = 36 nm, $\Phi_{em} = 40\%$). QD fluorescence decay was typically biexponential, as observed previously.¹³

2.7 Energy Transfer Analysis

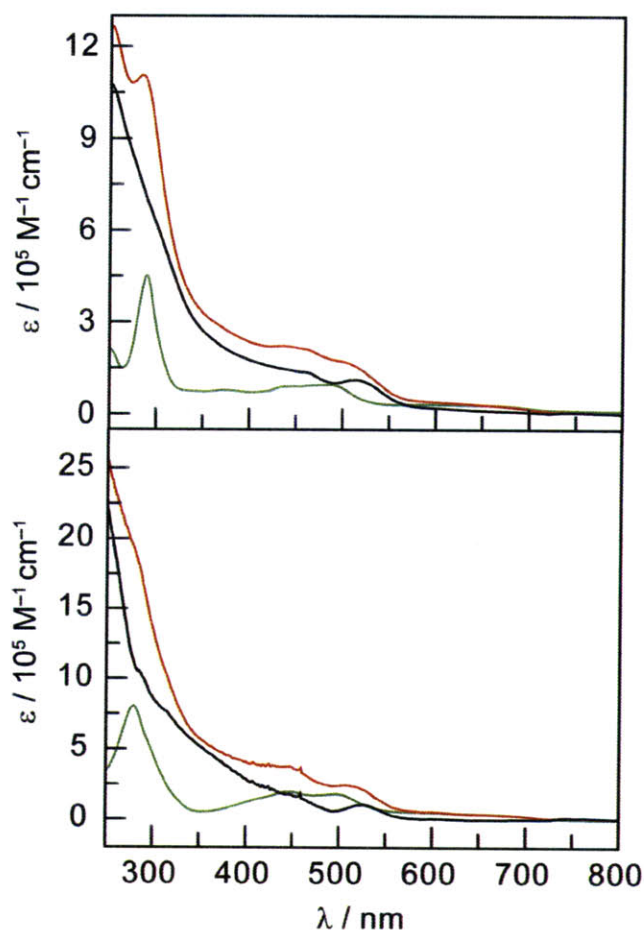


Figure 2.3. (Top) absorbance of the QD (—), 1 (—) and the QD-1 (—) conjugate. (Bottom) absorbance of the QD (—), 2 (—) and the QD-2 (—) conjugate.

The absorption spectra of **QD-1** and **QD-2** in Figure 2.3 match the composite sum of the QD and the Os(II)PP spectra. Accordingly, values of m (Table 2.1) were determined from the absorption spectra of **QD-1** and **QD-2** using the assumption that they were the sum of the absorptions of the free QD and Os(II)PP components. MLCT excitation ($\lambda_{\text{exc}} = 450 \text{ nm}$) of the Os(II)PP complexes within **QD-1** and **QD-2** conjugates yields an Os(II)-based emission that shifts to wavelengths shorter, by 35 and 49 nm, respectively, than that of the free complexes

(Figure 2.4). Selective excitation of the QD ($\lambda_{\text{exc}} = 355 \text{ nm}$) shows no additional changes in the Os(II)-based emissions. Comparison with the isolated Os(II)PP complexes excited at the same wavelengths exhibit an increase of the Os(II)PP emission within the conjugate whereas emission from the QD center is attenuated (Figure 2.4).

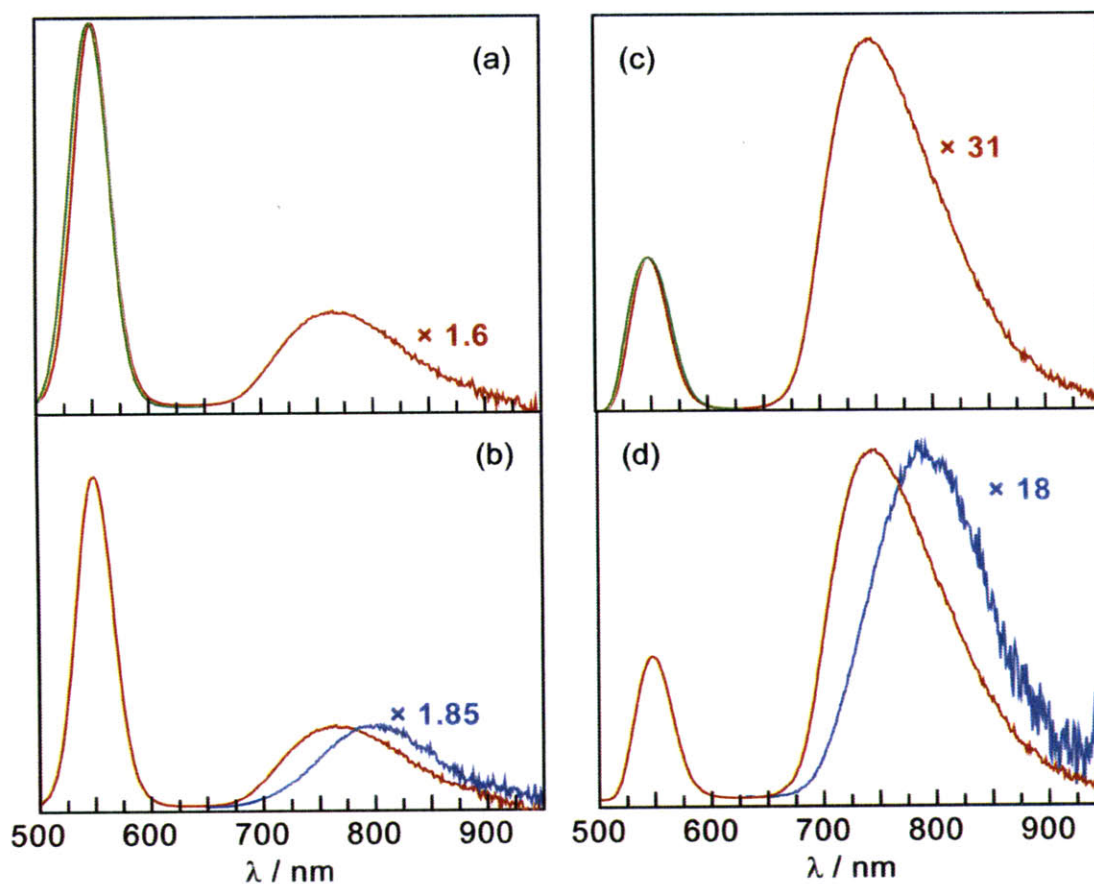


Figure 2.4. Steady-state emission spectra ($\lambda_{\text{exc}} = 450 \text{ nm}$) of the conjugates and their individual components in aqueous solution. Spectra were adjusted for concentration. (a) Spectra of the QD (—) and the QD-1 conjugate (—) with the same QD peak intensity. (b) Spectra of 1 (—) and QD-1 (—) with the same Os(II)PP emission peak intensity. (c) Spectra of the QD (—) and QD-2 (—) (1:135 QD:2 ratio) with the same QD peak intensity. (d) Spectra of 2 (—) and QD-2 (—) with the same Os(II)PP emission peak intensity.

The trend in the excited state lifetimes of the individual Os(II)PP and QD components as compared to the conjugates (see Table 2.1) concurs with the results of steady-state spectroscopy. The QD and the Os(II)PP centers of the conjugates both show biexponential decays.¹³ The increase in the steady-state emission of the Os(II)PP center within the conjugate is accompanied by a corresponding lifetime enhancement by a factor of nearly one order of magnitude. These results are in accordance with Os(II)PP-polymer systems, which also show 3-4-fold excited state lifetime enhancements.¹⁴ In turn, the lifetimes of the QD centers of the conjugates are diminished as compared to the QD alone.

To further quantify the efficiency of energy transfer, a lifetime analysis of the QD and conjugate was performed. A sample of **QD-2** possessing a larger QD:2 ratio (m) was employed for this study. The lifetime decays are shown in Figure 2.5 and results of the lifetime analysis are summarized in Table 2.2.

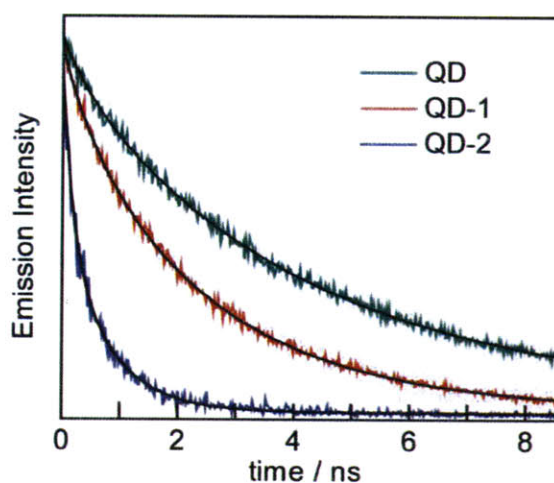


Figure 2.5. Time-resolved emission decay of the QD (—), QD-1 (—), and QD-2 (—). The quenching of the QD excited state is obvious from the accelerated decay.

The 67% energy transfer efficiency of **QD-1** accounts for the decrease in the steady-state emission of QD upon conjugation (as observed in Figure 2.4a); an energy transfer efficiency of 50% was calculated for the new **QD-2** sample. The distance parameters of energy transfer, R_0 and r listed in Table 2.2, were determined from eqs (2) and (4) using the listed Os(II)PP to QD ratios.

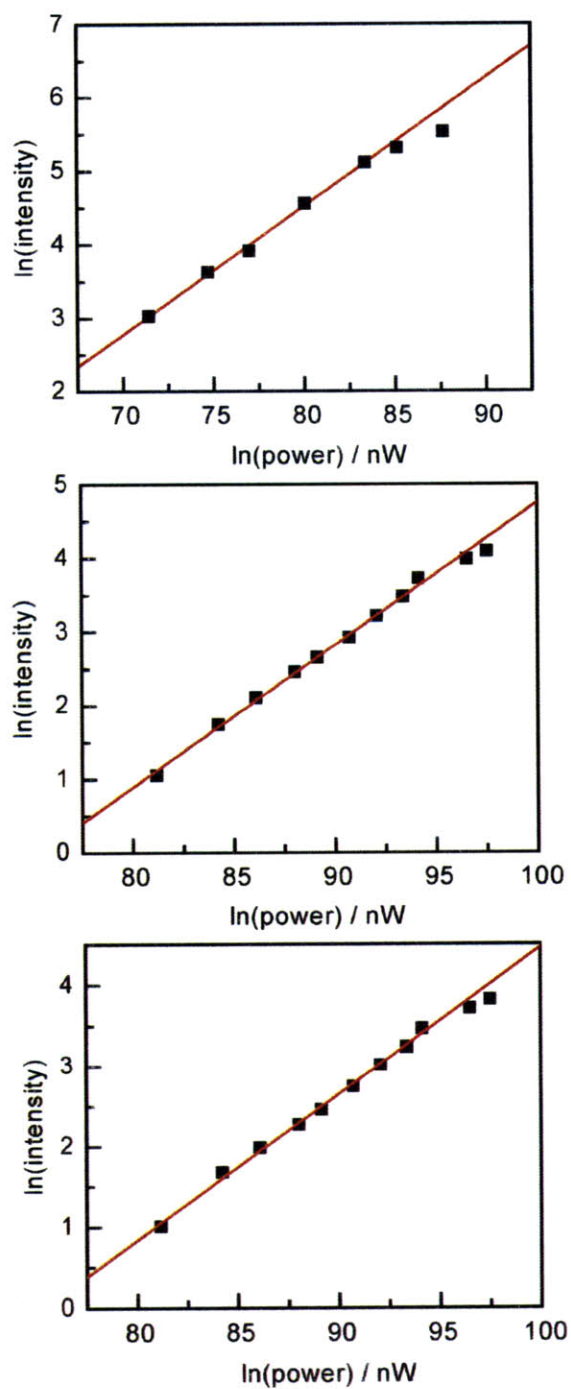


Figure 2.6. Energy dependence plots for the QD alone (slope = 1.75, top), QD in QD-2 (center, slope = 1.92), and 2 in QD-2 (slope = 1.82, bottom). The power listed was measured using a 20% beam pick-off.

Table 2.2. Förster Energy Transfer Parameters for QD-1 and QD-2

Complex	QD:Os(II)PP Ratio (m) ^a	r / nm ^b	R ₀ /	E ^d
QD-bpy ₂ OsNbpy (QD-1)	1:57	4.2	3.4	0.7
QD-DPPhen ₂ OsNbpy (QD-2)	1:13	4.0	4.0	0.5

^a Approximate ratios determined from the absorption spectra of the conjugate assuming it to reflect the composite sum of the QD and Os(II)PP complex. ^b Calculated from eq (2). ^c Calculated from eq (4). ^d Calculated from eq (3).

2.8 Two-photon Emission Studies of QD, **2**, and QD-2

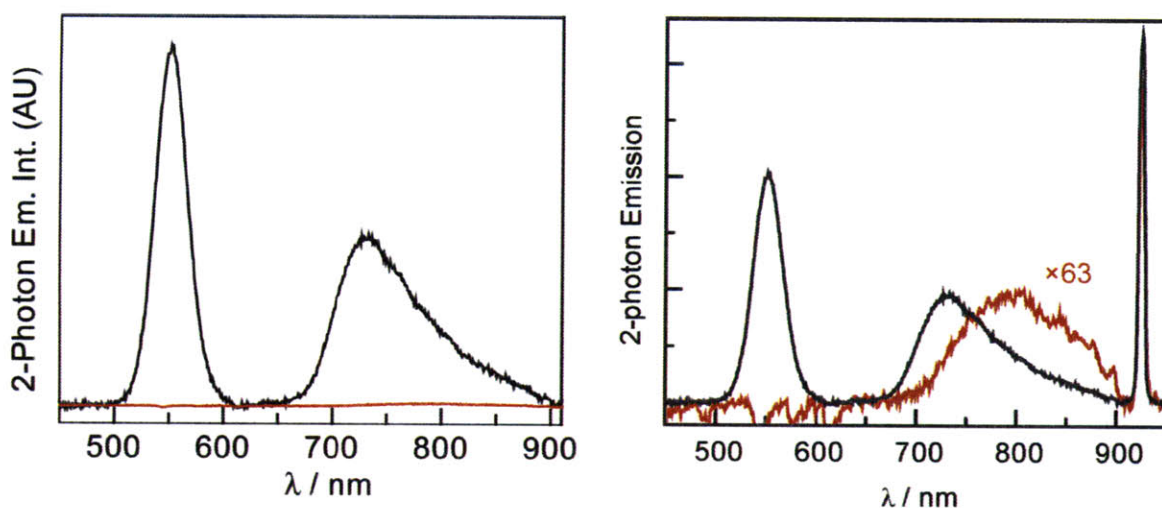


Figure 2.7. Two-photon emission of **2** (—) and the QD-2 (—) conjugate with the same Os(II)PP concentration.

The two-photon emission of the brighter **QD-2** and **2** are compared in Figure 2.7. For the purpose of this comparison the excitation wavelength must be chosen to excite **2** as well as the QD in the conjugate. A 920 nm two-photon excitation wavelength was chosen because it can excite both the QD and Os(II)PP centers within **QD-2** (at 460 nm) and scattered light at this wavelength is easily filtered from the emission of **2**. Emission from **2** was only observed when conjugated to QD, despite similar concentrations of **2** in **QD-2** and in a mixture of the complex

with QD (13 μM and 15 μM , respectively). Concentrations of more than 100 μM of **2** were required to observe any two-photon emission. Figure 2.6 depicts the quadratic power dependences found for both the emission of the QD and of **2** in the conjugate.

2.9 Oxygen Quenching of Phosphorescence

Oxygen efficiently quenches both the steady-state and time-resolved emission profiles of the Os(II)PP component of the **QD-1** and **QD-2** conjugates. Conversely, emission from the QD center of the conjugate is unaffected. The O_2 sensitivity of the complexes was initially quantified by integration of the area of the Os(II)PP emission under vacuum and under 1 atm of O_2 . **QD-1** exhibits a decrease in emission of 21% while emission from **QD-2** is slightly more attenuated (23%) (Figure 2.8).

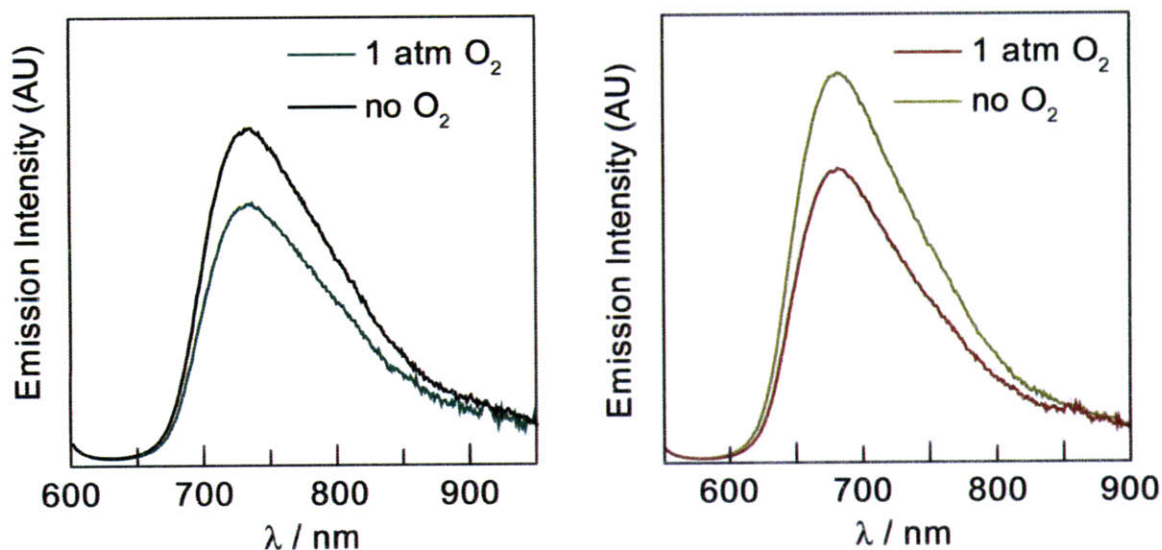


Figure 2.8. Emission profiles of QD-1 (—) and QD-2 (—) under vacuum and QD-1 (—) and QD-2 (—) under 1 atm of oxygen.

Phosphorescence lifetime decay curves of **1** and **2** were best fit to a single exponential when unconjugated to QD and to a biexponential when conjugated to QD. The long lifetime

component of the biexponential fits was used to determine the O₂ sensitivity of the conjugates. Consistent with steady-state emission quenching results, the lifetime of the Os(II)PP excited state in the **QD-1** conjugate decreases by 18% whereas the lifetime of the Os(II)PP excited state in the **QD-2** conjugate decreases by 23% upon exposure to 1 atm O₂ (Figure 2.9).

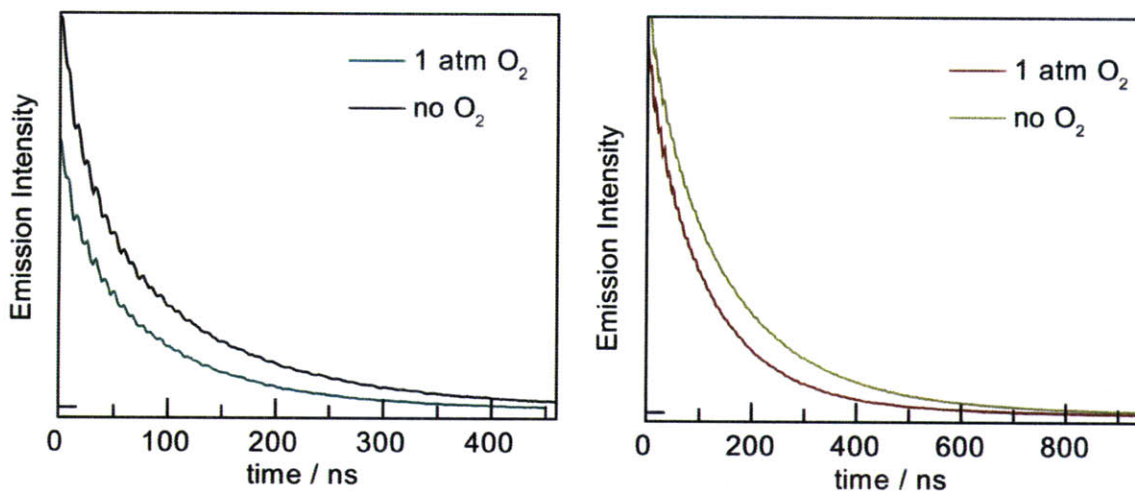


Figure 2.9. The excited state lifetime decay curves of **1** (—) and **2** (—) when conjugated to QD. The lifetimes of both **1** (—) and **2** (—) decrease upon transferring QD-1 and QD-2 from vacuum to oxygen.

Further investigation of the steady-state emission intensity attenuation of **QD-2** under multiple O₂ pressures yielded Figure 2.10. It can be seen the emission of the QD center remains unchanged, whereas that of **2** decreases with increasing O₂ pressure (left). An O₂ quenching rate constant of the conjugate is most reliably obtained from a fit of the lifetimes according to Stern-Volmer relation,

$$\frac{\tau_0}{\tau} = 1 + k_q \tau_0 [Q] \quad (1)$$

where τ_0 and τ are the lifetimes in the absence and presence, respectively, of O₂ at different pressures, k_q is the quenching constant, and pO₂ is the O₂ pressure. The Stern-Volmer fit of the lifetime data over an O₂ pressure range of 0-760 torr is linear and a quenching rate constant of

$1.8 \times 10^9 \text{ s}^{-1} \text{ M}^{-1}$ ($3000 \text{ s}^{-1} \text{ torr}^{-1}$) is obtained from the plot shown on the right.

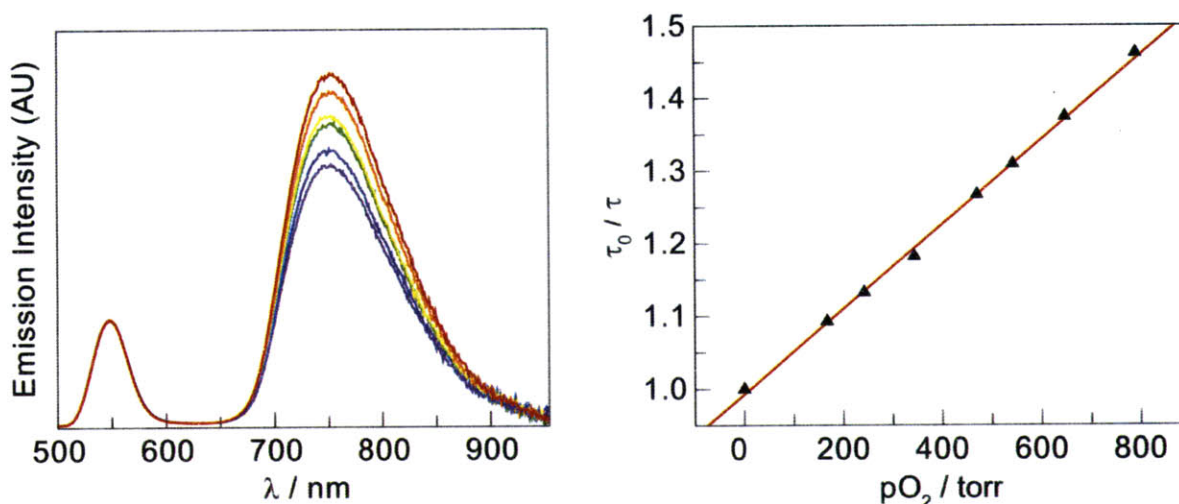


Figure 2.10. Emission from the Os(II)PP center of the QD-2 conjugate in the presence of 0 (—), 133 (—), 233 (—), 382 (—), 551 (—), and 760 (—) mmHg O₂ (left). Stern-Volmer plot of the excited state lifetime of the Os(II)PP center in the QD-2 conjugate vs. pO₂ (right). The Stern-Volmer slope yields a quenching rate constant of $1.8 \times 10^9 \text{ s}^{-1} \text{ M}^{-1}$ ($3000 \text{ s}^{-1} \text{ torr}^{-1}$).

2.10 Discussion

The extensive knowledge accrued of the photophysical properties of metal polypyridyl complexes^{15,16} provided the motivation for choosing **1** and **2** as O₂-sensing elements for a QD platform. **1** and **2** were conjugated to QDs via a carbodiimide linkage. Figure 2.1 shows the GFC traces obtained for mixtures of QD and **1** (Figure 2.1a) and QD and **2** (Figure 2.1b) in the presence (blue) and absence (red) of coupling agents. The peak centered at 14.5 min is characteristic of single QDs. Fractions containing single QDs were collected. Steady state emission spectra of the collected fractions confirm binding of **1** to the QD only when coupling agents were used. Compound **2** was present along with QD in the absence of coupling agent, indicating that **2** can non-specifically bind to the QD. Thus, the collected fractions of **QD-2** may

contain non-specifically bound **2**. However, the **QD-2** fractions consistently contained more **2** than the purified mixtures of the QD and **2**. Additionally, no appreciable loss of **2** occurred from the conjugates over a period of several days.

Compounds **1** and **2** possess absorption profiles that extend well into the red spectral region, thus leading to good spectral overlap (i.e., large J in eq 5) with the 550-nm emission band of the QDs. Moreover, the separation of the emission band of **1** and **2** from the emission profile of the QD engenders facile and accurate ratiometric sensing. Compound **2** is a superior sensor owing to the longer lifetime of the complex arising from the more rigid framework afforded by diphenylphenanthroline ligand.¹⁶ Notwithstanding, the lifetime is short enough that abbreviated wait times between measurements permits faster data collection as compared to compounds currently used to sense O₂ in biological environments.¹⁷

As revealed by the data in Table 2.1, which compiles the steady-state and time-resolved spectroscopic results of the materials used in this study, the emission of the Os(II)PP complexes blue-shifts upon conjugation to the QD. This blue-shift can be understood in the context of the physical properties of Os(II)PP excited states. MLCT excitation of metal polypyridyl complexes is associated with a marked increase in the molecular dipole owing to the intramolecular charge separation. For this reason, the emission energy and intensity are strongly dependent upon the polarity of the surrounding environment.^{18,19} High polarity environments tend to lower the energy of the thermally equilibrated excited state, thus resulting in a red-shift of the emission; conversely, lower polarity environments tend to result in a blue-shift in the emission. The shift of the emission band of the Os(II)PP centers to higher energy in the **QD-1** and **QD-2** constructs is consistent with exclusion of water from the solvation sphere of the Os(II)PP center upon conjugation to the encapsulating polymer of the QD. Attendant with the shift of the emission

band to higher energy, the lifetime of the excited state also increases as is predicted by energy gap law considerations.¹²

Emission from the Os(II)PP center is significantly increased when conjugated to the QD. The perturbation of the emission spectra of the native Os(II)PP centers conjugated to the QD can be seen in Figure 2.4b and Figure 2.4d. Little emission is observed from unconjugated Os(II)PP; consequently, sufficiently high concentrations of **1** and **2** were required for the quantification of the intensity differences of emission from Os(II)PP alone versus when conjugated to the QD. Similarly, high concentrations of QD conjugates (Figure 2.4a and c) were required for sufficient detection and accurate quantification of the FRET process. Of the two conjugates, the emission enhancement of **QD-2** was easiest to detect, as expected, since the ratio of QD to Os(II)PP and the spectral overlap between the absorption of Os(II)PP and the QD emission (overlap integral, J) is larger in **QD-2** than in **QD-1**. In fact, the quantum yield was enhanced from 1.3% to 23%, which is relatively high for room temperature phosphorescence. The shorter distance between QD and **2**, despite the larger size of **2**, is likely due to the greater hydrophobicity of **2** relative to **1**, thus allowing **2** to envelop itself in the hydrophobic interior of the polymer. This would allow for more efficient FRET at longer distances (eqs 3 and 5) as well as the exclusion of water from the solvation sphere, leading to brighter Os(II)PP emission.

The conjugate architecture confers the benefits of the two-photon absorption properties of the QD to the Os(II)PP center. Evidence for the enhanced two-photon absorption is provided in Figure 2.7. Here emission from **2** is observed in the conjugate, but not for unconjugated **2**, despite similar Os(II)PP concentrations for the two experiments. This observation is consistent with the preservation of FRET from the QD to Os(II)PP under two-photon excitation conditions. The two-photon emission of **2** when unbound only becomes visible when a concentration of 100

μM is attained, and even then, the emission was very weak. Comparison of this emission with the emission of the bound **2** shows an enhancement of more than 60 times when **2** is conjugated to the QD.

The conspicuous response of the Os(II)PP centers to O_2 is contrasted by an insensitivity of the QD emission. By examining the emission intensities from the QD and Os(II)PP centers and comparing their ratios with varying O_2 concentration, a ratiometric measurement of O_2 is obtained. Since the QD and Os(II)PP emission peaks are well separated, a third point may be taken at the baseline between the two emission bands, thus eliminating errors due to autofluorescence and other causes of baseline variation. Initially, the amount of O_2 quenching was ascertained at the extremes of 0 and 760 mm Hg of O_2 (Figure 2.8 and Figure 2.9). Stern-Volmer analysis of the oxygen quenching of emission intensity and lifetime from the Os(II)PP center of **QD-2** conjugate yields an appreciable quenching rate constant. The observed quenching rate constant of $3000 \text{ s}^{-1} \text{ torr}^{-1}$ translates to $1.8 \times 10^9 \text{ s}^{-1} \text{ M}^{-1}$. This value is commensurate with metal polypyridyl complexes bound to polymers and cyclodextrins.²⁰ The conjugation of the metal complex to the QD thus does not significantly occlude oxygen from interacting with the metal polypyridyl excited state. The Stern-Volmer analysis also shows the oxygen sensitivity of the conjugate spans the range 0-760 torr. However, oxygen pressures relevant for biological measurements range from 0-160 torr,^{21,22} where the sensor has a low dynamic range. Thus, modification of the sensor to achieve information on oxygen levels in biology requires probes with longer lived excited states. Additionally, biocompatibility may be impacted by non-specific binding interactions between the probe and biological media, perturbing the oxygen sensing properties of the sensor. Such problems are addressed by the

addition of polyethylene glycol-based ligands, which have shown significant resistance to non-specific binding in the biological milieu.^{23,24} These experiments are explored in Chapter 3.

2.11 Conclusions

In summary, a QD construct for O₂ sensing has been established based on a FRET signal transduction mechanism. The value of the QD construct comes from the differential responses of the QD and FRET dye acceptor. The QD emission remains constant with changing O₂ levels, while that of the Os(II)PP dye acceptor is quenched with increasing O₂ pressure. These differential responses provide a basis for a ratiometric O₂ sensing response. Moreover, the signal transduction and ratiometric properties are maintained under two-photon excitation. Such a sensor is attractive for highly scattering environments in biology, and is mandatory for imaging in tumors. However, the oxygen sensing range is broad. We desire a specific, low oxygen pressure sensitivity requiring new phosphors with longer excited state lifetimes. These phosphors will be discussed in following chapters.

2.12 Experimental Section

Materials. The following chemicals were use as received: ammonium hexachloroosmate (NH₄OsCl₆), 4,7-diphenyl-1,10-phenanthroline (Ph₂phen), 2,2'-bipyridine (bpy), sodium hydrogen sulfite (NaHSO₃), 4,4'-dimethyl-2,2'-bipyridine, selenium dioxide (SeO₂), 4-dimethylaminopyridine (DMAP), *tert*-butyl 6-aminohexylcarbamate, triethylamine (TEA), ammonium hexafluorophosphate (NH₄PF₆), hexafluorophosphoric acid (HPF₆, 60% in water), polyacrylic acid (PAA), *n*-octylamine, N-hydroxysuccinimide (NHS), 3-sulfo-N-hydroxysuccinimide (S-NHS), anhydrous N,N-dimethylformamide (DMF, 99%), tetramethylammonium hydroxide, and

rhodamine 6G from Sigma-Aldrich; selenium, silver nitrate (AgNO_3), diethylzinc, tri-n-octylphosphine (TOP, 97%), and dimethylcadmium from Strem; 1-ethyl-3-(3-dimethylamino-propyl) carbodiimide hydrochloride ($\text{EDC}\cdot\text{HCl}$), hexamethyldisilathiane (Fluka); 1-hydroxy-benzotriazole (HOBt) (NovaBiochem); magnesium sulfate (MgSO_4) (EMD); trifluoroacetic acid (TFA, 99.9%) (J. T. Baker); and hexylphosphonic acid (HPA) (Alfa Aesar). Tri-n-octylphosphine oxide (TOPO) and hexadecylamine were distilled from 90% reagent grade materials (Sigma-Aldrich). 4'-methyl-2,2'-bipyridine-4-carboxylic acid (Cbpy),²⁵ *bis*(4,7-diphenyl-1,10-phenanthroline)osmium(II) chloride [$\text{Os}(\text{Ph}_2\text{phen})_2$] Cl_2 and *bis*(2,2'-bipyridine)-osmium(II) chloride [$\text{Os}(\text{bpy})_2$] Cl_2 ,²⁶ *tris*(2,2'-bipyridine)-ruthenium(II), *tris*(2,2'-bipyridine)-osmium(II), *bis*(2,2'-bipyridine)(4'-methyl-2,2'-bipyridine-4-carboxylic acid)-osmium(II) *bis*(hexafluorophosphate) [$\text{Os}(\text{bpy})_2\text{Cbpy}](\text{PF}_6)_2$ and *bis*(4,7-diphenyl-1,10-phenanthroline)(4'-methyl-2,2'-bipyridine-4-carboxylic acid)osmium(II) *bis*(hexafluorophosphate) [$\text{Os}(\text{Ph}_2\text{phen})_2\text{Cbpy}](\text{PF}_6)_2$ ²⁷ were prepared as previously described.

***Tert*-butyl-6-(4'-methyl-2,2'-bipyridine-4-carboxamido)hexylcarbamate (Nbpy-BOC).**

Cbpy (0.5051 g, 2.350 mmol, 1 eq.), $\text{EDC}\cdot\text{HCl}$ (0.9049 g, 4.720 mmol, 2 eq.), HOBt (0.6332 g, 4.686 mmol, 2 eq.), DMAP (0.0583 g, 0.4772 mmol, <1 eq.) and N-BOC-1,6-diaminohexane (1.1952 g, 5.5250 mmol, 2.3510 eq.) were combined in a solution of 0.1 mL of TEA in methylene chloride (150 mL) followed by stirring under N_2 overnight. The solution was then washed with water (4×100 mL), dried over MgSO_4 , and the solvent was removed by rotary evaporation. The solid was dissolved in a few mL of ethyl acetate, loaded onto a Chromatotron plate (alumina, 2 mm), and eluted with ethyl acetate. The first band to elute was collected and the solvent removed *in vacuo* yielding 0.4986 g of the white ligand (51.43%). ^1H NMR (300 MHz, CD_3OD , 25 °C) δ = 1.42, (s, 9H, *t*Bu), 1.47, (m, 6H, $-\text{CH}_2-$), 1.67 (m, 2H, $-\text{CH}_2-$), 2.41 (s, 3H,

bpy-CH₃), 3.04 (t, 2H, amide-CH₂-), 3.42 (t, 2H, amide-CH₂-), 7.32 (d, 1H, bpy-H), 7.76 (d, 1H, bpy-H), 8.22 (s, 1H, bpy-H), 8.54 (d, 1H, bpy-H), 8.66 (m, 1H, bpy-H), 8.80 (d, 1H, bpy-H).

Bis(2,2'-bipyridine)(N-(6-aminohexyl)-4'-methyl-2,2'-bipyridine-4-carboxamide)-osmium(II) bis(hexafluorophosphate) [Os^{II}(bpy)₂(Nbpy)](PF₆)₂ (1). **1** was prepared using synthetic methods similar to those employed for the preparation of [Os^{II}(bpy)₂Cbpy](PF₆)₂.²⁷ Os^{II}(bpy)₂Cl₂ (0.1430 g, 0.2493 mmol, 1.000 eq.) and Cbpy (0.1199 g, 0.2496 mmol, 1.001 eq.) were combined in degassed ethylene glycol and heated at 90 °C under N₂ for 24 h. The solution was cooled to room temperature and a saturated aqueous solution of ammonium hexafluorophosphate (20 mL) was added to cause a dark solid to precipitate. The solid was isolated by filtration, washed with water, ether, and dried under vacuum overnight. The crude product was purified by column chromatography (neutral alumina) with 1:1 toluene:acetonitrile eluent. The *tert*-butylcarbamate (BOC) protecting group was removed by stirring the complex in 1:1 methylene chloride:trifluoroacetic acid (CH₂Cl₂:TFA, 10 mL) for 1 h, followed by removal of the solvent *in vacuo*. The product was dissolved in acetone (20 mL), precipitated upon addition of ether (100 mL), isolated by filtration, and dried under vacuum yielding a black-green solid (0.1328 g, 65.29). ¹H NMR (300 MHz, CD₃CN, 25 °C) δ = 1.36 (m, 6H, -CH₂-), 1.61 (m, 4H, -CH₂-), 2.61 (s, 3H, bpy-CH₃), 3.36 (m, 2H, amide-CH₂-), 7.16 (d, 1H, bpy-H), 7.29 (m, 4H, bpy-H), 7.42 (d, 1H, bpy-H), 7.63 (m, 4H, bpy-H), 7.71 (m, 2H, bpy-H), 7.84 (m, 4H, bpy-H), 8.48 (s, 4H, bpy-H), 8.68 (s, 1H, bpy-H), 8.99 (t, 1H, amide-H), 9.21 (s, 1H, bpy-H). MALDI-TOF Calcd. (Found): [M – 2PF₆]²⁺ 816.29 (816.15); M – BOC – PF₆⁺ 1061.31 (1061.28); [M – BOC – 2PF₆]²⁺ 916.35 (916.35).

Bis(4,7-diphenyl-1,10-phenanthroline)(N-(6-aminohexyl)-4'-methyl-2,2'-bipyridine-4-carboxamide)osmium(II) bis(hexafluorophosphate) [Os^{II}(Ph₂phen)₂(Nbpy)](PF₆)₂ (2).

Os(Ph₂phen)₂Cl₂ (0.1111 g, 0.1198 mmol, 1.000 eq.) and Cbpy (0.1158 g, 0.2410 mmol, 2.011 eq.) were combined in degassed ethylene glycol and heated at 90 °C under N₂ for 24 h. The solution was cooled to room temperature and a saturated aqueous solution of ammonium hexafluorophosphate (20 mL) was added to precipitate a dark solid. The solid was isolated by filtration, washed with water, ether, and dried under vacuum overnight. The crude product was purified by column chromatography (neutral alumina) with 1:1 toluene:acetonitrile eluent. The *tert*-butylcarbamate (BOC) protecting group was removed by stirring the complex in 1:1 methylene chloride (CH₂Cl₂:TFA, 10 mL) for 1 h, followed by removal of the solvent *in vacuo*. The product was dissolved in acetone (20 mL), precipitated upon addition of ether (100 mL), isolated by filtration, and dried under vacuum as above to yield a black-brown solid (0.0376 g, 26.9%). ¹H NMR (300 MHz, CD₃CN, 25 °C) δ = 1.36 (m, 6H, -CH₂-), 1.61 (m, 4H, -CH₂-), 2.65 (s, 3H, bpy-CH₃), 3.39 (m, 2H, amide-CH₂-), 7.14 (d, 1H, bpy-H), 7.49 (d, 2H, ligand-H), 7.62 (m, 20H, phenyl-H), 7.68 (m, 4H, ligand-H), 7.87 (d, 1H, ligand-H), 8.00 (m, 2H, ligand-H), 8.18 (m, 6H, ligand-H), 8.74 (s, 1H, bpy-H), 8.95 (t, 1H, amide-H), 9.26 (s, 1H, bpy-H). MALDI-TOF Calcd. (Found): [M – 2PF₆]²⁺ 1168.42 (1168.24); [M – BOC – PF₆]⁺ 1413.43 (1413.15); [M – BOC – 2PF₆]²⁺ 1268.47 (1268.16).

N-octylamine modified polyacrylic acid (PAA-OA). PAA (0.4949 g, 1800 MW, 1.0 eq.) was functionalized with 40% *n*-octylamine groups by adopting a previously reported method.²⁸ Briefly, the acid, NHS (0.0553 g, 0.4804 mmol, 0.1723 eq.), and EDC (0.5436 g, 2.836 mmol, 1.017 eq.) were combined in DMF (3 mL) under N₂ for 1 h, followed by addition of *n*-octylamine (0.6 mL, 3.6 mmol, 1.3 eq.) and left stirring overnight. After the DMF was removed *in vacuo*, water (5 mL) was used to precipitate the polymer and tetramethylammonium hydroxide (0.7491 g, 4.135 mmol, 1.483 eq.) was added to re-dissolve the solid, overnight. After washing

the solution with ethyl acetate (3 × 20 mL), the polymer was precipitated with concentrated hydrochloric acid (HCl, 0.34 mL, 4.1 mmol, 1.5 eq.), washed with water (2 × 3 mL), and dried *in vacuo*. Water (5 mL) and a sodium hydroxide solution (1.5 mL, 3 M) were added to the solid. Filtration and drying *in vacuo* yielded a somewhat sticky white solid (0.1848 g, 22.97%).

Tri-octylphosphineoxide-capped nanocrystals (TOPO-QDs). ($\text{Cd}_x\text{Zn}_{1-x}\text{Se}$) $\text{Cd}_y\text{Zn}_{1-y}\text{S}$ core-shell nanocrystals (**TOPO-QD**) were prepared as previously reported.²⁹ Briefly, ZnSe QDs were prepared by rapidly injecting diethylzinc (0.7 mmol) and tri-n-octylphosphine selenide (TOPSe, 1 mmol) dispersed in tri-n-octylphosphine (TOP, 5 mL) into a round bottom flask containing degassed hexadecylamine (7 g) at 310 °C. The solution was immediately cooled to 270 °C and QD growth was allowed to proceed for 2 h to furnish a solution of ZnSe QDs ($\lambda_{1\text{stAbs}} = 350$ nm). Aliquots of 1/3 of the above ZnSe QD lot were further modified by slowly adding a solution of dimethylcadmium (0.5 mmol) and TOPSe (1.2 mmol) in TOP (1.2 mL) to the ZnSe QDs in a solvent of TOPO (16 g) and hexylphosphonic acid (HPA, 4 mmol) under N_2 at 160 °C. After stirring for 48 h, $\text{Cd}_x\text{Zn}_{1-x}\text{Se}$ core shell QDs ($\lambda_{1\text{st abs}} = 473$ nm, $\lambda_{\text{PLmax}} = 513$ nm, FWHM = 40 nm) were obtained. The QDs were isolated by precipitation twice with methanol. A $\text{Cd}_y\text{Zn}_{1-y}\text{S}$ shell was grown by redissolving the QDs in TOPO (10 g) and HPA (2.4 mmol) and introducing a solution of dimethylcadmium, diethylzinc, and hexamethyldisilathiane (2 eq. vs. total moles metal added) in TOP (8 mL) drop wise at 150 °C. The QDs were annealed overnight (80 °C) to furnish **TOPO-QDs** ($\lambda_{\text{PLmax}} = 548$ nm, FWHM = 36 nm).

Water-soluble nanocrystals (QDs). The **TOPO-QDs** (10 mg) were isolated by repeated precipitation from hexanes with methanol and re-dissolved in a minimal amount of CHCl_3 . **PAA-OA** (50 mg) was dissolved in CHCl_3 (5 mL), added drop wise to the QD solution, and left

stirring overnight. After removing the CHCl_3 by vacuum, sodium bicarbonate buffer (pH \sim 8.5, 2 mL) was added to redissolve the QDs. The solution was then centrifuged (3900 rpm \times 5 min), decanted, and dialyzed (with 50 kDa MW cutoff spin concentrators, Millipore) to furnish aqueous QDs ($\lambda_{\text{PLmax}} = 549$ nm, FWHM = 27 nm, $\Phi = 40\%$).

QD-1 and QD-2 conjugates. Two methods were employed in the synthesis of the conjugates. In the first method, a solution of QD (1.60×10^{-4} M, 1 mL) was combined with 2-(N-morpholino)ethanesulfonic acid (MES) buffer (1 mL). The acid groups on QD were converted to esters of NHS through addition of an EDC/NHS solution (0.5 mM in each, 1 mL) (10 min). The precipitate was isolated by centrifugation and dried under vacuum. The QD precipitates were dissolved in sodium bicarbonate buffer (1.5 mL) and solutions of either **1** (4.365 mM, 0.200 mL, 0.873 mmol) or **2** (1.712 mM, 0.400 mL, 0.685 mmol) in DMF (0.1 mg of each) were added. The solutions were left stirring overnight, dialyzed into pH 7 buffer (phosphate), and centrifuged to settle out any undissolved material. The second method used differed from the first in that a solution of QD (1.60×10^{-4} M, 100 μL) was combined an EDC/S-NHS solution (0.5 mM in each, 100 μL , PBS buffer) forming some precipitate. Typically, addition of the Os(II)PP complexes in aqueous solutions of millimolar concentrations followed by TEA (50 μL) yielded optically clear solutions. The solutions were left stirring for 90 minutes and then dialyzed into pH 8.3 buffer (NaHCO_3) and further isolated by gel filtration chromatography.

Physical measurements. ^1H NMR spectra were recorded on a Varian Mercury 300 MHz NMR at the MIT Department of Chemistry Instrumentation Facility (DCIF) and externally referenced to tetramethylsilane. MALDI-TOF mass spectrometry was performed on a Bruker Omiflex instrument in the DCIF using dithranol as the matrix. The instrument was calibrated

with a quadratic polynomial using a mixture of bradykinin fragment 1-7 (757.3997), angiotensin II (1046.5423), and P14R synthetic peptide (1533.8582) (Sigma) with dithranol as the matrix.

Gel filtration chromatography (GFC) was performed on an Akta Prime system (GE) with a Superose 6 crosslinked dextran column. The hydrodynamic radii of QDs and conjugates were estimated by comparing the elution volumes to those of protein molecular weight standards (Bio-Rad). The eluent from the column was detected with the UV absorbance at 280 nm and the fluorescence spectrum was recorded. One mL fractions were collected from a volume of 5 - 25 mL. Fractions were combined based on the GFC traces and further characterized.

UV-vis absorption spectra were recorded on a Spectral Instruments (SI) CCD array UV-vis spectrophotometer, a Cary 5000, or an HP 8453 diode array spectrophotometer. Steady-state emission spectra were recorded on an automated Photon Technology International (PTI) QM 4 fluorometer equipped with a 150-W Xe arc lamp and a Hamamatsu R2658 photomultiplier tube. Time resolved emission measurements for the QDs were made with a chirped-pulse amplified Ti:sapphire laser system using the frequency doubled (400 nm) pump light provided by a Ti:sapphire laser system (100 fs pulsewidth). The detector was a Hamamatsu C4334 Streak Scope streak camera that is previously described.³⁰ Time resolved emission measurements of the osmium complexes were made with pump light provided by the third harmonic (355 nm) of a Quanta-Ray Nd:YAG laser (Spectra-Physics) running at 10 Hz. The pump light was passed through a BBO crystal and split into a visible frequency and an infrared frequency. Lifetime measurements employed both the pump and visible beams to excite samples. The infrared light was used as the excitation source for two-photon measurements. The beam was focused onto the sample using a 100 mm focal length lens. A 900 nm short-pass filter was placed between the sample and a mounted 600 μ m fiber-optic cable with a collimating lens. The other end of the

cable was attached to an Ocean Optics QE65000 Spectrometer from which spectra were recorded. Power measurements were made by picking off 20% of the incident laser beam.

Relative quantum yields of samples, Φ_{sam} , were calculated using $[\text{Ru}^{\text{II}}(\text{bpy})_3](\text{PF}_6)_2$, $[\text{Os}^{\text{II}}(\text{bpy})_3](\text{PF}_6)_2$ or rhodamine 6G (R6G) in water as the reference according to:

$$\Phi_{sam} = \Phi_{ref} \left(\frac{A_{ref}}{A_{sam}} \right) \left(\frac{I_{sam}}{I_{ref}} \right) \left(\frac{\eta_{sam}}{\eta_{ref}} \right)^2 \quad (2)$$

A is the measured absorbance, η is the refractive index of the solvent, I is the integrated emission intensity, and Φ_{ref} is the emission quantum yield of the reference. Φ_{ref} was taken to be 0.053 for $\text{Ru}(\text{bpy})_3^{2+}$ and 0.90 for R6G in water.^{31,32} Using $\text{Ru}(\text{bpy})_3^{2+}$ as the emission standard, Φ was determined to be 0.031 for $\text{Os}(\text{bpy})_3^{2+}$ in water and used as an additional reference. Samples for phosphorescence quantum yield and time resolved spectroscopic measurements were freeze-pump-thaw degassed for 3 cycles to 10^{-6} torr. Unless otherwise noted, all spectroscopy was performed in reagent grade deionized water.

Energy transfer analysis. The efficiency of energy transfer from the NC to the osmium complex was evaluated using Förster analysis:

$$E = \frac{mk_{D-A}}{mk_{D-A} + \tau_D^{-1}} = \frac{mR_0^6}{mR_0^6 + r^6} \quad (3)$$

where k_{D-A} is the rate of energy transfer, r is the distance between the donor and acceptor, R_0 is the critical transfer distance or the distance at which half of the donor molecules decay by energy transfer, and m is the number of acceptor molecules per donor. Experimentally, E can be obtained as:

$$E = 1 - \frac{\tau_{D-A}}{\tau_D} \quad (4)$$

where τ_D is the lifetime of the NC donor alone and τ_{D-A} is the lifetime of the bound donor (**QD-1** or **QD-2**).

While E may be experimentally determined from the excited state lifetime quenching, additional information is needed to quantify R_0 , r , and m :

$$R_0 = \frac{9000 \ln 10 \kappa^2 \Phi_D J}{128 \pi^5 n^4 N} \quad (5)$$

$$J = \int_0^\infty dv \frac{f_D(v) e_A(v)}{v^4} \quad (6)$$

where κ^2 is the relative orientation factor of the dipoles, taken to be $2/3$, Φ_D is the quantum efficiency of the donor, N is Avogadro's number, and n is the index of refraction of the medium, which is taken to be 1.4 in aqueous solution. The constants may be incorporated into one value, which is simply multiplied by Φ_D . Similarly, the latter half of the equation may be represented as J , the overlap integral, where $F_D(\lambda)$ is the normalized intensity of the donor and $\epsilon_A(\lambda)$ is the extinction coefficient of the acceptor at λ .^{33,34} R_0 may thus be calculated for the overlap of the experimentally determined spectra.

The average number of osmium complexes attached to the donor, m , can be determined from the optical cross-sections of the donor and acceptor as well as the absorption spectra of the conjugated **QD-1** and **QD-2** systems. The absorption spectra of the conjugates may be taken as a sum of the absorption of the donor and acceptor. The donor:acceptor ratio and the concentrations of the conjugates may be calculated using the individual donor and acceptor absorption spectra, their known ϵ values, and Beer's law.

2.13 References

1. Briñas, R.P.; Troxler, T.; Hochstrasser, R.M.; Vinogradov, S.A. *J. Am. Chem. Soc.* **2005**, *127*, 11851-11862
2. Finikova, O.S.; Troxler, T.; Senes, A.; DeGrado, W.F.; Hochstrasser, R.M.; Vinogradov, S.A. *J. Phys. Chem. A* **2007**, *111*, 6977-6990.
3. Wu, C.; Bull, B.; Christensen, K.; McNeill, J. *Angew. Chem. Int. Ed.* **2009**, *121*, 2779-2783.
4. Xu, H.; Aylott, J.W.; Kopelman, R.; Miller, T.J.; Philbert, M.A. *Anal. Chem.* **2001**, *73*, 4124-4133.
5. Koo, Y.L.; Cao, Y.; Kopelman, R.; Koo, S.M.; Brasuel, M.; Philbert, M.A. *Anal. Chem.* **2004**, *76*, 2498-2505.
6. Finikova, O.S.; Chen, P.; Ou, Z.; Kadish, K.M.; Vinogradov, S.A. *J. Photochem. Photobiol. A: Chem.* **2008**, *198*, 75-84.
7. Coe, B. J. *Acc. Chem. Res.* **2006**, *39*, 383-393.
8. Lemerrier, G.; Bonne, A.; Four, M.; Lawson-Daku, L. M. *Compt. Rend. Chimie* **2008**, *11*, 709-715.
9. Walker, G. W.; Sundar, V. C.; Rudzinski, C. M.; Bawendi, M. G.; Nocera, D. G. *Appl. Phys. Lett.* **2003**, *83*, 3555-3557.
10. Vanderkooi, J. M.; Maniara, G.; Green, T. J.; Wilson, D. F. *J. Biol. Chem.* **1987**, *262*, 5476-5482.
11. Buckingham, D. A.; Dwyer, F. P.; Goodwin, H. A.; Sargeson, A. M. *Aust. J. Chem.* **1964**, *17*, 325-336.

12. Kober, E. M.; Caspar, J. V.; Lumpkin, R. S.; Meyer, T. J. *J. Phys. Chem.* **1986**, *90*, 3722-3734.
13. Fisher, B. R.; Eisler, H.-J.; Stott, N. E.; Bawendi, M. G. *J. Phys. Chem. B* **2004**, *108*, 143-148.
14. Clarke, Y.; Xu, W.; Demas, J. N.; DeGraff, B. A. *Anal. Chem.* **2000**, *72*, 3468-3475.
15. Kober, E. M.; Sullivan, B. P.; Dressick, W. J.; Caspar, J. V.; Meyer, T. J. *J. Am. Chem. Soc.* **1980**, *102*, 7383-7385.
16. Kalyansundaram, K. *Photochemistry of Polypyridine and Porphyrin Complexes*. Academic Press: San Diego, CA, 1992.
17. Dunphy, I.; Vinogradov, S. A.; Wilson, D. F. *Anal. Biochem.* **2002**, *310*, 191-198.
18. Caspar, J. V.; Meyer, T. J. *J. Am. Chem. Soc.* **1983**, *105*, 5583-5590.
19. Hauenstein, B. L. Jr.; Dressick, W. J.; Buell, S. L.; Demas, J. N.; DeGraff, B. A. *J. Am. Chem. Soc.* **1983**, *105*, 4251-4255.
20. Sacksteder, L.; Lee, M.; Demas, J.N.; DeGraff, B.A. *J. Am. Chem. Soc.* **1993**, *115*, 8230-8238.
21. Finikova, O.S.; Lebedev, A.Y.; Aprelev, A.; Troxler, T.; Gao, F.; Garnacho, C.; Muro, S.; Hochstrasser, R.M.; Vinogradov, S.A. *Chem. Phys. Chem.* **2008**, *9*, 1673-1679.
22. Helmlinger, G.; Yuan, F.; Dellian, M.; Jain, R. K. *Nat. Med.* **1997**, *3*, 177-182.
23. Liu, W.; Howarth, M.; Greytak, A. B.; Nocera, D. G.; Ting, A. Y.; Bawendi, M. B. *J. Am. Chem. Soc.* **2008**, *130*, 1274-1284.
24. Bentzen, E.L.; Tomlinson, I.D.; Mason, J.; Gresch, P.; Warnement, M.R.; Wright, D.; Sanders-Bush, E.; Blakely, R.; Rosenthal, S.L. *Bioconjugate Chem.* **2005**, *16*, 1488-1494.

25. McCafferty, D. G.; Bishop, B. M.; Wall, C. G.; Hughes, S. G.; Mecklenberg, S. L.; Meyer, T. J.; Erickson, B. W. *Tetrahedron* **1995**, *51*, 1093-1106.
26. Kober, E. M.; Caspar, J. V.; Sullivan, B. P.; Meyer, T. J. *Inorg. Chem.* **1988**, *27*, 4587-4598.
27. Dupray, L. M.; Meyer, T. J. *Inorg. Chem.* **1996**, *35*, 6299-6307.
28. Wu, X. Y.; Liu, H. J.; Liu, J. Q.; Haley, K. N.; Treadway, J. A.; Larson, J. P.; Ge, N. F.; Peale, F.; Bruchez, M. P. *Nat. Biotech.* **2003**, *21*, 41-46.
29. Ivanov, S. A.; Nanda, J.; Piryatinski, A. Achermann, M.; Balet, L. P.; Bezel, I. V.; Anikeeva, P. O.; Tretiak, S. Klimov, V. I. *J. Phys. Chem. B* **2004**, *108*, 10625-10630.
30. Damrauer, N. H.; Hodgkiss, J. M.; Rosenthal, J.; Nocera, D. G. *J. Phys. Chem. B* **2004**, *108*, 6315-6321.
31. Henderson, L. J. Jr.; Cherry, W. R. *J. Photochem.* **1985**, *28*, 143-151.
32. Magde, D.; Wong, R.; Seybold, P. G. *Photochem. Photobiol.* **2002**, *75*, 327-334.
33. Förster, T. *Ann. Phys.* **1948**, *2*, 55-75.
34. Lakowicz, J. R., *Principles of Fluorescence Spectroscopy*, 3rd ed.; Springer: New York, 2006.

Pd(II) *meso*-Tetra(4-carboxyphenyl) Porphyrin O₂ Sensors

3.1 Motivation

QD-Osmium polypyridine-based sensors provide a good proof of concept for QD enhancement of single molecule two-photon emission/absorption. However, the sensor is good for only high pressures of oxygen, and not the low levels present in biology (0-160 torr).¹ The sensitivity of the phosphor to oxygen is directly related to the lifetime of the via the Stern-Volmer equation described in Chapter 1. Generally, larger values of τ_0 allow for greater sensitivity to low oxygen pressures. Using a phosphor with a longer excited state lifetime should aid in obtaining a more sensitive oxygen response, which is required for dynamic measurements in biological environments.

3.2 Background

Current optical oxygen sensors range from polymers to metalloporphyrins to polypyridines.² Pd metalloporphyrins have been actively pursued due to their long lifetimes ($\tau_0 \sim 700 \mu\text{s}$).³ Pd-*meso*-tetra(4-carboxyphenyl) porphyrin (PdTCPP or R_0) has attracted particular interest due to its solubility in aqueous solutions, enabling its use in biological applications.⁴ However, as with the polypyridines, the two-photon absorptions of these phosphors are prohibitively low, in this case 1-6 GMs.⁵ Attachment of QDs to small molecule phosphors was shown to increase the two-photon emission by more than 60-fold in Chapter 2. Extension of this to the longer lifetime, brighter, R_0 would provide a bright sensor with oxygen sensitivity in the biological range.

QD sensor biocompatibility is enhanced with, smaller, and less charged QD scaffolds.⁶ These QD scaffolds are ligated by dithiol ligands appended with a PEG unit for added stability and water solubility. Well-developed syntheses of these ligands allow a variety of functionalities, including amines and carboxylic acids, to be employed at the ligand terminus. This allows

phosphors with carboxylic acid functionalities to be coupled to the QDs, whereas with the polymer encapsulated QDs provided only a carboxylic acid surface, requiring a phosphor with amine functionality. The dithiol ligands are exchanged with the native TOPO-based QD coordinating ligands, yielding smaller QDs, which have also been shown to extravasate in tumors. Extravasation of the QDs from the tumor vasculature allows imaging of the tumor interstitium. This chapter reports the conjugation of Pd metalloporphyrins to these new dithiol PEG scaffolds on QD surfaces.

3.3 Results and Discussion

3.4 R₀ as an Oxygen Sensor

The A₄ porphyrin, R₀, shown in Figure 3.1 has been used as an oxygen sensor in several cases due to its favorable photophysical properties (long lifetime, decent phosphorescence quantum yield). This A₄ porphyrin is characterized by its four carboxylic acid functionalities, terminating the phenyl units. These acid groups present a functional handle for attachment of the porphyrin to QDs. The incorporation of palladium(II) into the porphyrin center generates a very stable phosphor. The absorption spectrum of the porphyrin is shown in Figure 3.2. Metallation increases the symmetry of the porphyrin leading to a single Q-band, with a small shoulder. This absorption profile allows us to study the energy transfer within the QD-R₀ system by tuning the QD emission, thus varying the amount of overlap (J in eq 6) between the porphyrin absorption and QD emission bands. The excited state of the porphyrin is characterized by a long excited state lifetime (450 μ s)⁷ and a red emission, which is well-suited for biological applications due to the window of minimal absorption described in Chapter 1.

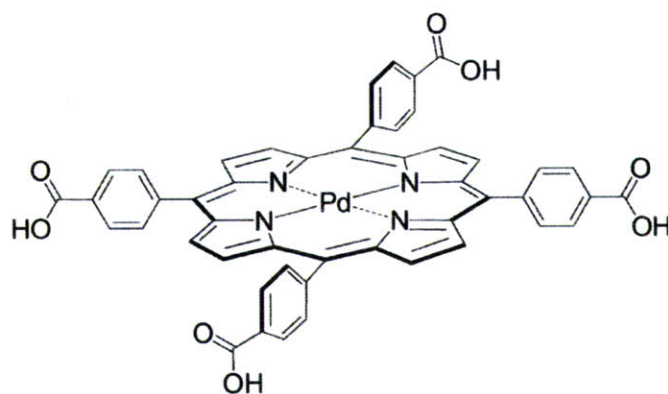


Figure 3.1. Pd meso-tetra(4-carboxyphenyl) porphyrin.

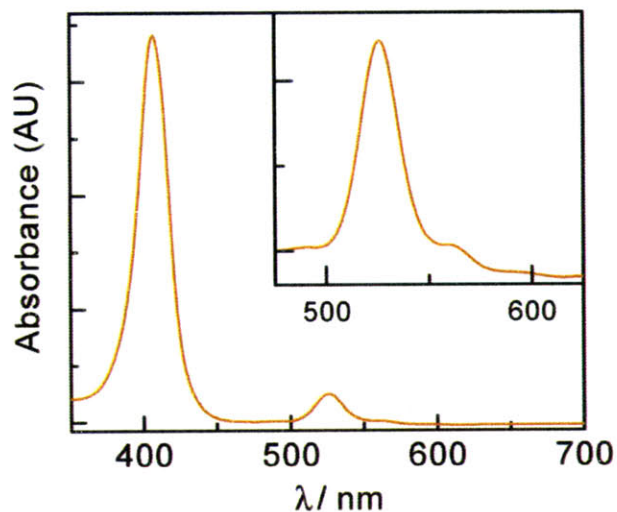


Figure 3.2. Absorption spectrum of R_0 . The incorporation of the Pd metal leads to a single Q-band with a small shoulder.

The long excited state lifetime of R_0 engenders oxygen sensitivity at low pressures (pO_2). Detailed procedures for oxygen measurements can be found in the experimental section. Briefly, oxygen pressures were varied by displacement of oxygen with argon gas while monitoring the pO_2 using an Ocean Optics fiber optic oxygen sensor. Figure 3.3 shows the excited state oxygen dependence using both steady-state and time resolved spectroscopic methods. It is immediately

apparent from the large decrease in intensity of the steady-state emission (Figure 3.3, left) between 0% oxygen and 6% oxygen (~46 torr) that the porphyrin is well suited to measuring very low oxygen pressures. Characterization of the porphyrin excited state decay with respect to oxygen is shown on the right side of Figure 3.3. Oxygen measurements were limited to pressures below about 200 torr to focus on the biologically relevant pressure range.

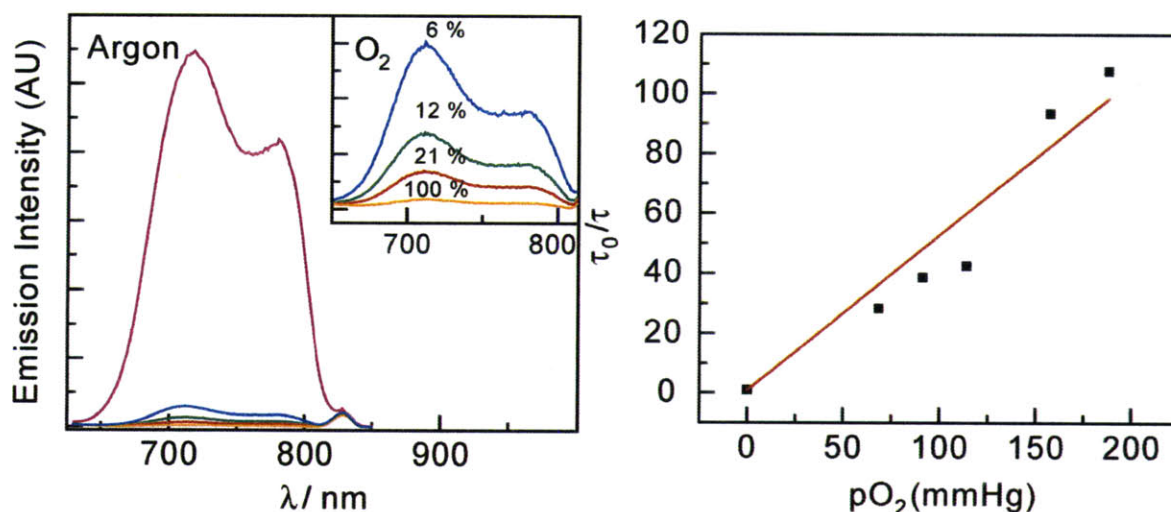
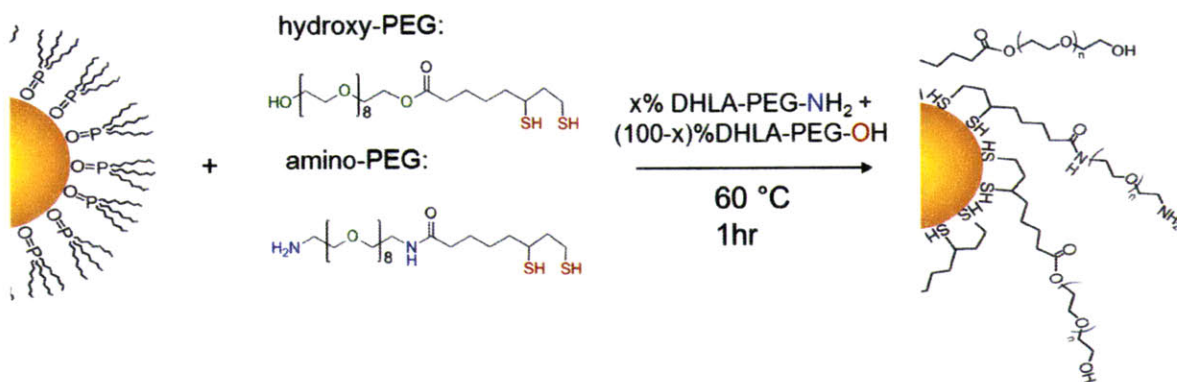


Figure 3.3. R_0 Steady-state emission with varying oxygen levels (left). R_0 Stern-Volmer plot using time-resolved emission lifetimes (right). A k_q value of $380 \text{ torr}^{-1} \text{ s}^{-1}$ was calculated. Samples were bubbled with argon gas and the oxygen levels (%) were monitored using an Ocean Optics fiber optic oxygen sensor.

3.5 Synthesis of QD- R_0 Sensors

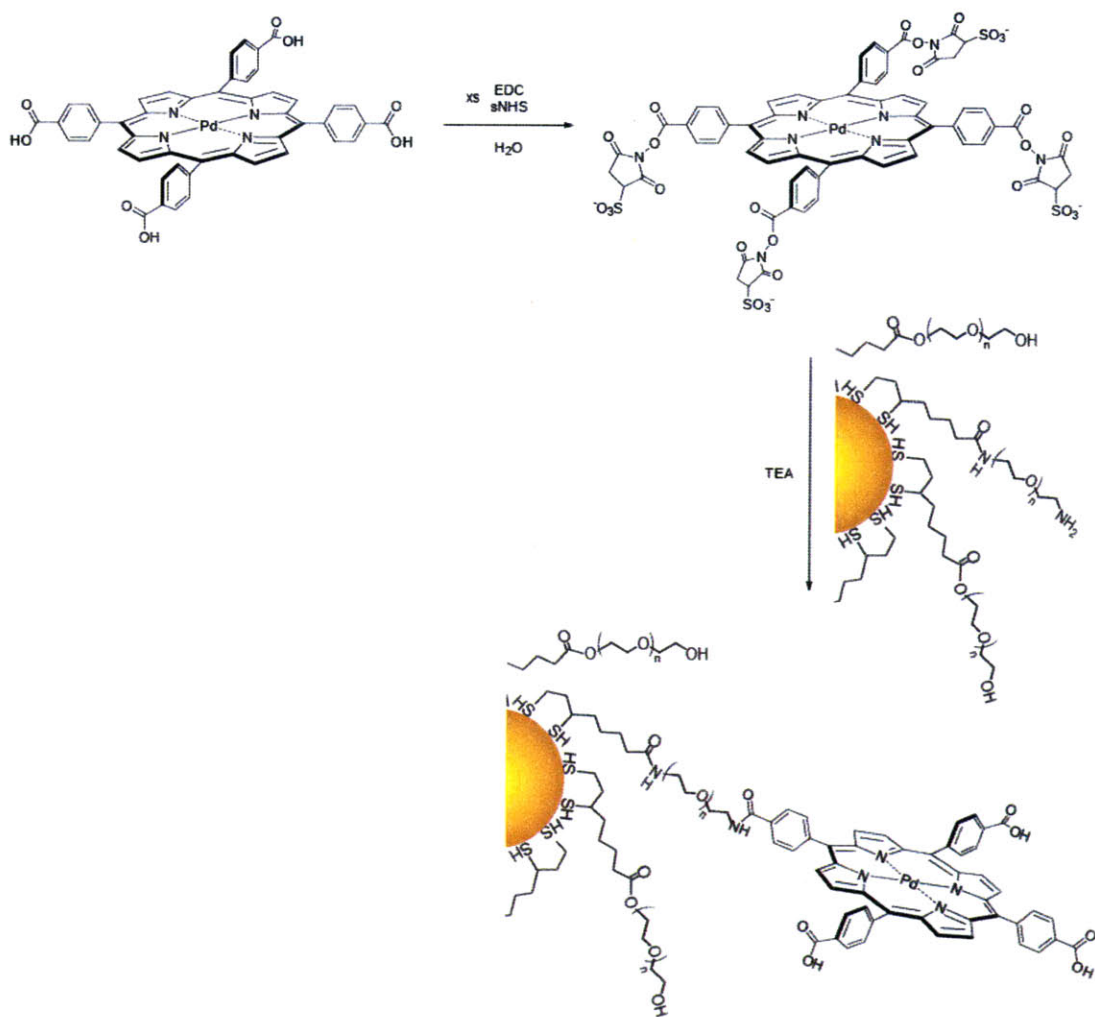
Established methods of QD water solubilization and amide bond formation were used to generate R_0 -QD oxygen sensors.⁶ Briefly, the dithiol-based PEG ligands were synthesized by coupling amine-functionalized PEG with thioctic acid followed by reduction to the dihydrolipoic acid-based ligand.⁶ Scheme 3.1 depicts the water solubilization of TOPO capped QDs through exchange of the native organic ligands with hydroxy-PEG or a mixture amino-PEG and hydroxy-PEG in organic solvent with gentle heating. Although QDs with a higher percentage of amine

ligands present more sites for coupling to the acid-functionalized porphyrin, the surface charge from the amines was found by Liu *et. al.* to cause non-specific binding *in-vivo*. Limiting the percentage of amines to 20% was found to be sufficient for prevention of these undesired binding interactions.



Scheme 3.1. Cap exchange of TOPO-QDs with hydroxy and amine terminated PEG dithiol ligands yielding water soluble dots. The percent of amino-PEG used may be varied to allow more sites for coupling of phosphors.

Attachment of R₀ to the DHLA-PEG QDs through carbodiimide coupling generated oxygen sensitive QDs. Scheme 3.2 shows the synthesis of these oxygen sensitive QDs. Briefly, R₀ is activated with sulfo-NHS, generating a more reactive ester, followed by amide bond formation with 50% amino-PEG QDs. Use of larger amounts of porphyrin yielded aggregated samples, likely due to the multiple carboxylic acid groups present on the porphyrin, presenting a means for cross-linking between the QDs and porphyrins. Upon decreasing the equivalents of porphyrin:QD and reducing the percentage of amino-PEG ligand to 20%, samples with significantly less aggregation were produced. Samples purified by GFC were isolated initially as unaggregated QDs that were bound to R₀.



Scheme 3.2. Coupling of R_0 to the amino-PEG ligands on the QDs yields phosphorescent QDs.

3.6 Purification of R_0 -QD Sensors

Though initially unaggregated, GFC showed that aggregation of the QD- R_0 samples did occur over time leading to eventual sensor precipitation. Figure 3.4 shows a GFC trace of QDs water-solubilized with 50% hydroxy-PEG and 50% amino-PEG DHLA-based ligands. The absorption of the QDs at 280 nm is presented with respect to elution time. The QDs show a characteristic peak around 16 minutes. Fraction 11 of the initial QD sample (black) was collected and re-

purified on the GFC to examine the possibility of aggregation over time. The blue trace in Figure 3.4 shows the absorption at 280 nm of the re-purified QD sample. The shoulder around $t = 15$ minutes is characteristic of sample aggregation. The column used in the latter purification was equilibrated with free DHLA-PEG ligand prior to addition of the QD sample to help prevent sample aggregation during purification. The large absorption seen at 20-22 minutes is likely due to these small unbound ligands.

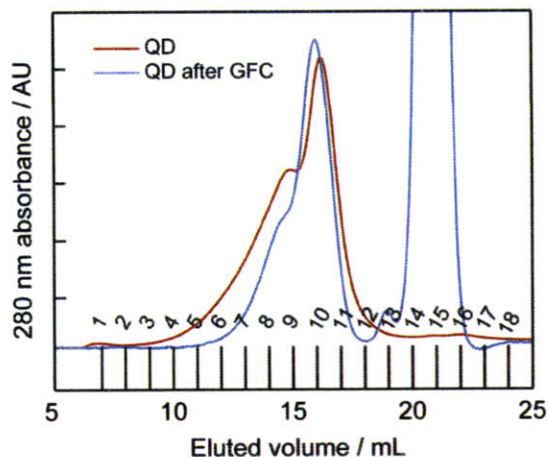


Figure 3.4. GFC trace of QDs with 50% amino-PEG ligands and 50% hydroxyl-PEG ligands. Aggregation can be seen in the purified QD sample (blue) indicating likely aggregation over time.

The porphyrin was determined to greatly increase the amount of sample aggregation, even at very low concentrations. GFC traces of samples consisting of QD: R_0 ratios of approximately 1:2 and 1:1 are presented in Figure 3.5 (left and right, respectively). There is significant aggregation present in both samples. The aggregation is also significantly more than that found with the QDs alone (Figure 3.4), likely indicating cross-coupling between the QDs and porphyrins or the presence of hydrophobic interactions between the QDs and porphyrins.

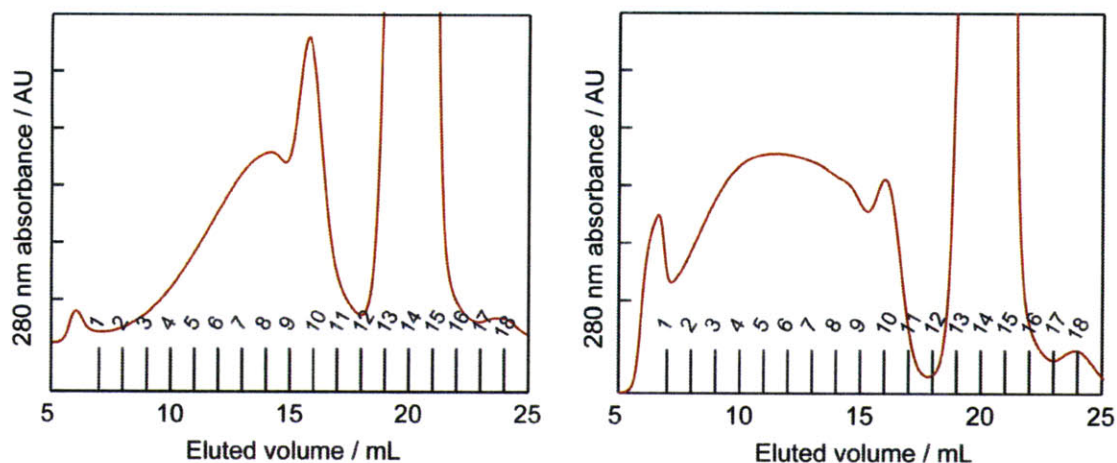


Figure 3.5. Coupling of R_0 to 50% amino-PEG QDs in ratios (R_0 to QD) of 1:1 (left) and 2:1 (right).

As mentioned in Section 3.5, decreasing the percentage of amino-PEG ligands used to water solubilize the QDs can dramatically decrease the amount of sample aggregation. This has been shown to be related to a decrease in charge.⁶ A GFC trace of the 280 nm absorption of a 20% amino-PEG QD sample is shown in Figure 3.6 (left). Again, the sample is eluted on the column in the presence of excess DHLA-PEG ligand to help prevent aggregation. On the right side of Figure 3.6, a GFC trace of a coupling reaction between 20% amino-PEG QDs and R_0 is shown. The increase in aggregation can be seen in the presence of a larger shoulder at shorter times (10-14 minutes). However, the aggregation is significantly decreased from the 50% amino-PEG QD coupling reactions, as seen by the GFC traces in Figure 3.5.

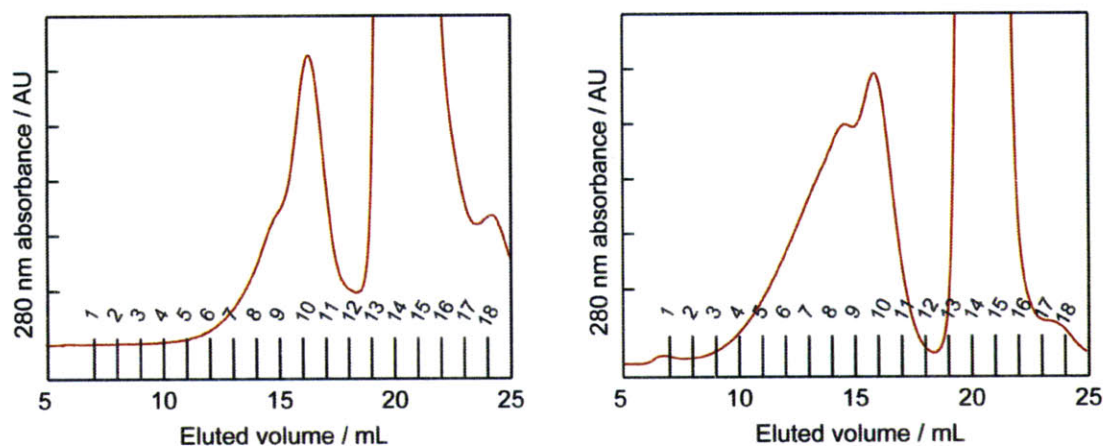


Figure 3.6. GFC traces of 20% amino-PEG QDs alone (left) and coupled with R_0 (right).

Our ability to better control the aggregation of the QDs and R_0 through GFC purification and variation of the coupling conditions facilitates the synthesis of QD- R_0 oxygen sensors. Collection of single QD fractions after GFC purification bypasses cross-coupling issues due to the presence of multiple carboxylic acid groups. Limiting the amount of R_0 also helps minimize sample aggregation. Using 20% amino-PEG QDs, the procedure outlined in Scheme 3.2 was employed to afford three samples. The GFC traces of these samples are shown in Figure 3.7. Sample A contains only QDs, and shows the amount of aggregation present in a QD sample under the same reaction conditions (heated at 60 °C for an hour) as the samples with R_0 . Samples B and C were prepared with starting QD to R_0 ratios of 1:3.5 and 1:7.5 respectively. These ratios decreased to 1:2.5 and 1:4.5 after purification. Addition of more R_0 during coupling increased the amount of R_0 in the final sample, as expected. The GFC trace of sample C also shows more aggregation than B as indicated by the large shoulder present between 10 and 14 mL. The spectroscopic properties of the collected fractions were further examined to study the energy transfer from the QD to the porphyrins as well as determine the feasibility of the sensor for biological use.

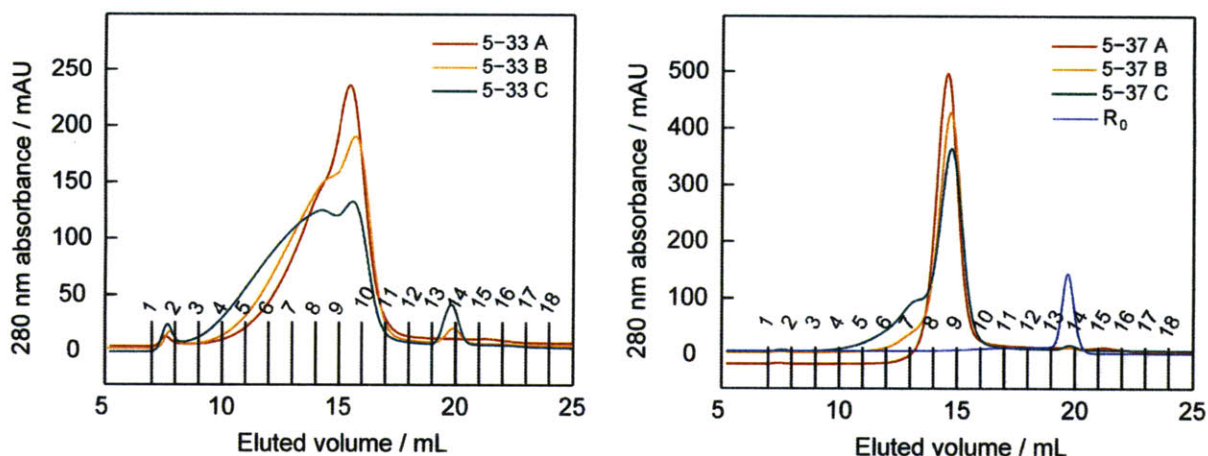


Figure 3.7. GFC traces of three reactions where the amount of R_0 is varied. Sample A is a control sample and thus contained no R_0 . The elution rate was 1 mL per minute so the x-axis may be read as minutes as well as mL.

3.7 Spectroscopic Properties of QD- R_0 : An Energy Transfer Study

The photophysical properties of the QDs, R_0 , and conjugates thereof were characterized by steady-state and time-resolved spectroscopies. The properties are summarized in Table 3.1 along with those of R_2 , a porphyrin based on R_0 , surrounded by a second-generation glycine dendrimer. The absorption spectrum of R_0 first seen in Figure 3.2 is presented again in Figure 3.8 along with the emission spectrum of **QD1**. The narrow Q-band absorption of R_0 overlaps well with the 526 nm emission of these QDs, an advantage of the ability to tune the QD emission wavelength. Calculation of the overlap, J , eq (6), between the absorption of R_0 and emission of **QD1** yields a value of $7.9 \times 10^{-14} \text{ cm}^3/\text{M}$. Upon conjugation of R_0 to the QDs, a red-shift in the absorption of the porphyrin Soret band is observed but there is negligible change in the Q-band in the QD conjugates. The Soret red-shift is similar in magnitude to that seen in the R_2 dendrimer encapsulated PdTCPP (R_0). The porphyrin emission is also slightly blue-shifted upon conjugation to the QDs, which is also seen in Oxyphor R_2 .

Table 3.1. Photophysical Properties of Palladium (II) *meso*-Tetra(4-Carboxyphenyl) Porphine-based Complexes and Their QD-Conjugates.

Complex	$\lambda_{\text{abs}} / \text{nm}$	$\lambda_{\text{em}} / \text{nm}$
Oxyphor R ₀ (PdTCPP) ^a	407, 525	714
Oxyphor R ₂ ^a	415, 524	700
QD1 ^b	504 ^d	526 ^b
QD2 ^c	612 ^d	623 ^c
QD1 - R ₀	417, 524, 505 ^d	529, 708
QD2 - R ₀	417, 525, 611 ^d	624, ~709 ^g

^a From reference 3. ^b $\lambda_{\text{exc}} = 350 \text{ nm}$, $\lambda_{\text{det}} = 525 \text{ nm}$. ^c $\lambda_{\text{exc}} = 350 \text{ nm}$, $\lambda_{\text{det}} = 625 \text{ nm}$. ^d Lowest energy exciton peak.

Selective excitation of the QD allows the energy transfer mechanism at play in the conjugates to be explored. Emission profiles of the QD-R₀ conjugates were examined with steady-state and time-resolved methods. The steady-state emission spectra of Samples **QD1-A**, **QD1-B**, and **QD1-C** as well as R₀ alone are shown in Figure 3.9. The spectra were corrected using the **QD1** concentration, as the QD is the significant absorber at 350 nm. The spectrum of R₀ alone was corrected using the R₀ concentration and absorbance at 350 nm. The narrow absorption of the porphyrin allows the QD to be selectively excited with 350 nm light, which should lead to phosphorescence due almost entirely to energy transfer.

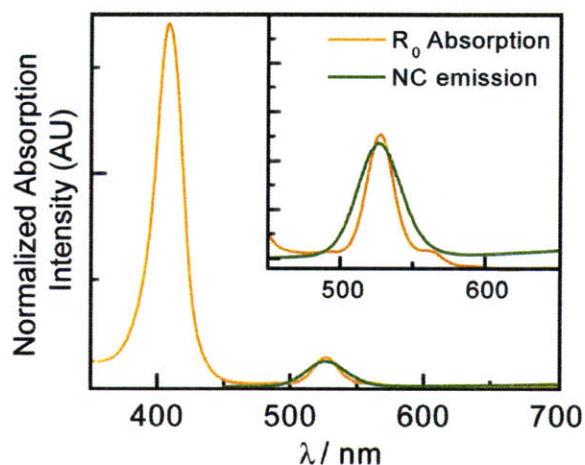


Figure 3.8. Absorption profile of R_0 and emission profiles of green emitting QDs (**QD1**) showing significant overlap for high energy transfer efficiency ($J = 7.9 \times 10^{-14} \text{ cm}^3/\text{M}$).

The enhancement of the porphyrin emission in the QD conjugate relative to the unconjugated porphyrin in Figure 3.9 is a strong indication of energy transfer from the QD to the porphyrin. The variation in QD: R_0 ratios between samples should manifest itself through increased QD emission quenching with higher concentrations of R_0 and a corresponding increase in the emission intensity of R_0 . It can be seen in Figure 3.9 that Sample **QD1-A**, which had no R_0 added, has a small emission peak near 700 nm, which may be due to the presence of R_0 . It is possible a small amount of R_0 present in the reaction mixture or on the GFC column during purification contaminated the sample. However, calculation of the QD: R_0 ratio from the absorption spectrum of Sample **QD1-A** showed a negligible amount of R_0 (<0.3 per QD). In addition, the QD emission in Sample **QD1-A** is smaller than that of the QD emission in Sample **QD1-B**. This is unexpected as the control sample (**QD1-A**) should yield the strongest QD emission, as there is negligible R_0 present to quench the QD emission through energy transfer. The QD emission in Sample **QD1-C** shows the smallest QD emission, as expected, but the R_0

emission is less than that in **QD1-B**. There is more R_0 in sample **QD-1C**, thus a larger emission from the porphyrin was expected.

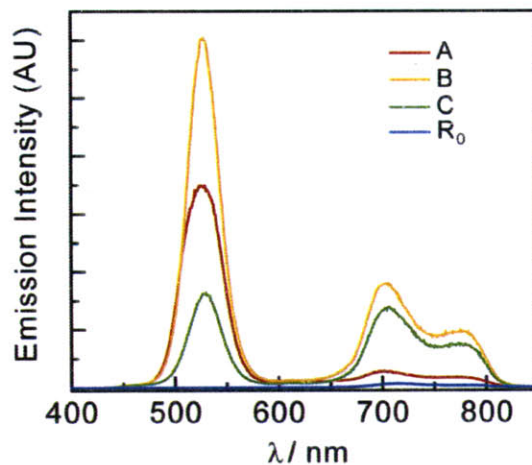


Figure 3.9. Emission spectra of green QD- R_0 samples with varying QD: R_0 ratios. All spectra were taken in the absence of oxygen.

There are a number of possibilities as to why these unexpected emission intensities may be seen. The samples were corrected using the QD concentration, which may not have been accurate as the absorbance at 350 nm differed between samples, with **QD1-A** being more concentrated. The samples were all purified using a similar method; however, small differences in the sample purification, such as the concentration of the sample when added to the GFC column or the concentration of excess ligand present in the sample, may have led to differences in brightness. The decreased emission of R_0 in **QD1-C** vs. **QD1-B** could be due to other interactions between the QD or QD ligands and R_0 , decreasing the QD and/or R_0 emission. More specifically, the carboxylic acid groups on the porphyrin may coordinate to the QD, changing both of their emission profiles or aggregation may occur over time due to the presence of the tetra-functional porphyrin. Despite the unexpected emission intensity differences between

samples, they show that there is energy transfer from the QD to the porphyrin. Figure 3.10 shows the degree of porphyrin emission enhancement relative to the porphyrin alone.

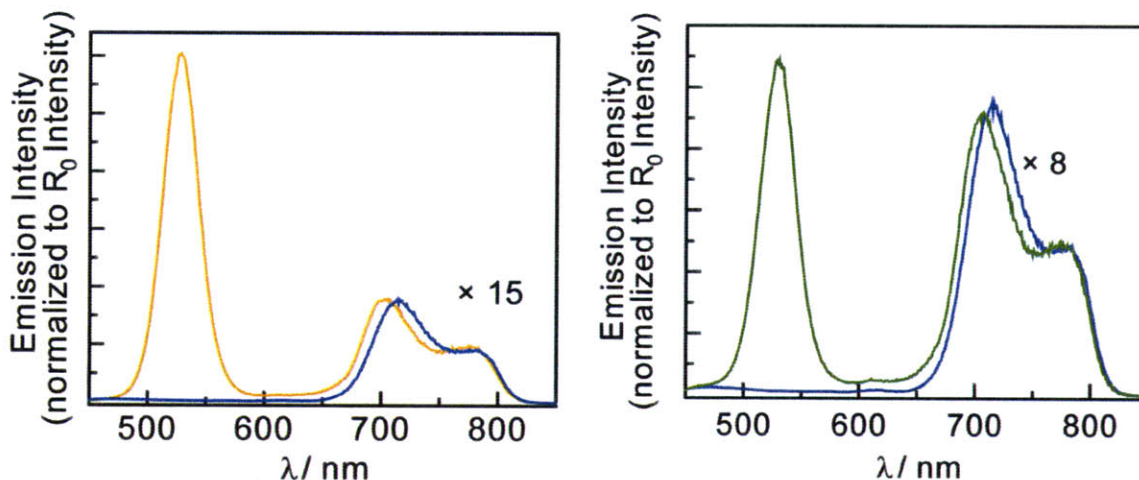


Figure 3.10. Emission enhancement of R_0 in Samples **QD1-B** (orange) and **QD1-C** (green) vs. R_0 alone (blue) through energy transfer from the QD. The emission of R_0 in **QD1-B** and **QD1-C** is enhanced about 15 times and 8 times respectively.

Further exploration of the QD to R_0 energy transfer was pursued through synthesis and characterization of a QD with red emission, where the porphyrin doesn't absorb. An analogous plot to Figure 3.8 for the red emitting QDs is shown in Figure 3.11. The 624 nm emission of the QDs overlaps very little with the porphyrin absorption, as seen in the Figure 3.11 inset. Calculation of the amount of overlap, eq (6), yields a value of $1.2 \times 10^{-15} \text{ cm}^3/\text{M}$, which is more than an order of magnitude smaller than that of the green QD samples (**QD1**). Table 3.1 lists spectroscopic properties of the **QD2** samples. As with the **QD1** samples, a red-shift in the Soret band of the porphyrin is observed while the Q-band absorption does not shift. A similar blue-shift in the porphyrin emission in the QD-conjugates vs. R_0 alone is also observed.

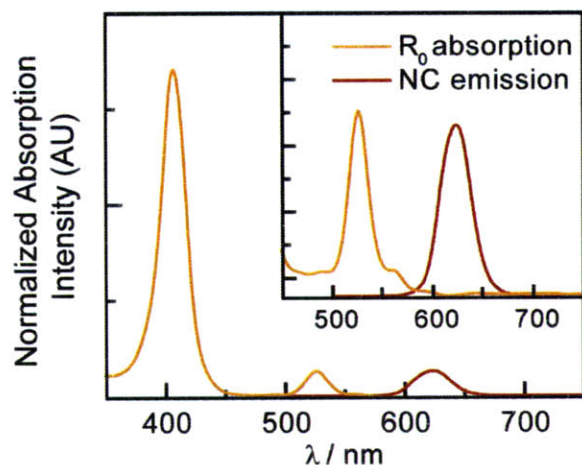


Figure 3.11. Absorption of R₀ (orange) and red QD emission (red) showing the lack of overlap, preventing FRET ($J = 1.2 \times 10^{-15} \text{ cm}^3/\text{M}$).

Steady-state emission spectra of samples with QD:R₀ ratios of 1:0 (**QD2-A**), 1:5 (**QD2-B**), and 1:9 (**QD2-C**) show a lack of energy transfer from the QD to the porphyrin (Figure 3.12). Selective excitation of the QD at 350 nm yields only the emission of the QDs at 624 nm. Despite the lack of energy transfer, we still observe a large quenching in the QD emission when R₀ is present. This confirms another process is contributing to the quenching of the QD emission, such as the aggregation or another type of interference with the QD surface chemistry.

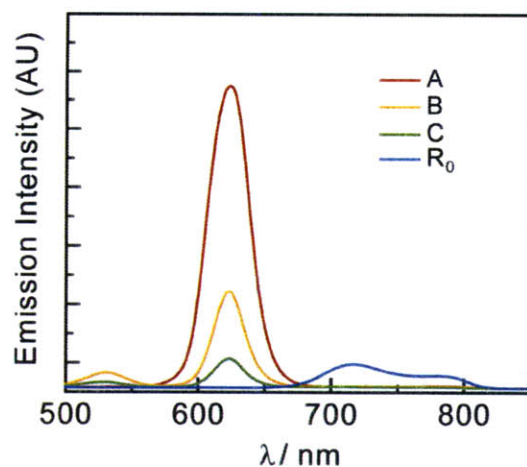


Figure 3.12. Emission spectra of red QD- R_0 samples with QD: R_0 ratios of 1:0 (red), 1:5 (orange) and 1:9 (green). The emissions of the samples are normalized to the QD concentration and the R_0 alone (blue) emission is normalized to its concentration. The spectra were taken in the absence of oxygen with 350 nm excitation.

3.8 Oxygen Quenching of Phosphorescence

Steady-state and time-resolved spectroscopies techniques were used to determine the viability of the QD- R_0 conjugates as oxygen sensors for tumor microenvironments. Steady-state emission data of the **QD1** samples display the expected quenching of the porphyrin phosphorescence by oxygen (Figure 3.13). There is no change in the QD emission intensity, indicating that the QD can act as an internal standard. The spectra in Figure 3.13 display the emissions of **QD1-A** (red), **QD1-B** (orange), **QD1-C** (green) and R_0 (blue) under vacuum. The corresponding emissions in the presence of ~ 760 torr of oxygen are shown in black.

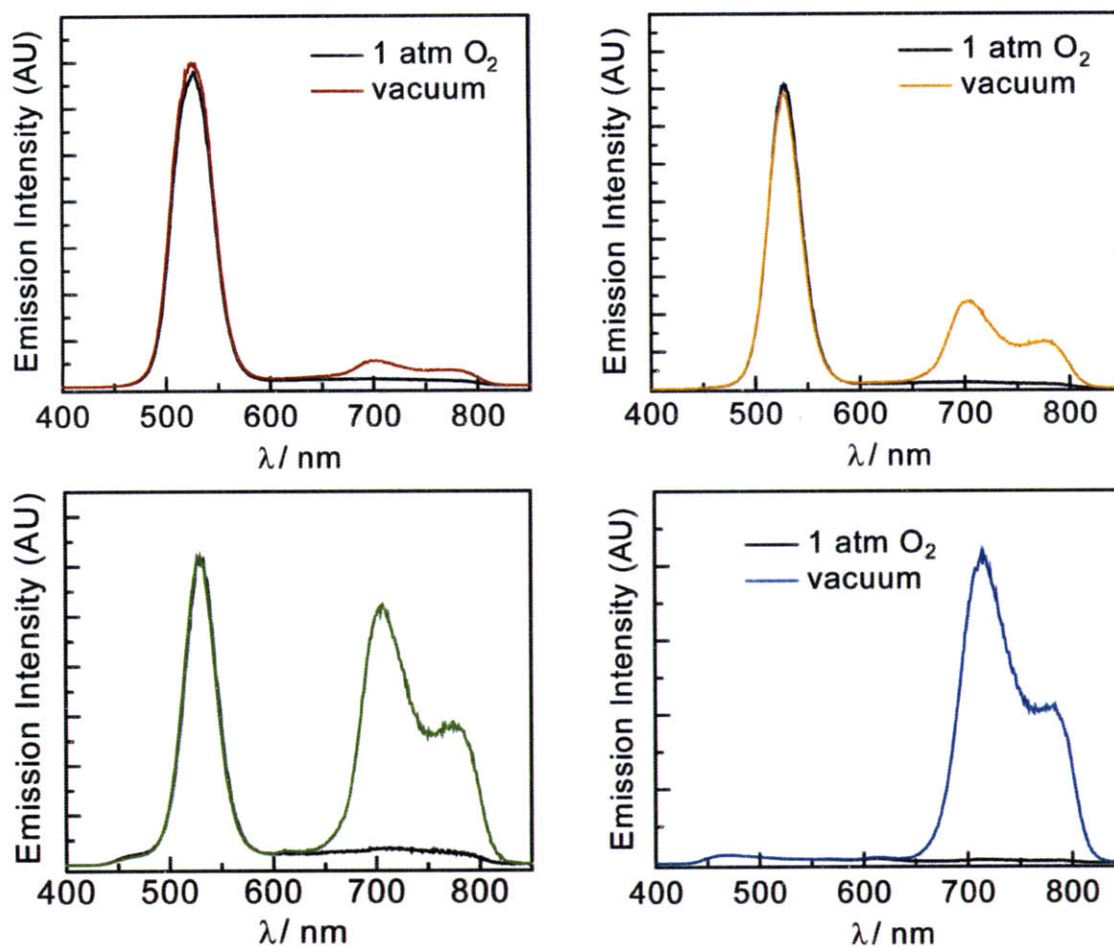


Figure 3.13. Emission spectra of samples **QD1-A** (red), **QD1-B** (orange), **QD1-C** (green), and **R₀** (blue) in the absence of oxygen as well as in the presence of oxygen (black).

Oxygen displacement was performed using several techniques all of which are detailed in the experimental section. The steady-state data presented in Figure 3.13 were obtained using the freeze-pump-thaw technique to remove oxygen. However, this technique was found to precipitate QDs water-solubilized with DHLA-PEG ligands. The QDs adhered to the glass of the sample holder after freezing, leading to changes in sample concentration and QD:R₀ ratio. For other samples, three alternative methods of oxygen removal were employed. Two were enzymatic methods of oxygen removal, using oxidation of either glucose by glucose oxidase or

ascorbate by ascorbate oxidase to consume O₂. Addition of argon or nitrogen gas was the third method employed. Both enzymatic methods provide the advantage of being able to titrate in a solution of glucose or ascorbic acid, allowing for step-wise oxygen removal. However, both methods require equilibration times of 30 minutes to an hour depending on the sample volume. They both also produce acid requiring adjustment of the solution pH over time, as QDs are sensitive to low pH (<6). Addition of argon gas was found to work the best for obtaining solutions of stable oxygen pressure for time-resolved excited state measurements.

Time-resolved measurements agreed with the oxygen sensitivity of the QD-R₀ conjugates indicated by steady-state measurements. The excited state lifetime of the porphyrin was found to decrease with increasing oxygen pressure. A Stern-Volmer plot of a QD-R₀ conjugate is shown in Figure 3.14. An approximate k_q value of 750 torr⁻¹ s⁻¹ was calculated from the data. As argon was added to the solution, the oxygen level decreased and lifetime measurements were taken at points when the pO₂ had stabilized, as determined by the fiber optic oxygen sensor. Over time, sample precipitation was observed and no emission could be detected after reaching a pO₂ of 20 torr. The k_q value was significantly larger than the k_q value for R₀ alone, indicating that the oxygen sensitivity had decreased. The QD-R₀ sensor was sensitive to higher oxygen pressures than R₀ alone. This was unexpected as the porphyrin is likely to be somewhat shielded from oxygen by the DHLA-PEG ligands, which would decrease the k_q value. Also, the excited state decays of R₀ bound to the QD in the absence of oxygen were much shorter than those of R₀ alone. Further attempts to quantify and improve the sensor yielded similar trends. Aggregation of the samples is likely to decrease the lifetime of the excited state, and thus the oxygen sensitivity. This can occur through self-quenching of the porphyrin excited state or perhaps even quenching of the porphyrin excited state by the QDs.

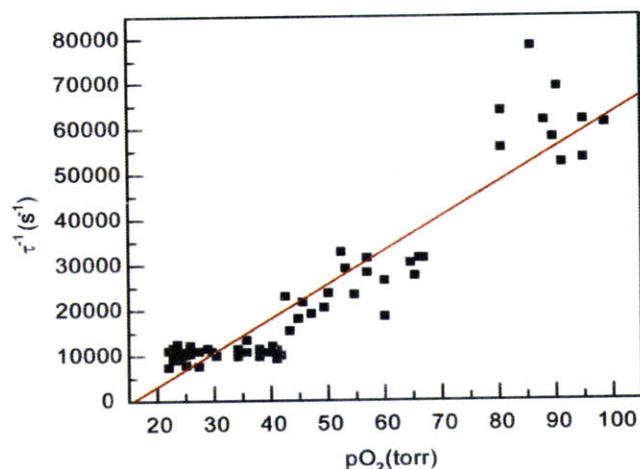


Figure 3.14. Stern-Volmer plot of the oxygen response of a QD-R₀ Sensor. An approximate k_q value of $750 \pm 40 \text{ torr}^{-1} \text{ s}^{-1}$ was calculated. The oxygen level didn't reach 0 before sample decomposition, so the plot is τ^{-1} vs. pO_2 .

3.9 Conclusions

A new type of QD-porphyrin conjugate system was investigated. Energy transfer was found to occur between the QDs and porphyrin. Despite advances in developing a QD conjugate that is more finely tuned to O_2 pressure ranges needed for tumor metabolic profiling, a more biocompatible QD scaffold and a phosphor with oxygen sensitivity in the desired biological range is needed. The QD-porphyrin conjugates showed extensive aggregation, which increased over time. The aggregation resulted from cross-linking between the QDs and porphyrin, which occurs due to the multiple carboxylic acid groups on the porphyrin. Future work addresses the issue of aggregation through synthesis of porphyrins with a single functional group.

3.10 Experimental Section

Materials. The following chemicals were used as received: cadmium oxide (CdO), decylamine, N-hydroxysuccinimide (NHS), 3-sulfo-N-hydroxysuccinimide (S-NHS), anhydrous

N,N-dimethylformamide (DMF, 99%), glucose, ascorbate, glucose oxidase, catalase, ascorbate oxidase, and rhodamine 6G from Sigma-Aldrich; tri-n-octylphosphine (TOP, 97%), and dimethylcadmium from Strem; 1-ethyl-3-(3-dimethylaminopropyl)carbodiimide hydrochloride (EDC•HCl) and 1-hydroxybenzotriazole (HOBT) from NovaBiochem; Oxyphor R₀ (Oxygen Enterprises); selenium shot and 1-tetradecylphosphonic acid (98%, TDPA) (Alfa Aesar); trifluoroacetic acid (TFA, 99.9%) (J. T. Baker). Diethyl zinc (ZnEt₂) bis(trimethylsilyl)sulfide [(TMS)₂S] (Fluka); tri-n-octylphosphine oxide (TOPO) and hexadecylamine were distilled from 90% reagent grade materials (Sigma-Aldrich). Trioctylphosphine selenide (TOPSe) was prepared by dissolving 5.92 g selenium shot in 50 mL TOP. Amino-PEG and hydroxyl-PEG were prepared as previously described.⁶

CdSe/CdZnS Nanocrystals (TOPO-QDs). CdSe QDs overcoated with alloyed CdZnS were prepared by using modified literature methods.^{8,9} Briefly, CdO (0.128 g, 1.0 mmol), TDPA (0.418 g, 1.5 mmol) and TOPO (6 g, 15.5 mmol) were degassed at 320 °C for 1 hour. The resulting clear, colorless solution was cooled to 270 °C under N₂ and 1.5 M TOPSe (5 mL, 7.5 mmol) was rapidly injected into the flask. The resulting solution was heated at 220 °C until the first absorption feature of the core CdSe QDs was 470 nm. The bare CdSe NCs were precipitated twice with butanol and methanol and dispersed in 4 mL hexanes. The QDs were subsequently overcoated by injecting a hexane solution of the bare CdSe into a degassed solvent of TOPO (10 g, 25.9 mmol) and HPA (0.4 g, 2.4 mmol,). The hexane was removed in vacuo at 80 °C from the CdSe cores. Decylamine (0.25 mL, 1.3 mmol) was added to the solution, which was then stirred for 2 hours. Using a syringe pump, two separate solutions of (TMS)₂S in 5 mL TOP and a 90:10 molar ratio of ZnEt₂ and CdMe₂ in 5 mL TOP were added to the CdSe solution at 130 °C over the course of two hours. Amounts of (TMS)₂S, ZnEt₂ and CdMe₂ were chosen to yield a ~3

monolayer coating of ZnS on the bare CdSe QDs, using the methods of Dabboussi et al.⁸ yielding the QDs (FWHM = 32 nm Φ = 58%).

CdSe/CdZnS Nanocrystals (TOPO-QD2s). CdSe NCs overcoated with alloyed CdZnS were prepared using modified literature methods.^{8,10,11} A vial containing cadmium 2,4-pentanedionate (0.317 g, 0.00100 mol) and dodecanal (0.50 mL, 0.0023 mol) in TOP (6.0 mL, 0.0135 mol) was degassed at 180 °C for an hour. TOPO (6.25 g, 0.0162 mol), HDA (5.75 g, 0.0238 mol), and TOP (3.4 mL, 0.0076 mol) were combined and degassed at 360 °C for 1 hour. The vial mixture was cooled to room temperature yielding a homogenous, bright yellow solution. TOPSe (1.5 M, 4 mL) was added and the contents of the vial were rapidly injected into the three-neck flask. Heating was immediately stopped to obtain QDs with a first absorption feature of 596 nm. The bare CdSe QDs were precipitated twice with butanol and methanol and dispersed in 4 mL hexanes. The QDs were then overcoated by injecting the hexane solution of the core CdSe into a degassed solvent of distilled TOPO (10.0 g, 0.0259 mol) and HPA (0.40 g, 0.0024 mol). The hexane was removed in vacuo at 80 °C, and decylamine (0.50 mL, 0.0020 mol) was added. After stirring for 1 hour, the solution temperature was raised to 140 °C. Using a syringe pump, two separate solutions of (TMS)₂S in 5 mL TOP and a 80:20 molar ratio of ZnEt₂ and CdMe₂ in 5 mL TOP were added into the CdSe solution over the course of two hours. Exact amounts were chosen to yield a ~2.5 monolayer coating of ZnS on the bare CdSe QDs, using the methods of Dabboussi et al.⁸ yielding the QDs (FWHM = 26 nm).

Water-soluble nanocrystals (QD1s). The **TOPO-QD1s** were isolated by repeated precipitation from hexanes with a mixture of n-butanol and methanol and re-dissolved in a minimal amount of CHCl₃. In a separate vial, DHLA-hydroxyPEG (100 mg) and DHLA-aminoPEG (125 μ L, 20% methanolic solution) were stirred and the solvent evaporated. Under

N₂, the chloroform QD solution was injected into the ligand mixture and stirred vigorously. The solvent of the QD-ligand mixture was removed and the reaction was stirred at 60 °C for three hours. Upon removing the reaction from heat, ethanol (0.5 mL) and chloroform (0.1 mL) were added. The QDs were precipitated from solution with hexanes (1 mL). The solution was then centrifuged (3900 rpm × 5 min), decanted, and dialyzed (with 50 kDa MW cutoff spin concentrators, Millipore) to furnish aqueous QDs ($\lambda_{\text{PLmax}} = 526 \text{ nm}$, $\Phi = 16\%$).

Water-soluble nanocrystals (QD2s). The **TOPO-QD2s** were isolated by repeated precipitation from hexanes with a mixture of n-butanol and methanol and re-dissolved in a minimal amount of CHCl₃. In a separate vial, DHLA-hydroxyPEG (100 mg) and DHLA-aminoPEG (125 μL , 20% methanolic solution) were stirred and the solvent evaporated. Under N₂, the chloroform QD solution was injected into the ligand mixture and stirred vigorously. The solvent of the QD-ligand mixture was removed and the reaction was stirred at 60 °C for three hours. Upon removing the reaction from heat, ethanol (0.5 mL) and chloroform (0.1 mL) were added. The QDs were precipitated from solution with hexanes (1 mL). The solution was then centrifuged (3900 rpm × 5 min), decanted, and dialyzed (with 50 kDa MW cutoff spin concentrators, Millipore) to furnish aqueous QDs ($\lambda_{\text{PLmax}} = 623 \text{ nm}$).

QD1-R₀ and QD2-R₀ conjugates. A solution of QDs were dialyzed (with 50 kDa MW cutoff spin concentrators, Millipore) twice into DI H₂O and then into pH 8.3 sodium bicarbonate buffer (30 mM) yielding a QD solution with an estimated concentration of 3 μM . A solution of Oxyphor R₀ (0.37 mM, MES buffer pH ~6) was activated with EDC (2.2 mM, 6 eq.) and s-NHS (4.4 mM, 12 eq.) for 25 minutes. This mixture was added to the QD solution and stirred for 1.5

hours. The reaction mixture was dialyzed (with 50 kDa MW cutoff spin concentrators, Millipore) into borate buffer (pH 9) and further isolated by gel filtration chromatography.

Physical measurements. ^1H NMR spectra were recorded on a Varian Mercury 500 MHz NMR at the MIT Department of Chemistry Instrumentation Facility (DCIF) and externally referenced to tetramethylsilane. MALDI-TOF mass spectrometry was performed on a Bruker Omnicflex instrument in the DCIF using dithranol as the matrix. The instrument was calibrated with a quadratic polynomial using a mixture of bradykinin fragment 1-7 (757.3997), angiotensin II (1046.5423), and P14R synthetic peptide (1533.8582) (Sigma) with dithranol as the matrix.

Gel filtration chromatography (GFC) was performed on an Akta Prime system (GE) with a Superose 6 crosslinked dextran column. The hydrodynamic radii of QDs and conjugates were estimated by comparing the elution volumes to those of protein molecular weight standards (Bio-Rad). The eluent from the column was detected with the UV absorbance at 280 nm and the fluorescence spectrum was recorded. One mL fractions were collected from a volume of 5 - 25 mL. Fractions were combined based on the GFC traces and further characterized.

UV-vis absorption spectra were recorded on a Spectral Instruments (SI) CCD array UV-vis spectrophotometer, a Cary 5000, or an HP 8453 diode array spectrophotometer. Steady-state emission spectra were recorded on an automated Photon Technology International (PTI) QM 4 fluorometer equipped with a 150-W Xe arc lamp and a Hamamatsu R928 photomultiplier tube. Time resolved emission measurements for the QDs were made with a chirped-pulse amplified Ti:sapphire laser system using the frequency doubled (400 nm) pump light provided by a Ti:sapphire laser system (100 fs pulsewidth). The detector was a Hamamatsu C4334 Streak Scope streak camera that has been previously described.¹² Time resolved emission measurements of the porphyrin complexes were made with pump light provided by the third harmonic (355 nm)

of a Quanta-Ray Nd:YAG laser (Spectra-Physics) running at 10 Hz. The pump light was passed through a BBO crystal and split into a visible frequency and an infrared frequency. Lifetime measurements employed both the pump and visible beams to excite samples.

Relative quantum yields of samples, Φ_{sam} , were calculated using rhodamine 590 or rhodamine 6G (R6G) as the reference according to:

$$\Phi_{sam} = \Phi_{ref} \left(\frac{A_{ref}}{A_{sam}} \right) \left(\frac{I_{sam}}{I_{ref}} \right) \left(\frac{\eta_{sam}}{\eta_{ref}} \right)^2 \quad (2)$$

A is the measured absorbance, η is the refractive index of the solvent, I is the integrated emission intensity, and Φ_{ref} is the emission quantum yield of the reference. Φ_{ref} was taken to be 0.94 for rhodamine 590 in methanol¹³ or 0.90 for R6G in water.^{14,15} Samples for phosphorescence quantum yield and time resolved spectroscopic measurements were prepared using one of three methods: freeze-pump-thaw degassing for 3 cycles to 10^{-6} torr, addition of argon gas, or addition of an oxygen consuming enzyme (ascorbic oxidase or glucose oxidase). Unless otherwise noted, all spectroscopy was performed in reagent grade deionized water.

Energy transfer analysis. The efficiency of energy transfer from the NC to the porphyrin complex may be evaluated using Förster analysis:

$$E = \frac{mk_{D-A}}{mk_{D-A} + \tau_D^{-1}} = \frac{mR_0^6}{mR_0^6 + r^6} \quad (3)$$

where k_{D-A} is the rate of energy transfer, r is the distance between the donor and acceptor, R_0 is the critical transfer distance or the distance at which half of the donor molecules decay by energy transfer, and m is the number of acceptor molecules per donor. E may be experimentally determined from the excited state quenching of the donor.

To quantify R_0 , r , and m , the following equation may be used:

$$R_0 = \frac{9000 \ln 10 \kappa^2 \Phi_D J}{128 \pi^5 n^4 N} \quad (5)$$

$$J = \int_0^\infty dv \frac{f_D(v) e_A(v)}{v^4} \quad (6)$$

where κ^2 is the relative orientation factor of the dipoles, taken to be $2/3$, Φ_D is the quantum efficiency of the donor, N is Avogadro's number, and n is the index of refraction of the medium, which is taken to be 1.4 in aqueous solution. The constants may be incorporated into one value, which is simply multiplied by Φ_D . Similarly, the latter half of the equation may be represented as J , the overlap integral, where $F_D(\lambda)$ is the normalized intensity of the donor and $\epsilon_A(\lambda)$ is the extinction coefficient of the acceptor at λ .^{2,16} R_0 may thus be calculated for the overlap of the experimentally determined spectra.

The average number of porphyrin complexes attached to the donor, m , can be determined from the optical cross-sections of the donor and acceptor as well as the absorption spectra of the conjugated **QD1-R₀** and **QD2-R₀** systems. The absorption spectra of the conjugates may be taken as a sum of the absorption of the donor and acceptor. The donor:acceptor ratio and the concentrations of the conjugates may be calculated using the individual donor and acceptor absorption spectra, their known ϵ values, and Beer's law.

Oxygen Sensing Calibration. An external method of oxygen calibration was required when enzymatic or gas displacement methods for oxygen removal were employed. A fiber optic oxygen sensor (Ocean Optics) shown in Figure 3.15 supplied the external calibration source. The sensor uses a fiber optic cable for both excitation of Ru(bpy)₃ embedded in a polymer matrix and

detection of the emission from the $\text{Ru}(\text{bpy})_3$. The emission lifetime of the $\text{Ru}(\text{bpy})_3$ is calibrated to oxygen levels of zero and air using Ocean Optics software.

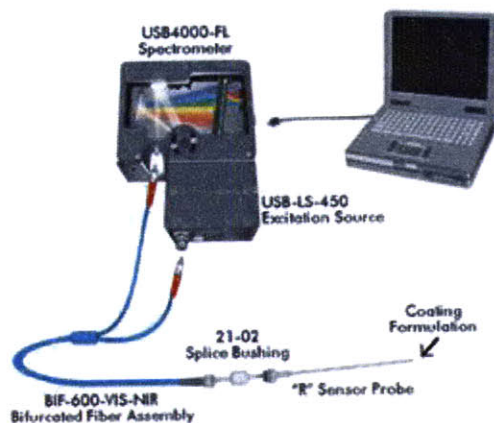


Figure 3.15. Ocean Optics oxygen sensing system. A bifurcated fiber optic cable sends an optical excitation to the phosphor-based probe tip. The excited state lifetime of the phosphor is monitored by the spectrometer and converted to an oxygen level using software.

The oxygen level in the sample was calibrated by insertion of the $\text{Ru}(\text{bpy})_3$ probe into the sample within the cell. Addition of argon gas, as shown in Figure 3.16, while stirring was used to adjust the oxygen level. The solution was allowed to equilibrate with the headspace until the oxygen pressure read by the sensor stabilized.

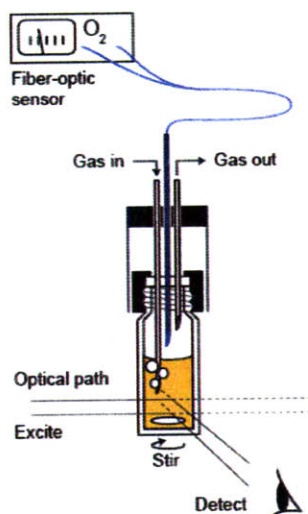


Figure 3.16. Method for controlling and monitoring oxygen levels using nitrogen or argon gas flow. A gas inlet and outlet are accompanied by a fiber optic oxygen probe within the cell. Oxygen levels are monitored and correlated with the sensor emission profile for calibration.

Enzymatic methods for oxygen removal involve titration of solutions with known concentration of glucose or ascorbate. The oxidizing enzyme (glucose oxidase or ascorbate oxidase, respectively) is present in the sample solution prior to the addition of any glucose or ascorbate. Thus, upon addition of a small volume of glucose or ascorbate solution, the enzyme removes a certain amount of oxygen from solution. The oxygen level is measured with a similar set up to that shown in Figure 3.16; however, there is no gas inlet or outlet, only a syringe for injection of glucose or ascorbate solution.

3.11 References

1. Helmlinger, G.; Yuan, F.; Dellian, M.; Jain, R. K. *Nat. Med.* **1997**, *3*, 177-182.
2. Lakowicz, J. R. *Principles of Fluorescence Spectroscopy*, 2nd ed.; Kluwar Academic/Plenium Publishing: New York, **1999**.
3. Dunphy, I.; Vinogradov, S.A.; Wilson, D.F. *Anal. Biochem.* **2002**, *310*, 191-198.
4. Lo, L. W.; Koch, C. J.; Wilson, D. F. *Anal. Biochem.* **1996**, *236*, 153-160.
5. Kruk, M.; Karotki, A.; Drobizhev, M.; Kuzmitsky, V.; Gael, V.; Rebane, A. *J. Lumines.* **2003**, *105*, 45-55.
6. Liu, W.; Howarth, M.; Greytak, A. B.; Zheng, Y.; Nocera, D. G.; Ting, A. Y.; Bawendi, M. G. *J. Am. Chem. Soc.* **2008**, *130*, 1274-1284.
7. Vinogradov, S. A.; Lo, L.; Wilson, D. F. *Chem. Eur. J.* **1999**, *5*, 1338-1347.
8. Dabbousi, B. O.; Rodriguez-Viejo, J.; Mikulec, F. V.; Heine, J. R.; Mattoussi, H.; Ober, R.; Jensen, K. F.; Bawendi, M. G. *J. Phys. Chem. B* **1997**, *101*, 9463-9475.
9. Aldana, J.; Wang, Y. A.; Peng, X. *J. Am. Chem. Soc.* **2001**, *123*, 8844-8850.
10. Murray, C. B.; Norris, D. J.; Bawendi, M. G. *J. Am. Chem. Soc.* **1993**, *115*, 8706-8715.
11. Hines, M. A.; Guyot-Sionnest, P. *J. Phys. Chem.* **1996**, *100*, 468-471.
12. Damrauer, N. H.; Hodgkiss, J. M.; Rosenthal, J.; Nocera, D. G. *J. Phys. Chem. B* **2004**, *108*, 6315-6321.
13. Holzer, W.; Gratz, H.; Schmitt, T.; Penzkofer, A.; Costela, A.; Garcia-Moreno, I.; Sastre, R.; Duarte, F. *J. Chem. Phys.* **2000**, *256*, 125-136..
14. Henderson, L. J. Jr.; Cherry, W. R. *J. Photochem.* **1985**, *28*, 143-151.
15. Magde, D.; Wong, R.; Seybold, P. G. *Photochem. Photobiol.* **2002**, *75*, 327-334.

16. Förster, T. *Ann. Phys.* **1948**, 2, 55-75.

Chapter 4

Synthesis of Phosphorescent A₃B Porphyrins for O₂ Sensing

4.1 Motivation

As described in Chapter 3, difficulties in synthesis of a QD-porphyrin oxygen sensor were due in part to use of a tetra-carboxylic acid functionalized porphyrin. Moving to porphyrins with only one functional group should in principle help prevent the aggregation and cross-coupling. The tailorability of the porphyrin synthesis also allows platinum(II) porphyrins to be synthesized in conjunction with their palladium(II) analogs to permit a side-by-side comparison of the two systems to allow for the range of oxygen sensitivity to be discerned.

This Chapter examines another new technology. The use of a water solubilizing imidazole polymer developed by Liu *et. al.* yields significantly more stable QDs than the DHLA-PEG ligands used in Chapter 3. The polymer also provides a method for porphyrin water solubilization prior to QD attachment by coupling the porphyrin to the polymer. We now examine two methods for synthesis of A₃B porphyrins and initial experiments on their coupling to an imidazole polymer.

4.2 Nitration of Tetraphenyl Porphyrin

4.2.1 Background

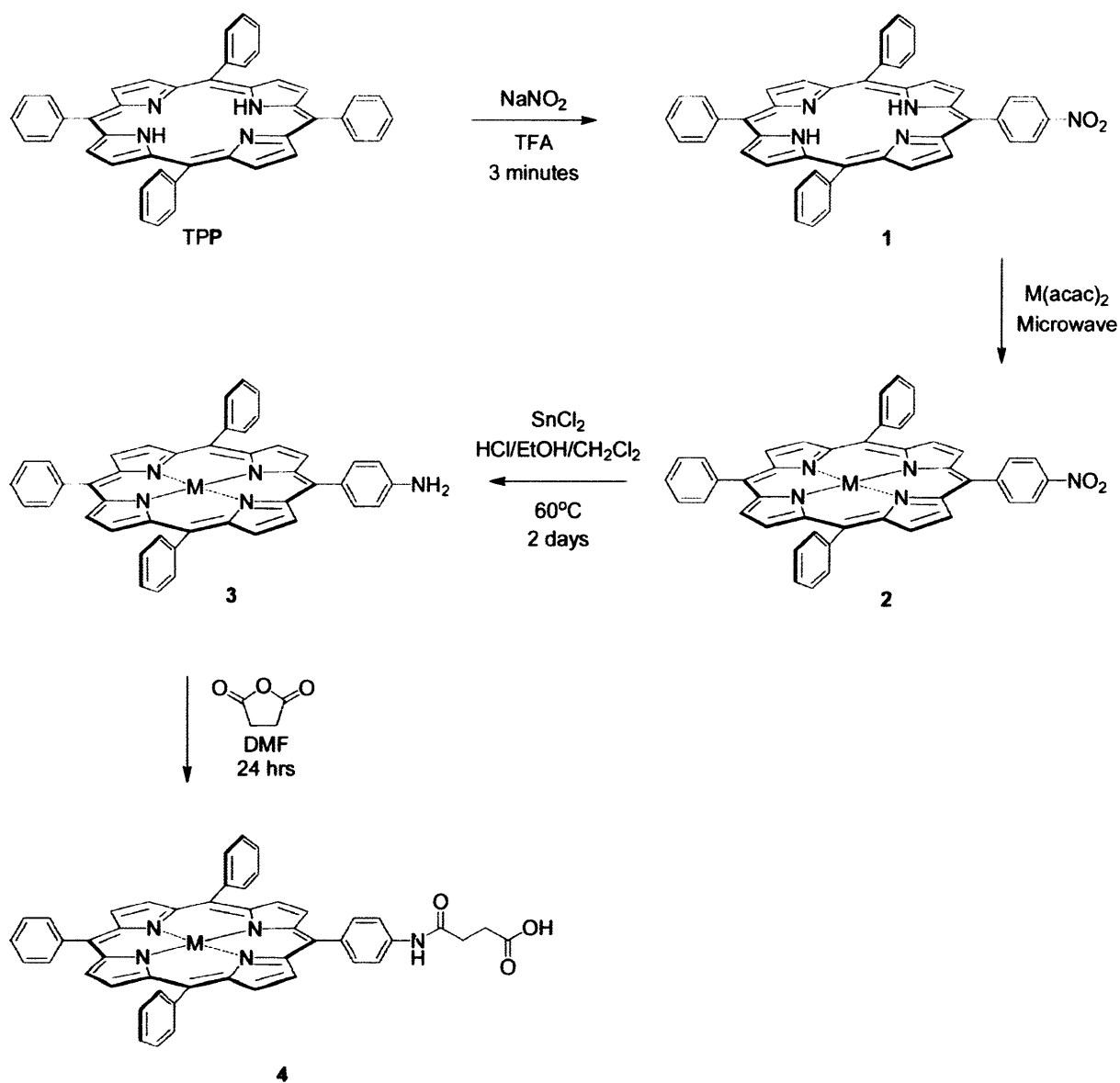
Obtaining asymmetric porphyrins can be synthetically challenging.¹ Methods usually involve condensation reactions in which a variety of products are obtained resulting in low yields and the resulting products can be difficult to isolate. One strategy for obtaining asymmetric porphyrins more readily has been to impart the asymmetry after porphyrin formation. The synthetic method outlined in this section describes a method for obtaining A₃B porphyrins using nitration of tetraphenyl porphine based on literature procedures.² The nitro group is further manipulated to obtain porphyrins with functionalities such as aniline¹ or a carboxylic acid.³

The QDs available for conjugation present carboxylic acid functionality (Chapter 2). Water-solubilization methods developed by Liu *et. al.* afforded an assortment of ligands for QD coordination that also presented amine and hydroxy functionalities (Chapter 3). Acid groups can couple directly to the surfaces of these QDs. This section addresses the challenges in obtaining good quantities of mono-functionalized porphyrin, and integration of such a porphyrin with an imidazole polymer for QD water-solubilization.

4.2.2 Results and Discussion

4.2.3 Synthesis

The synthetic scheme for synthesis of an A₃B porphyrin depicted in Scheme 4.1 yielded phosphorescent porphyrins with a single functional group. Modified literature procedures⁴⁵ were used and are described in detail in the experimental section. Tetraphenyl porphyrin was nitrated using sodium nitrite in TFA resulting in **1**. **1** was reacted with M(acac)₂ (M = Pd^{II} or Pt^{II}) in a microwave reactor, yielding the metallated complex. Microwave reaction temperatures of 180 °C for palladium and 250 °C for platinum were required for insertion of the metal into the porphyrin. Reduction of the nitro group with SnCl₂ in a mixture of HCl, water, ethanol, and dichloromethane for 2 days yielded the aniline porphyrin. **4** was obtained by reaction with a cyclic anhydride (succinic anhydride is shown in Scheme 4.1) and its presence was confirmed by MALDI. However, the resulting porphyrins were extremely insoluble and could not be isolated.



Scheme 4.1. Synthesis of an A₃B porphyrin through nitration, metallation, reduction, and amide bond formation with succinic anhydride. An additional step, reaction with *tert*-butyl 6-aminohexylcarbamate followed by deprotection, could yield a free amine, which is preferable for amide bond formation (as opposed to an aniline).

The synthesis uses tetraphenyl porphine as a synthon/starting material, in contrast to other methods of porphyrin synthesis, which involve condensation. This method of generating a single functional group on the porphyrin was pursued because the condensation of A₄ porphyrins tends to be more straightforward than condensation of asymmetric porphyrins, as only one type of aldehyde is used.

Literature procedures were modified due to the need for phosphorescent porphyrins containing Pd or Pt. Palladium(II) and platinum(II) acetyl acetate were used as the metal sources in place of halogen-based starting materials (PtCl₂ or PdCl₂). These materials are more prone to oxidation than the acac complexes, and they are known to lead to plating out of the metal much faster in microwave reactors.⁴ Plating of the metal to the sides of the reaction tube reflects the microwaves and prevents accurate reading of the temperature within the tube. Metallation of the porphyrin after reduction of the nitro group was found to oxidize the aniline. The aniline free-base porphyrin was reacted with a cyclic anhydride to protect the aniline from oxidation but, the amide bond was found to break during metallation, likely due to the high reaction temperatures required. For these reasons, compound **1** was metallated before reduction of the nitro group. Compound **2** was significantly less soluble than the free-base porphyrin, which may be reduced in HCl alone. This decreased solubility required significantly longer reaction times of multiple days, as indicated in Scheme 4.1. The resulting aniline could be isolated in good yield (~90%). Reaction of either the Pd or Pt porphyrin with a cyclic anhydride (succinic or diglycolic) yielded insoluble product in a variety of solvents. Despite the appearance of product as indicated by MALDI, only starting material was isolated.

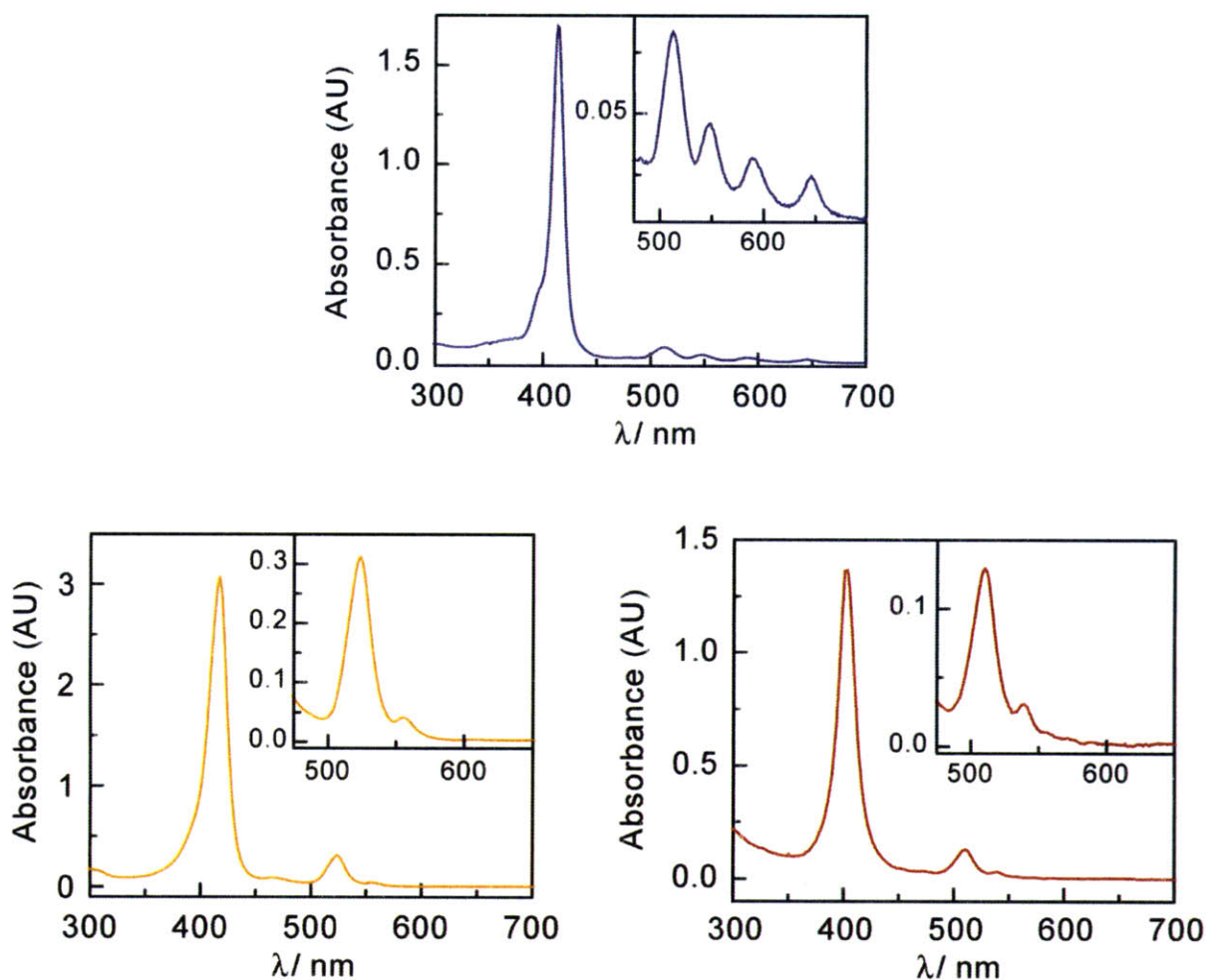


Figure 4.1. Absorption spectra of TPPNH₂COCH₂CH₂COOH (purple, top), PdTPPNH₂ (orange, bottom left), and PtTPPNH₂ (right, red). Incorporation of the metal dramatically changes the lower energy absorption of the porphyrin.

4.2.4 Spectroscopic Properties

The isolated materials from Scheme 4.1 showed spectra that are characteristic of porphyrins. The free-base porphyrins show high energy absorption band (Soret) and lower energy bands resulting from the splitting of the Q(0,0) transition into Q_x(0,0) and Q_y(0,0), which each have vibronic overtones. Upon metallation, there is a small shift in the Soret band and the Q-band is defined by a single peak with a small shoulder as the porphyrin goes from D_{2h} to D_{4h} symmetry.

Compound **Pd3** displays absorption bands shifted slightly to the red from those of **Pt3** (Figure 4.1). There was no significant difference in the absorption spectra of compounds **2** and **3** for either platinum or palladium. Absorption and emission spectra of the compound **4** derivatives were not obtained due to their insolubilities.

4.3 Statistical Synthesis of M^{II} 5-(4-carboxyphenyl)-10,15,20-triphenylporphyrin

4.3.1 Background

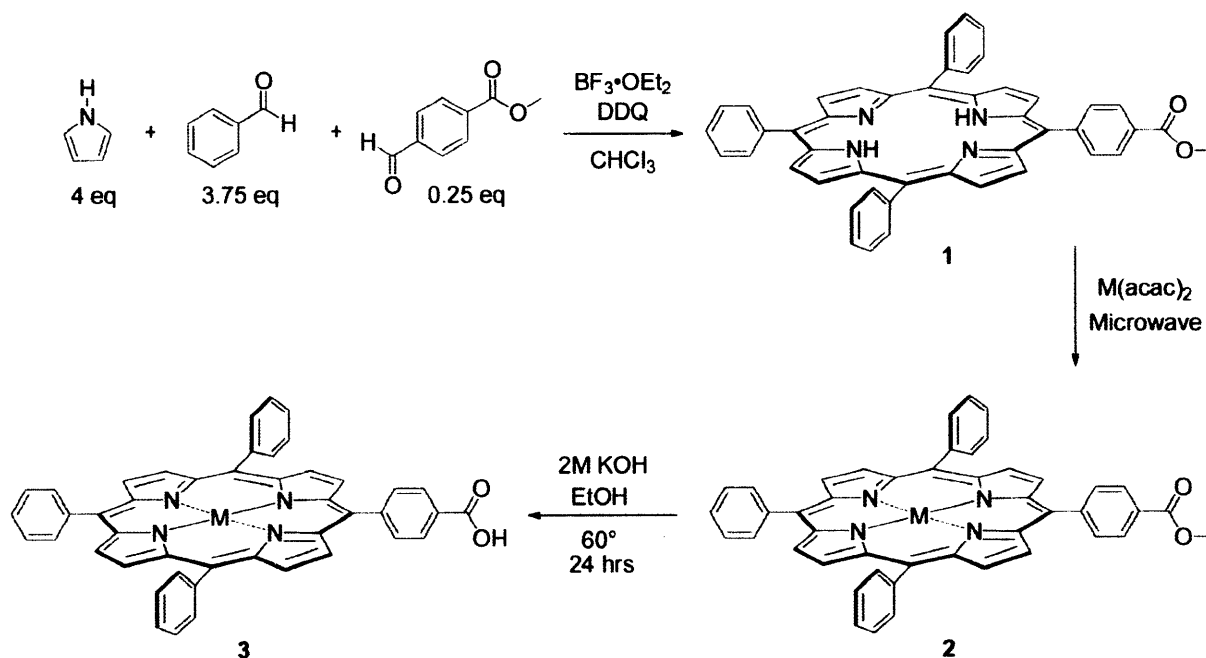
Statistical synthesis is used for formation of a variety of porphyrins.⁶⁻⁹ It provides the advantage of yielding porphyrin in one reaction step, although this reaction step tends to be very low yielding. A single functional group may be introduced through use of different aldehydes in the initial condensation reaction. Synthetic diversity can also be achieved through aldehyde variation, as a wide variety of aldehydes are readily available. The synthesis and spectroscopic analysis of two Pd and Pt porphyrins, each possessing a single carboxylic acid functionality, is described in this section.

4.3.2 Results and Discussion

4.3.3 Synthesis Pt^{II} 5-(4-carboxyphenyl)-10,15,20-triphenylporphyrin

Despite the rather low yielding condensation reaction, Pt 5-(4-carboxyphenyl)-10,15,20-triphenylporphyrin can be easily generated through the synthetic route outlined in Scheme 4.2, which is based on literature procedures.^{8,9} Initially, porphyrin **1** is generated through condensation of pyrrole with benzaldehyde and methyl 4-formyl benzoate. The ester of the porphyrin is more soluble in organics and thus can be isolated through column chromatography more readily. Additionally, the ester also proves to be more stable to some of the more harsh reaction conditions shown in Scheme 4.2. In fact, the initial reaction route pursued basic

hydrolysis of **1**, yielding 5-(4-carboxyphenyl)-10,15,20-triphenylporphyrin. However, the microwave metallation of this porphyrin was found to generate the A₄ tetraphenyl porphine likely due to decarboxylation. Metallation of **1** followed by basic hydrolysis of **2** provided better yields of **3**.



Scheme 4.2. Statistical synthesis of M^{II} 5-(4-carboxyphenyl)-10,15,20-triphenylporphyrin (MTPPCOOH) where M is palladium or platinum.

Although the basic hydrolysis of **2** may be performed in a microwave reactor in somewhat shorter times, more traditional reaction methods described in the experimental section allowed hydrolysis of more product, due to the low solubility of **2** and the small volume of the microwave tube. The analogous Pd compound was synthesized by Mr. Christopher Lemon and further analysis of both complexes is presented in the following section.

4.3.4 Spectroscopic Properties of Compounds **Pt3** and **Pd3**

The absorption and emission properties of compounds **Pt3** and **Pd3** show narrow absorptions and oxygen sensitive emissions, as summarized in Table 4.1. Figure 4.2 shows the absorption and emission spectra of **Pd3** (orange, bottom) are red-shifted from those of **Pt3** (red, top). The absorption spectra (left) of these complexes show a Q-band with a small vibrational overtone at the expected wavelengths of 510 nm for **Pt3** and 523 nm for **Pd3**. A broader band further to the red can be seen in both absorption spectra. This band may be due to a small amount of coordination from the carboxylic acid group to the metals present, leading to additional splitting of the Q-band. The emission spectra indicate a strong response to oxygen. Phosphorescence of the compounds is observed in the absence of oxygen (colored), while little to no phosphorescence observed in the presence of oxygen (black). The excited state lifetimes were also found to be sensitive to oxygen. The excited state lifetime of **Pd3** was 219 μ s in the absence of oxygen and 3.17 μ s in air. Similarly, the excited state of **Pt3** was quenched from 120 μ s to 0.725 μ s. Lifetimes of Pd porphyrins tend to be longer than those of Pt porphyrins, which agrees with the porphyrins examined here.

Table 4.1. Spectroscopic and Photophysical Properties of Porphyrin Complexes.

Complex	$\lambda_{\text{abs}} / \text{nm}$	$\lambda_{\text{em}} / \text{nm}$	$\tau_{\text{em}} / \mu\text{s}$
Pd3 ^a	415, 523, 553, ^c 595 ^c	694, 765 ^c	219 ^d , 3.17 ^e
Pt3 ^b	401, 510, 539, ^c 582 ^c	661, 725 ^c	120 ^d , .755 ^e
PolyPt3 ^b	308, 402, 510, 540, ^c 586 ^c		57.3, ^d 12.4 ^d ; 6.38, ^e 1.03 ^e

^a $\lambda_{\text{exc}} = 524 \text{ nm}$, $\lambda_{\text{det}} = \text{nm}$. ^b $\lambda_{\text{exc}} = 510 \text{ nm}$, $\lambda_{\text{det}} = \text{nm}$. ^c Shoulder. ^d In the absence of oxygen. ^e In air. Polymer lifetime values were fit to biexponentials. Both values for τ are given.

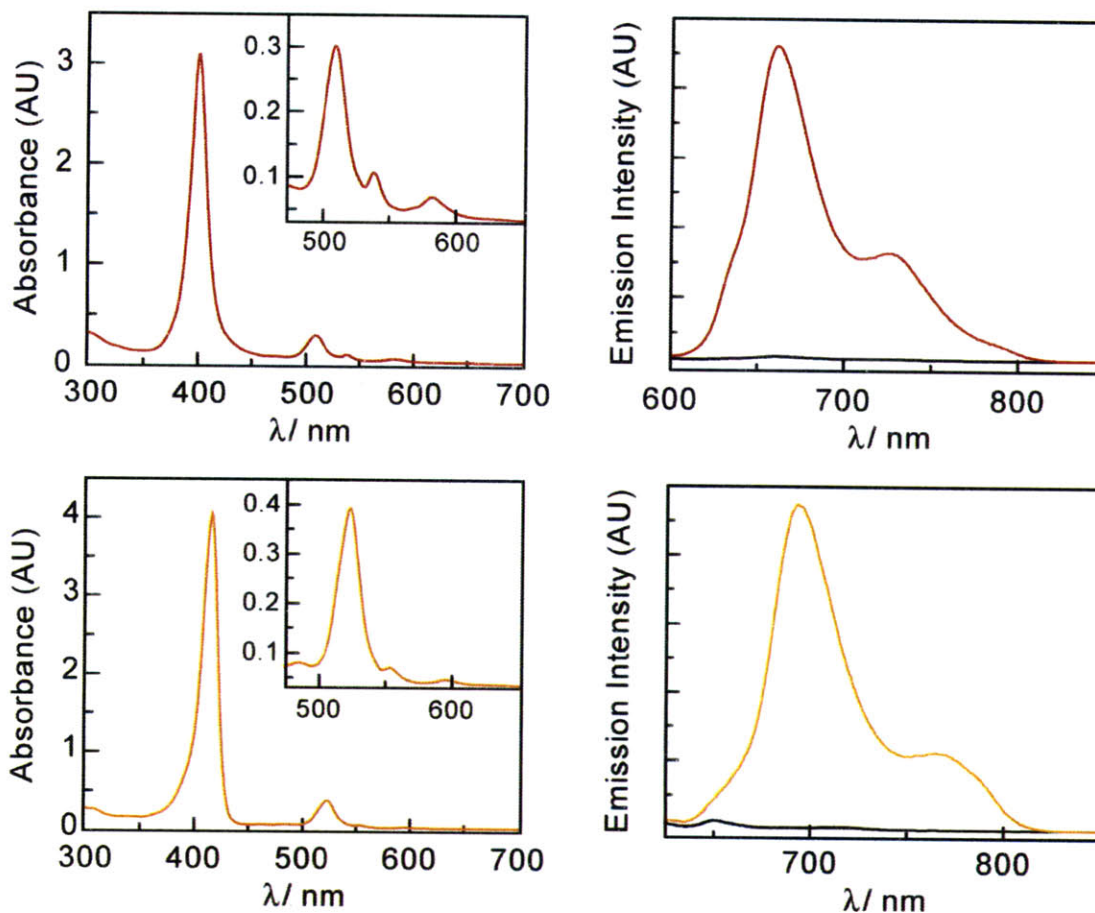
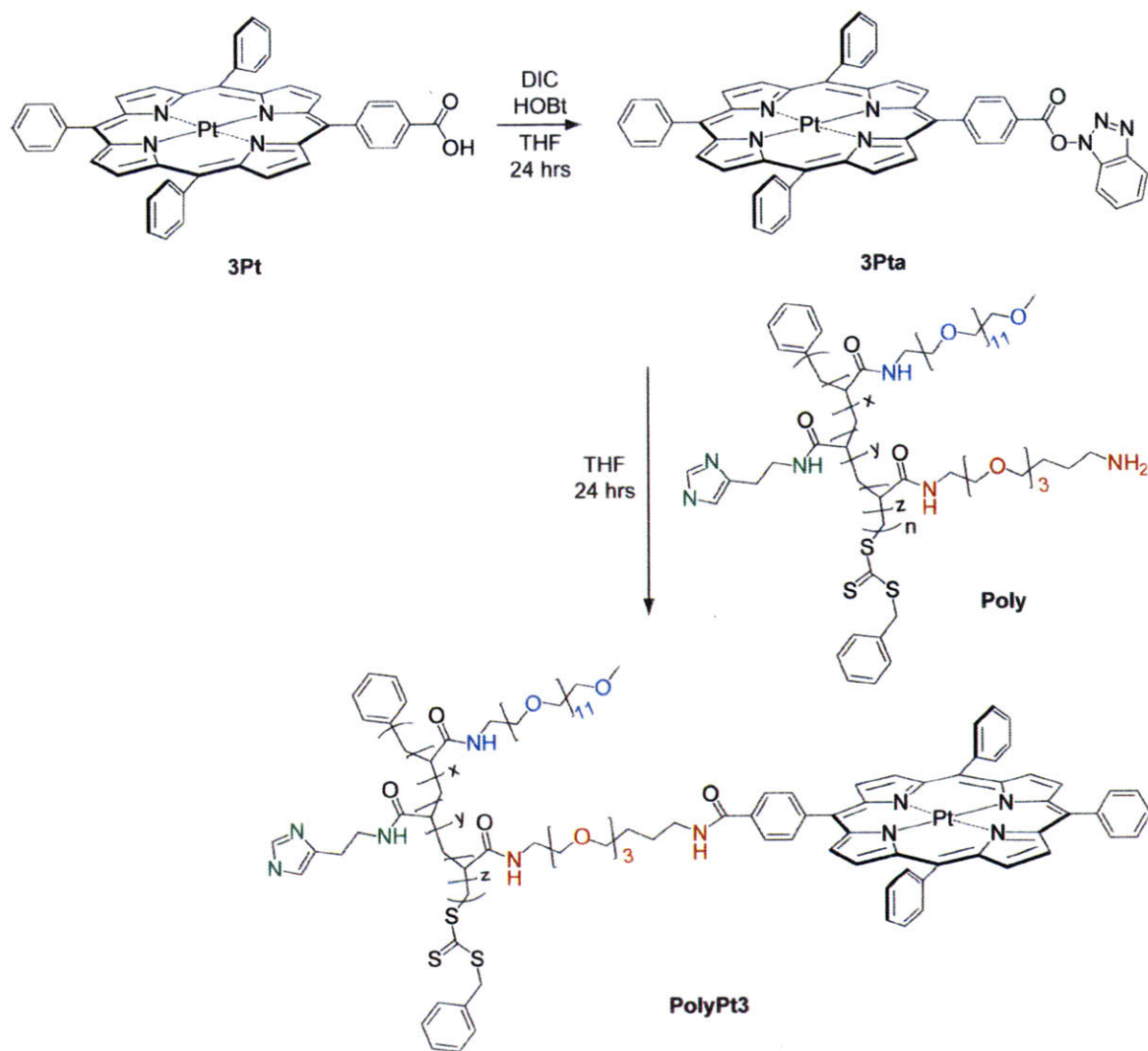


Figure 4.2. Absorption (left) and emission (right) spectra of **Pt3** (red) and **Pd3** (orange). The emission spectra are shown under vacuum (colored) and in air (black). The emissions of both phosphors are almost completely quenched in the presence of air. All spectra were taken in THF.

4.3.5 Synthesis and Purification of a Phosphorescent Imidazole Polymer

The hydrophobicity of **3** prevents synthesis of a QD-**3** sensor through methods employed in Chapters 2 and 3, which require aqueous conditions. However, covalent attachment of **3** to an imidazole-based polymer (shown as **Poly** in Scheme 4.3) used for QD water-solubilization brings the porphyrin into aqueous solution. The synthesis of the imidazole polymer developed by Liu *et. al.* has been previously described.¹⁰ Synthesis of three monomers chosen for QD binding (green, imidazole based), water solubility (blue, PEG based), and porphyrin binding (red, amine

based) followed by polymerization of those monomers yielded the imidazole polymer (**Poly**) shown in Scheme 4.3. Formation of the porphyrin benzotriazole ester (**3Pta**) through DIC coupling, followed by reaction with the **Poly** yielded a phosphorescent polymer (**PolyPt3**), which after purification, was soluble in water. Further details are described in the experimental.



Scheme 4.3. Attachment of **Pt3** to the imidazole polymer through DIC coupling.

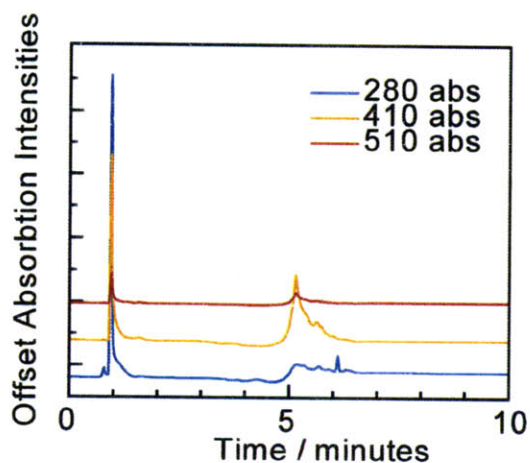


Figure 4.3. HPLC traces of during the purification of **polyPt3**. The absorbances at 280 (blue), 410 (orange), and 510 (red) are shown with respect to elution time.

Purification of the crude **polyPt3** using HPLC yielded the traces shown in Figure 4.3. The polymer was monitored at 280 nm and the porphyrin was monitored at 410 and 510 nm. The polymer absorbs only at ~ 300 nm, where the porphyrin absorbs little. The simultaneous presence of strong porphyrin absorption (400 nm and 510 nm) in conjunction with 300 nm absorption of the polymer is a strong indicator for porphyrin bound to polymer.

Collection of fractions at 1 minute intervals allowed further spectroscopic analysis of the samples. From Figure 4.3, polymer and porphyrin absorptions can be seen at an elution time of about 1 minute. Additional porphyrin absorption is seen at an elution time of 5 minutes. Comparison of the absorption spectra of the 1 minute and 5 minute fractions is shown in Figure 4.4. While the 5 minute fraction shows porphyrin absorption, it shows little absorption near 300 nm. The 1 minute fraction shows both significant porphyrin and polymer absorptions. Thus, the 1 minute fraction was used in further experiments.

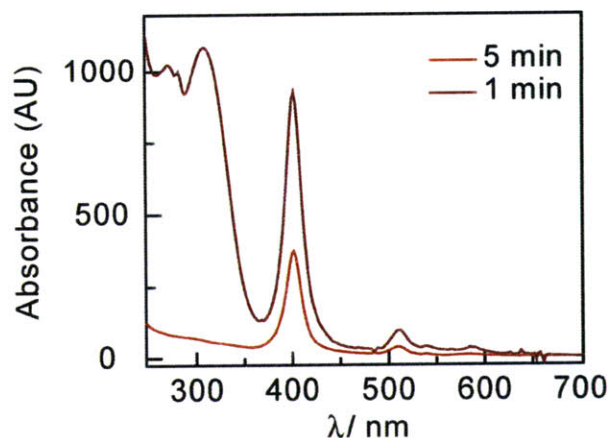


Figure 4.4. Absorption spectra of the fractions collected at 5 minutes (red) and 1 minute (dark red).

4.3.6 Spectroscopic Properties of PolyPt3 (Polymer Bound Pt3)

The polymer bound **Pt3** (**polyPt3**) showed similar absorption properties of **Pt3** alone, but with a significant difference in the excited state lifetime. Comparison of the absorption and emission properties of **Pt3** and **polyPt3** are given in Table 4.1. There is little to no shift in the porphyrin absorption despite the change in solvent from THF to water. The additional absorption at 308 nm is due to the presence of the polymer. Excited state lifetimes of **polyPt3** were fit to biexponential functions, as is generally required for porphyrins interacting with polymers, due to the presence of multiple porphyrin environments.^{11,12} The excited state lifetimes were significantly shorter for **polyPt3** than **Pt3**. We ascribe this to the aqueous conditions of the former; water is known to deactivate excited states through vibrational coupling.¹³ Despite the shorter lifetimes, **polyPt3** shows a significant response to oxygen (see Table 4.1).

4.4 Conclusions

The variety of synthetic methods available for synthesis of asymmetric porphyrins provided a framework within which to generate phosphorescent porphyrins (Pd or Pt) with a single functional group. Although not all synthetic methods attempted were successful, the generation of compounds **Pt3** and **Pd3** is an important step in achieving QD-porphyrin oxygen sensors. The poor solubility of the Pt and Pd porphyrins can be circumvented by attaching them to a more soluble entity, such as the water-soluble imidazole polymer. This polymer not only engendered increased solubility of the porphyrin in organic solvents, it made the porphyrin soluble in water. This enables a more facile synthesis of a QD-porphyrin conjugate as the porphyrin-QD linkage may be formed prior to QD water solubilization. Addition of organics to QDs in aqueous solutions to enable coupling with a hydrophobic molecule has proven difficult, often leading to QD precipitation or quenching of the QD excited state emission. The water soluble QD-porphyrin constructs provide QD-phosphors sensitive to lower oxygen pressures than found in the Os-QD sensors discussed in Chapter 2.

4.5 Experimental Section

Materials. The following chemicals were use as received: Tetraphenyl porphine, sodium nitrite, sodium bicarbonate, benzonitrile (PhCN), pyridine (Py), triethylamine (TEA), anhydrous N,N-dimethylformamide (DMF, 99%), tin (II) chloride (SnCl₂), tetrahydrofuran (THF, inhibitor free), benzaldehyde, methyl-4-formyl benzoate, boron trifluoride (BF₃•OEt₂), 2,3-dichloro-5,6-dicyanobenzoquinone (DDQ), and rhodamine 6G (Sigma-Aldrich); platinum(II) acetyl acetonate and palladium(II) acetyl acetonate (Strem); 1-hydroxybenzotriazole (HOBt) and

diisopropylcarbodiimide (DIC) (NovaBiochem); and trifluoroacetic acid (TFA, 99.9%) (J. T. Baker). Pyridine was distilled from reagent grade materials (Sigma-Aldrich).

5-(4-Nitrophenyl)-10,15,20-triphenylporphyrin (TPPNO₂). The title compound was prepared similarly to the procedure described by Luguya *et. al.* Briefly, TPP (1.00 g, 1.63 mmol) was dissolved in TFA (100 mL) followed by addition of NaNO₂ (200 mg, 2.90 mmol) while stirring. The mixture was poured into 500 mL cold water after 3 minutes and extracted with dichloromethane until the aqueous layer was colorless. Saturated NaHCO₃ was added to the organic layer, restoring the purple color of the porphyrin, and the organic layer was collected again. The solvent was removed *in vacuo* and the compound was purified on a silica column eluting with 4:1 CH₂Cl₂:hexanes. Removal of the solvent *in vacuo* yielded the compound (440 mg, 41%). ¹H NMR (500 MHz, CDCl₃, 25 °C) δ = 8.98 (m, 6H), 8.78 (d, 2H), 8.56 (d, 2 H), 8.30 (m, 8 H), 7.79 (m, 9H). MALDI-TOF Calcd. (Found): [M]⁺ 658.23(658.59)

5-(4-Aminophenyl)-10,15,20-triphenylporphyrin (TPPNH₂). To a solution of TPPNO₂ (68.9 mg, 0.104 mmol) in hydrochloric acid (12 M, 10 mL), tin(II) chloride (118.8 mg, 0.627 mmol) was added while stirring. The solution was heated at 65 °C under nitrogen for an hour whereupon it was poured into cold water (100 mL) and brought to pH 8 with ammonium hydroxide. The solution was extracted using dichloromethane, as above. Removal of the solvent *in vacuo* followed by purification on an alumina column eluting with 4:1 CH₂Cl₂:hexanes yielded the porphyrin (56.7 mg, 86.2%). ¹H NMR (500 MHz, CDCl₃, 25 °C) δ = 8.96 (s, 2H), 8.84 (s, 6H), 8.20 (m, 6H), 7.98 (d, 2H), 7.75 (m, 9H), 7.07 (d, 2H), 4.02 (s, 2H). MALDI-TOF Calcd. (Found): [M]⁺ 629.26(628.39).

Platinum(II) 5-(4-Nitrophenyl)-10,15,20-triphenylporphyrin (PtTPPNO₂). TPPNO₂ (444 mg, 0.674 mmol) and Pt(acac)₂ (291.7mg, 0.7417 mmol) were combined with a stir bar in a

microwave tube. Benzonitrile (3 mL) was added and the tube was heated in a microwave reactor at 250 °C for 15 minutes. The solvent was removed and part of the crude material (180.4 mg) was purified on a silica column eluting with 3:2 CH₂Cl₂:hexanes with 1% TFA yielding the metallated porphyrin (131.3 mg, 72.78%). MALDI-TOF Calcd. (Found): [M]⁺ 852.18(852.3).

Platinum(II) 5-(4-Aminophenyl)-10,15,20-triphenylporphyrin (PtTPPNH₂). PtTPPNO₂ (131.3 mg, 0.1539 mmol) was dissolved in a minimal amount of CH₂Cl₂. HCl (6 mL, 12 M), EtOH (10 mL) and SnCl₂ (141.4 mg, 0.9173 mmol) were added to the flask and the mixture was refluxed for 2 days. The flask was cooled in an ice water bath and 50 mL of cold H₂O was added. After neutralization with NaOH (2 M) the product was extracted with CH₂Cl₂ (3 × 50 mL) and washed twice with DI H₂O (100 mL). The CH₂Cl₂ was removed *in vacuo* and the crude material was purified on an alumina column eluting with 3:2 CH₂Cl₂. After removing the solvent, PtTPPNH₂ was isolated (113.5 mg, 89.6%). ¹H NMR (500 MHz, CDCl₃, 25 °C) δ = 8.87 (d, 2H), 8.76 (m, 6H), 8.16 (d, 6H), 7.92 (d, 2H), 7.74 (m, 9H), 7.01 (d, 2H), 3.98 (s, 2H). MALDI-TOF Calcd. (Found): [M]⁺ 822.21(822.50).

Palladium(II) 5-(4-Nitrophenyl)-10,15,20-triphenylporphyrin (PdTPPNO₂). TPPNO₂ (56.3 mg, 0.0853 mmol) and Pd(acac)₂ (97.3 mg, 0.433 mmol) were combined with a stir bar in a microwave tube. A minimal amount of pyridine (~1 mL) was added and the tube was heated in a microwave reactor at 180 °C for 20 minutes. Water was added to the crude material, followed by extraction with CH₂Cl₂ (3 × 25 mL). The crude material was not isolated further before reduction.

Palladium(II) 5-(4-Aminophenyl)-10,15,20-triphenylporphyrin (PdTPPNH₂). PdTPPNO₂ (131.3 mg, 0.1539 mmol) was dissolved in a minimal amount of CH₂Cl₂. HCl (10 mL, 12 M)

and SnCl₂ (220.4 mg, 0.9173 mmol) were added to the flask and the mixture was refluxed for 2 hours. The flask was cooled in an ice water bath and 100 mL of cold H₂O was added. After neutralization with NaOH (2 M) the product was extracted with CH₂Cl₂ (3 × 55 mL) and washed twice with DI H₂O (50 mL). The CH₂Cl₂ was removed *in vacuo* and the crude material was purified on an alumina column eluting with 3:2 CH₂Cl₂. After removing the solvent, PdTPPNH₂ was isolated (20.8 mg, 89.6%). ¹H NMR (500 MHz, CDCl₃, 25 °C) δ = 8.86 (m, 6H), 8.69 (d, 2H), 8.60 (d, 2H), 8.34 (d, 2H), 8.16 (m, 6H), 7.74 (m, 9H). MALDI-TOF Calcd. (Found): [M]⁺ 822.21(822.50).

5-(4-methoxycarbonyl phenyl)-10,15,20-triphenylporphyrin (TPPCOOMe, 1). To a round bottom flask with degassed CHCl₃ (425 mL), pyrrole (0.275 mL, 4.00 mmol), benzaldehyde (379 μL, 3.75 mmol), and methyl-4-formyl benzoate (41.3 mg, .251 mmol) were added. After degassing for another hour, BF₃•OEt₂ (168 μL, 1.32 mmol) was added drop wise. An hour later, DDQ (0.6802 g, 3.000 mmol) was added followed by an additional hour of stirring. Triethyl amine (1.84 mL, 13.2 mmol) was then added to the reaction mixture followed by a final 10 minutes of stirring. After removal of the solvent, the crude product was purified using silica chromatography eluting with 3:2 CH₂Cl₂:hexanes. Removal of the solvent yielded **1** (114.0 mg, 16.9%). ¹H NMR (500 MHz, CD₂Cl₂, 25 °C) δ = 8.87 (m, 6H), 8.80 (d, 2H), 8.45 (d, 2H), 8.32 (d, 6H), 7.77 (m, 9H), 4.12 (s, 3H) MALDI-TOF Calcd. (Found): [M]⁺ 672.75(672.17).

Platinum(II) 5-(4-methoxycarbonyl phenyl)-10,15,20-triphenylporphyrin (PtTPPCOOMe, Pt2). **1** (64.5 mg, 0.0959 mmol) and Pt(acac)₂ (116.0 mg, 0.295 mmol) were added to a microwave tube containing a stir bar. Benzonitrile (~3 mL) was added to rinse the solids to the bottom of the tube. The tube was heated in a microwave reactor at 250 °C for 15 minutes. Silica chromatography of the crude material eluting with 4:1 hexanes:CH₂Cl₂ followed

by solvent removal yielded **Pt2** (41.3 mg, 49.8%). MALDI-TOF Calcd. (Found): [M]⁺ 865.20(866.84).

Platinum(II) 5-(4-carboxyphenyl)-10,15,20-triphenylporphyrin (PtTPPCOOH, Pt3). Pt2 (41.3 mg, 0.0477 mmol) was suspended in CH₂Cl₂ (50 mL), KOH (2 M, 50 mL), and EtOH (50 mL). The solution was refluxed at 75 °C for 24 hours. The porphyrin was extracted using CH₂Cl₂ (3 × 50 mL) and the solvent was removed *in vacuo*. Silica chromatography on the crude material eluting with CH₂Cl₂ yielded **Pt3** (22.0 mg, 54.0%). ¹H NMR (500 MHz, CD₂Cl₂, 25 °C) δ = 8.77 (m, 4H), 8.73 (d, 2H), 8.44 (d, 2H), 8.29 (d, 2H), 8.14 (d, 4H), 7.71 (m, 9H). MALDI-TOF Calcd. (Found): [M]⁺ 851.19(851.45).

Imidazole polymer bound platinum(II) 5-(4-carboxyphenyl)-10,15,20-triphenylporphyrin (PolyPt3). Pt3 (6.6 mg, 0.0077 mmol) was dissolved in THF (0.5 mL), and HOBt (55.0 mg, 0.407 mmol) followed by DIC (60 μL, 0.383 mmol) and an additional 1 mL of THF was added. The reaction was monitored by TLC (silica, CH₂Cl₂). After 24 hours, a solution of the imidazole polymer (4 mg, 25% amino-PEG₃, 50% imidazole, 25% methoxy-PEG) was added to the porphyrin mixture. After another 24 hours, the mixture was purified on a biobeads column (THF, SX1) and fractions were collected. After the solvent removal, the first fraction was dissolved in PBS. Further purification of the water soluble fraction using HPLC (95% NaHCO₃, 5% THF to 5% NaHCO₃, 95% THF over 10 minutes) yielded **PolyPt3** (1.7 mg).

Physical measurements. ¹H NMR spectra were recorded on a Varian Mercury 500 MHz NMR at the MIT Department of Chemistry Instrumentation Facility (DCIF) and externally referenced to tetramethylsilane. MALDI-TOF mass spectrometry was performed on a Bruker Omnicflex instrument in the DCIF using dithranol as the matrix. The instrument was calibrated

with a quadratic polynomial using a mixture of bradykinin fragment 1-7 (757.3997), angiotensin II (1046.5423), and P14R synthetic peptide (1533.8582) (Sigma) with dithranol as the matrix.

UV-vis absorption spectra were recorded on a Spectral Instruments (SI) CCD array UV-vis spectrophotometer, a Cary 5000, or an HP 8453 diode array spectrophotometer. Steady-state emission spectra were recorded on an automated Photon Technology International (PTI) QM 4 fluorometer equipped with a 150-W Xe arc lamp and a Hamamatsu R928 photomultiplier tube. Time resolved emission measurements of the porphyrin complexes were made with pump light provided by the third harmonic (355 nm) of a Quanta-Ray Nd:YAG laser (Spectra-Physics) running at 10 Hz. The pump light was passed through a BBO crystal and split into a visible frequency and an infrared frequency. Lifetime measurements employed both the visible beam to excite samples.

Relative quantum yields of samples, Φ_{sam} , were calculated using rhodamine 6G (R6G) in water as the reference according to:

$$\Phi_{sam} = \Phi_{ref} \left(\frac{A_{ref}}{A_{sam}} \right) \left(\frac{I_{sam}}{I_{ref}} \right) \left(\frac{\eta_{sam}}{\eta_{ref}} \right)^2 \quad (2)$$

A is the measured absorbance, η is the refractive index of the solvent, I is the integrated emission intensity, and Φ_{ref} is the emission quantum yield of the reference. Φ_{ref} was taken to be 0.90 for R6G in water.^{14,15}

4.6 References

1. Luguya, R.; Jaquinod, L.; Fronczek, R. R.; Vicente, M. G. H.; Smith, K. M. *Tetrahedron* **2004**, *60*, 2757-2763.
2. Kruper, W. J., Jr.; Chamberlin, T. A.; Kochanny, M. *J. Org. Chem.* **1989**, *54*, 2753-2756.
3. Sibrian-Vazquez, M.; Jensen, T.J.; Fronczek, F. R.; Hammer, R. P.; Vicente, M. G. H. *Bioconj. Chem.* **2005**, *16*, 852-863.
4. Dean, M. L.; Schmink, J. R.; Leadbeater, N. E.; Brückner, C. *Dalton Trans.* **2008**, *10*, 1341-1345.
5. Gabrielsson, A.; Lindsay Smith, J.; Perutz, R. N. *Dalton Trans.* **2008**, 4259-4269.
6. Rothmund, P. *J. Am. Chem. Soc.* **1936**, *58*, 625-627.
7. Lindsey, J. S.; Schreiman, I. C.; Hsu, H. C.; Kearney, P. C.; Marguerettaz, A. M. *J. Org. Chem.* **1987**, *52*, 827-836.
8. Dogutan, K. K.; Bediako, D. K.; Teets, T. S.; Schwalbe, M.; Nocera, D. G. *Org. Lett.* **2010**, *12*, 1036-1039.
9. Jiang, M. Y.; Dolphin, D. *J. Am. Chem. Soc.* **2008**, *130*, 4236-4237.
10. Liu, W.; Greytak, A. B.; Lee, J.; Wong, C. R.; Park, J.; Marshall, L. F.; Jiang, W.; Curtin, P. N.; Ting, A. Y.; Nocera, D. G.; Fukumura, D.; Jain, R. K.; Bawendi, M. G. *J. Am. Chem. Soc.*, **2010**, *132*, 472-483.
11. Dunphy, I.; Vinogradov, S.A.; Wilson, D.F. *Anal. Biochem.* **2002**, *310*, 191-198.
12. Sinks, L. E.; Robbins, G. P.; Roussakis, E.; Troxler, T.; Hammer, D. A.; Vinogradov, S. A. *J. Phys. Chem. B* **2010**, *114*, 14373-14382.

13. Hauenstein, B. L. Jr.; Dressick, W. J.; Buell, S. L.; Demas, J. N.; DeGraff, B. A. *J. Am. Chem. Soc.* **1983**, *105*, 4251-4255.
14. Henderson, L. J. Jr.; Cherry, W. R. *J. Photochem.* **1985**, *28*, 143-151.
15. Magde, D.; Wong, R.; Seybold, P. G. *Photochem. Photobiol.* **2002**, *75*, 327-334.

Chapter 5

Luminescent Ruthenium Protein Scaffolds

Parts of this Chapter have been published:

Winter, M. B.; Mclaurin, E. J.; Reece, S. Y.; Olea, C.; Nocera, D. G.; Marletta, M. A. "Ru-Porphyrin Scaffolds for Sensing O₂" *J. Am. Chem. Soc.* **2010**, *132*, 5582-5583.

5.1 Motivation

The Marletta Lab at UC Berkeley has found the H-NOX (Heme Nitric oxide / O₂ binding) protein *Thermoanaerobacter tengcongensis* (*Tt* H-NOX) preferably binds O₂ over NO.¹ This is unusual for this family of proteins, which selectively bind NO. To explore the mechanism for this selectivity, we examine the accessibility of the heme to oxygen. Incorporation of an unnatural, luminescent porphyrin in place of the native heme allows spectroscopic exploration of oxygen diffusion into the heme domain through quenching of the porphyrin luminescence by oxygen. This chapter examines oxygen levels at the heme domain within Ru *Tt* H-NOX, comparing them with those of the O₂ binding protein Myoglobin (Mb) and examines the utility of Ru *Tt* H-NOX as an O₂ sensor.

5.2 Background

Quenching of luminescence is a well-established technique for examining small molecule diffusion within proteins.²⁻⁸ Substitution of a luminescent porphyrin for that of a heme can yield insight into the accessibility of the heme to small molecule quenchers of luminescence, namely O₂ and NO. Traditional methods for unnatural porphyrin incorporation into hemoproteins have limited their utility as biological tools. Harsh, denaturing conditions are typically required to remove native heme from proteins,^{9,10} dramatically decreasing the number of useful protein constructs. A recently reported method for incorporating unnatural porphyrins into hemoproteins during protein expression¹¹ avoids these harsh conditions.

The complex ruthenium(II) CO mesoporphyrin IX (RuMP) (Figure 5.1) exhibits bright, O₂-sensitive phosphorescence⁷ and is an ideal cofactor for protein-based sensors because it presents a proximal axial ligation site¹⁶ useful for stabilizing a porphyrin-protein complex. Myoglobin (Mb)

and the H-NOX (Heme Nitric oxide / OXygen binding) domain from the thermophilic bacterium *Thermoanaerobacter tengcongensis* (*Tt* H-NOX) are robust scaffolds for RuMP sensors, as they can be readily modified with genetically-encoded affinity tags and site-directed mutagenesis.^{12,13} In addition, *Tt* H-NOX is stable under extreme temperatures (>70 °C).¹³

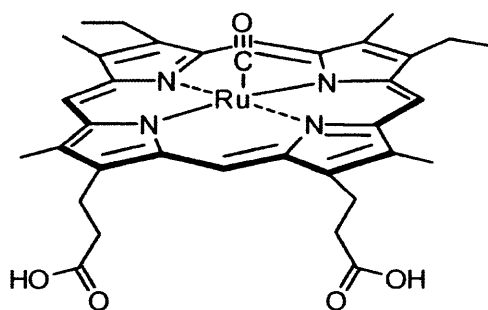


Figure 5.1. Chemical structure of M mesoporphyrin IX, where M is Ru in the unnatural porphyrin and Fe in the natural heme.

5.3 Results

5.3.1 Ru *Tt* H-NOX

Details for preparation and characterization of RuMP-substituted *Tt* H-NOX (Ru *Tt* H-NOX) are described in the experimental section. Briefly the Marletta Lab synthesized RuMP in a manner similar to published methods¹⁶ and incorporated it into *Tt* H-NOX during anaerobic protein expression. Ru *Tt* H-NOX was isolated with a stoichiometric amount of porphyrin and there was no detectible porphyrin loss for >24 hours under biological conditions (mouse plasma, 37 °C).

Crystallization of the purified Ru *Tt* H-NOX, work done at UC Berkeley, shows proper porphyrin insertion and preservation of the protein fold (Figure 5.2). Key contacts between the

protein and porphyrin are preserved, such as coordination of the proximal histidine to Ru and hydrogen bonding between the distal porphyrin ligand and a tyrosine residue.

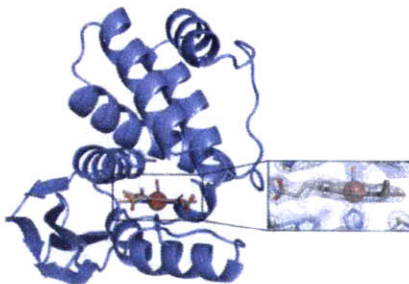


Figure 5.2. Structure of Ru *Tt* H-NOX showing the position of the Ru MP IX.

Steady-state and time-resolved spectroscopies were employed to examine the spectral properties of RuMP bound to the protein scaffold. The UV-visible spectrum for Ru *Tt* H-NOX shows a Soret band at 400 nm and α and β bands at 555 nm and 524 nm respectively (Figure 5.3). Steady-state emission spectra reveal red luminescence with a fairly low quantum yield (1.7×10^{-4} , red). The Ru *Tt* H-NOX emission is quenched in the presence of oxygen (orange). Time-resolved emission spectroscopy conducted to further probe the spectral features of the porphyrin-protein complex yielded single-exponential emission decays. The lifetimes of the Ru *Tt* H-NOX excited state in the presence and absence of oxygen are given in Table 5.1. The lifetime of Ru *Tt* H-NOX is quenched from 7.7 μ s to 2.9 μ s upon going from argon to air.

Measurement of the Ru *Tt* H-NOX excited state lifetime at several O₂ concentrations is presented on the right side of Figure 5.3. The data were analyzed according to the Stern-Volmer (SV) equation for O₂ quenching:

$$\frac{\tau_0}{\tau} = 1 + k_q \tau_0 [Q] \quad (9)$$

where τ_0 and τ are the excited state lifetimes in the absence and presence of quencher, respectively, k_q is the quenching constant, and pO_2 is the oxygen pressure. This analysis yielded a bimolecular quenching constant, k_q , of $1350 \text{ mmHg}^{-1} \text{ s}^{-1}$ ($8.2 \times 10^8 \text{ M}^{-1} \text{ s}^{-1}$). Emission quenching was observed to be linear across the biologically relevant range of O_2 concentrations (Figure 5.3, right).¹⁴

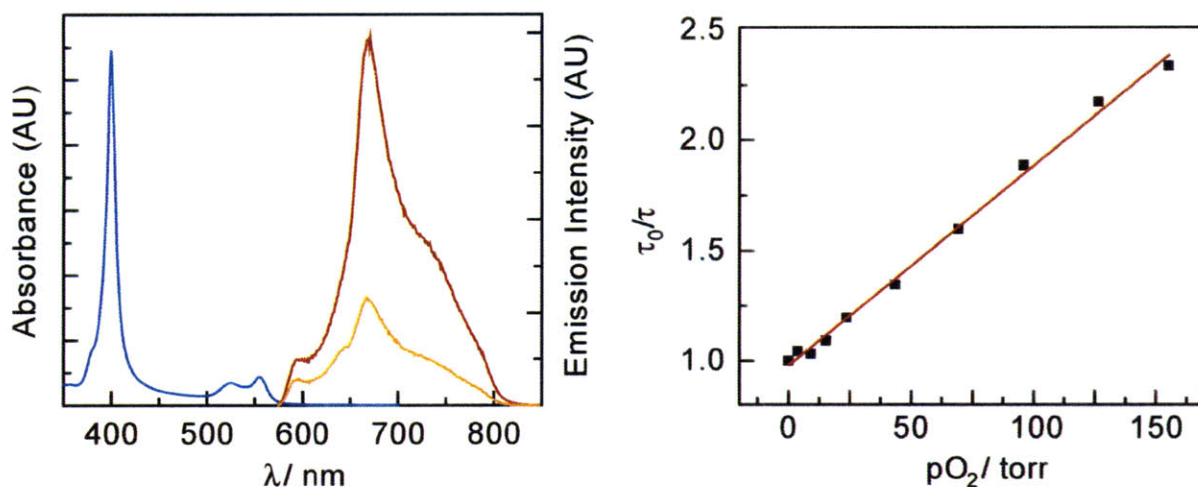


Figure 5.3. Absorption and emission spectra of Ru *Tt* H-NOX (left). The emission spectra are shown in the presence (orange) and absence (red) of oxygen. Stern-Volmer plot of Ru *Tt* H-NOX yielding a k_q of $1350 \text{ s}^{-1} \text{ torr}^{-1}$ (right).

Table 5.1. Steady-state and Time-resolved Emission Properties of Ru *Tt* H-NOX and Ru Myoglobin.

Protein	$\lambda_{\text{abs}} / \text{nm}$	$\lambda_{\text{em}}^a / \text{nm}$	Φ_{em}^c	$\tau_{\text{em}}^d / \mu\text{s}$	$k_q (\text{mmHg}^{-1} \text{ s}^{-1})$
Ru <i>Tt</i> H-NOX	400, 524, 555	668, $\sim 734^b$	1.7×10^{-4}	2.9, ^e 7.7 ^f	1350
Ru Mb	397, 518, 553	663, $\sim 733^b$	4.8×10^{-5}	12.2, ^e 37.3 ^f	~ 300

^a $\lambda_{\text{exc}} = 550 \text{ nm}$. ^b Shoulder. ^c $\lambda_{\text{exc}} = 550 \text{ nm}$, argon. ^d $\lambda_{\text{exc}} = 550 \text{ nm}$, $\lambda_{\text{det}} = 640 \text{ nm}$. ^e In air. ^f In argon.

5.3.2 Ru Mb

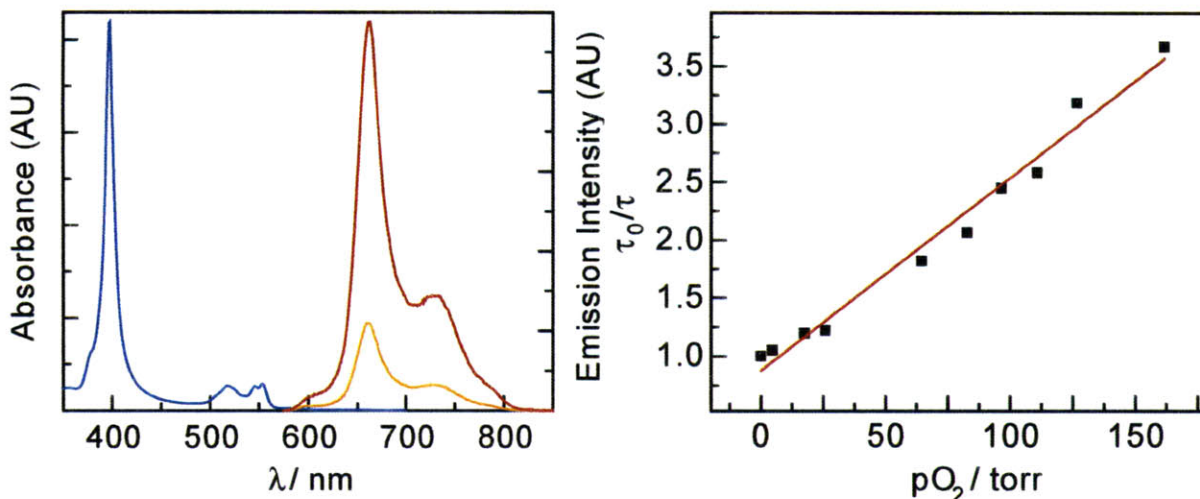


Figure 5.4. Absorption and emission spectra of Ru Mb (left). Emission spectra are shown in the absence (red) and the presence (orange) of oxygen. Stern-Volmer plot of the oxygen sensitivity of Ru Mb.

Ru Mb was prepared similarly to Ru *Tt* H-NOX. Incorporation of RuMP into Mb during anaerobic protein expression yielded Ru Mb, which was isolated with a stoichiometric amount of porphyrin. The UV-visible spectrum for Ru Mb shows a Soret band at 397 nm (Figure 5.4, left and Table 5.1). The α band at ~ 550 nm for Ru Mb is split, as observed previously.¹⁶ Excitation into the α band yields a sharp, oxygen sensitive emission band with a small shoulder and a quantum yield of 4.8×10^{-5} . Excited state lifetimes under anaerobic and aerobic conditions are given in Table 5.1. Further examination of the Ru Mb luminescence with respect to oxygen is shown in Figure 5.4 (right). Analysis using eq (9) yielded a k_q of $\sim 300 \text{ mmHg}^{-1} \text{ s}^{-1}$. However, changes in the absorption spectrum of Ru Mb after collection of the excited state lifetime data used in the SV analysis shows decomposition (Figure 5.5).

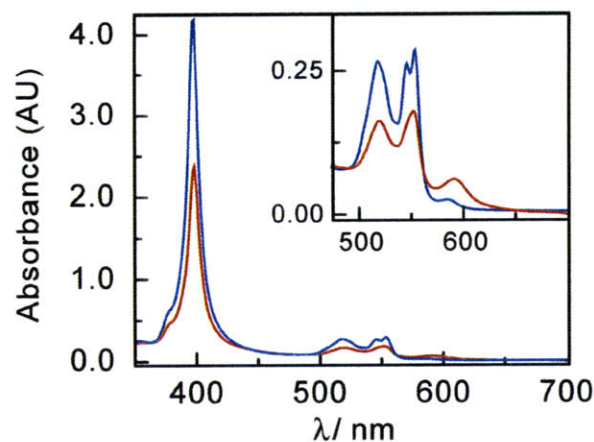


Figure 5.5. Absorption spectrum of Ru Mb before (blue) and after (red) laser excitation over a period of 8 hours.

5.4 Discussion

The high-resolution (2.00 Å) structure of Ru *Tt* H-NOX (Figure 5.2) is the first crystal structure of a Ru porphyrin bound to a protein and demonstrates that the unnatural porphyrin maintains key contacts with surrounding heme pocket residues. In fact, comparison of heme-bound *Tt* H-NOX with its Ru analogue indicates little perturbation of the protein fold (Figure 5.6).

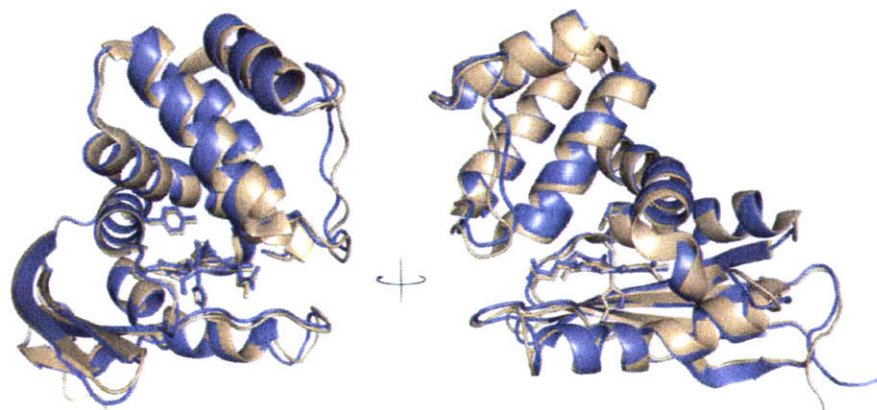


Figure 5.6. Overall alignment showing secondary structural elements of Ru *Tt* H-NOX (—) and heme-bound *Tt* H-NOX (molecule B, PDB 1U55)¹ (—) (~90° rotation shown).

Absorption spectra of both proteins show similar features, but the small differences highlight the complexity of the coordination environments within these proteins. The Soret, α , and β bands appear at similar wavelengths for both proteins. However, the α band of Ru Mb shows two peaks instead of one. This splitting at ~ 550 nm has been suggested to occur due to bending of the CO with respect to the metal center, as opposed to a linear arrangement found in the RuMP complex alone.¹⁵

Comparison of the steady-state emission spectra of Ru *Tt* H-NOX and Ru Mb reveals that O₂ appreciably quenches the emission of both proteins (Figure 5.3 and Figure 5.4, respectively). The emission of Ru Mb was blue-shifted as compared to Ru *Tt* H-NOX (Table 5.1) and the emission quantum yield was lower (4.8×10^{-5} vs. 1.7×10^{-4}). Although this could be attributed to a more polar coordination environment,¹⁶ the origins of the effect are difficult to resolve due to different porphyrin binding modes, solvent accessibilities, and heme pocket electrostatics in the two scaffolds. Such complexities could also account for the differences in emission peak shapes and excited state lifetimes ($\tau_0 = 37.3 \mu\text{s}$ for Ru Mb vs. $7.7 \mu\text{s}$ for Ru *Tt* H-NOX, respectively) that were observed.

Further examination of the excited state lifetime dependence on oxygen concentration provided additional evidence for the different porphyrin binding modes. SV plots for Ru *Tt* H-NOX and Ru Mb yielded k_q values of $1350 \text{ mmHg}^{-1} \text{ s}^{-1}$ and $\sim 300 \text{ mmHg}^{-1} \text{ s}^{-1}$, respectively. The uncertainty in the k_q value of Ru Mb is due to decomposition of the protein, observed through the absorption spectra (Figure 5.5). The decomposition may be due to loss of the CO ligand or oxidation of the Ru^{II} to Ru^{III}.¹⁶ The bimolecular quenching constants indicate that although the protein blocks O₂ from exhibiting diffusion-limited quenching,¹⁶ diffusion of O₂ through the

protein is still highly rapid. Taken together, these data indicate a substantially different conformation and/or chemical environment for RuMP in Mb and *Tt* H-NOX. Indeed, the crystal structure of Mb reveals that the heme is partially exposed to solvent,¹² whereas the heme in *Tt* H-NOX is buried within the protein matrix (Figure 5.2).

5.5 Conclusions

In summary, a new expression-based strategy for synthesis of RuMP proteins has yielded information about the accessibility of the heme domain within the proteins to oxygen. The spectroscopic data exemplified the differences between the Mb and *Tt* H-NOX domains. Additionally, Ru *Tt* H-NOX was found to be extremely stable and sensitive to O₂ levels within the biological range. This, along with the stability of Ru *Tt* H-NOX in mouse plasma, indicates the sensor has the ability to monitor O₂ levels in complex biological environments. Further exploration and improvement of *Tt* H-NOX sensors is presented in Chapter 6.

5.6 Experimental Section

Materials. The following chemicals were use as received: triruthenium dodecacarbonyl (Ru₃(CO)₁₂), D-(+)-glucose, triethanolamine hydrochloride (TEA), deoxyribonuclease I (DNase I), sodium phosphate (Na₂HPO₄), benzamidine hydrochloride, imidazole, and tris base from Sigma-Aldrich; hemin and mesoporphyrin IX dihydrochloride from Frontier Scientific; ampicillin, terrific broth (TB), isopropyl-β-D-thiogalactopyranoside (IPTG), and N-2-hydroxyethyl piperazine-N'-ethanesulfonic acid (HEPES) from Research Products International Corp.; glacial acetic acid and dimethylsulfoxide (DMSO) from EMD Chemicals, Inc.; sodium chloride (NaCl) and glycerol from Fisher Scientific; 4-(2-aminoethyl)-benzenesulfonyl fluoride

hydrochloride from Biosynth International, Inc.; Bio-Rad Protein Assay from Bio-Rad Laboratories, Inc. DNA primers for PCR amplification and site-directed mutagenesis were synthesized by Elim Biopharmaceuticals, Inc. and Integrated DNA Technologies, respectively. Ru(bpy)₃ was prepared as previously described.¹⁷

Ru^{II}(CO) mesoporphyrin IX. Synthesis and all subsequent manipulations of RuMP were carried out in low light. RuMP was prepared through modification of known methods.³ Triruthenium dodecacarbonyl, Ru₃(CO)₁₂, (180 mg, 0.282 mmol) and mesoporphyrin IX dihydrochloride (60 mg, 0.094 mmol) were refluxed, under N₂, in ~30 mL glacial acetic acid for 24-36 h. Reaction progress was monitored with UV-vis spectroscopy. The reaction product was cooled in an ice bath, precipitated through the drop wise addition of chilled ddH₂O, and collected on Whatman grade 42 filter paper (55 mm, Whatman International Ltd.), yielding a deep red-purple solid, which was formed quantitatively, as judged by UV-vis spectroscopy. The product was washed with several volumes of chilled ddH₂O and dried overnight under house vacuum. ESI-MS Calcd. (Found): [M – H]¹⁻ 693.2 (693.2).

Plasmids for protein expression. The gene for *Tt* H-NOX (residues 1-188 of *Tt*Tar4H from *Thermoanaerobacter tengcongensis*) was PCR amplified from an expression plasmid for insertion into the pCW vector. The 5' oligo, GGA ATT CCA TAT GAA GGG GAC AAT CGT CGG, was used to introduce a NdeI restriction endonuclease site. The 3' oligo, GCT CTA GAT CAG TGG TGG TGG TGG TGG TG, was used to introduce a XbaI restriction endonuclease site. The PCR product was double digested with XbaI and NdeI and ligated into the pCW plasmid. A stop codon was subsequently introduced at the 3' end of the *Tt* H-NOX gene using site-directed mutagenesis following the Quikchange protocol (Stratagene). The 5' oligo was GTT TTT GAG TAT AAG AAA AAT TGA GAG CAC CAC CAC CAC CAC, and the 3'

oligo was GTG GTG GTG GTG GTG GTG CTC TCA ATT TTT CTT ATA CTC AAA AAC. Sequencing of the final *Tt* H-NOX construct was carried out by Elim Biopharmaceuticals, Inc.

The mouse Mb construct in the pCW plasmid was used as described previously.⁴ The construct contained a N-terminal hexa-histidine tag to aid in purification.

Protein expression and incorporation of Ru¹¹¹CO mesoporphyrin IX. A modified method for unnatural porphyrin incorporation was used to express *Tt* H-NOX and Mb containing RuMP.⁴ Overnight cultures of RP523 *E. coli* cells were grown anaerobically in Hungate tubes (Bellco Glass, Inc.) as described,⁴ except antibiotic selection was carried out with 75 µg/mL ampicillin. TB media (9 L) containing 75 µg/mL ampicillin was sparged overnight in a 10 L fermentor vessel with house N₂ that had been passed through a 0.22 µm filter (Millipore). Sterile 0.2% D-(+)-glucose was added to the media immediately prior to inoculation with the overnight culture. The expression culture was grown at 37 °C to an OD₆₀₀ of 0.8-1.0 in the fermentor vessel while being continuously sparged with N₂. The media was then cooled to 25 °C and the fermentor was covered in aluminum foil before the addition of 3-6 µg/mL RuMP (from an ~200X stock in DMSO). Expression was induced with 1 mM IPTG and induction was allowed to occur for 18-22 h at room temperature while the culture was continuously sparged with N₂. *E. coli* pellets were harvested in the dark and stored at -80 °C following centrifugation.

Purification of *Tt* H-NOX and myoglobin containing Ru¹¹¹CO mesoporphyrin IX.

Purification of *Tt* H-NOX⁵ and Mb⁴ were carried out as described previously but with some modifications. All manipulations of Ru *Tt* H-NOX and Ru Mb during the purification were performed in the dark and/or behind aluminum foil.

For Ru *Tt* H-NOX, cell pellets (from 9 L of *E. coli* expression) were slowly thawed using warm water and re-suspended in ~100 mL of buffer A (50 mM TEA, pH 7.5, 50 mM NaCl), which also contained 1 mM 4-(2-aminoethyl)-benzenesulfonylfluoride hydrochloride and DNase I. The resuspended cells were lysed 3 times with an EmulsiFlex-C5 homogenizer (Avestin, Inc.) at 4 °C between 50,000 and 150,000 psi. The lysate was then heat-denatured at 70 °C for 30 minutes using a water bath. All further manipulations were carried out at 4 °C. The lysate underwent centrifugation with an Optima XL-100K ultracentrifuge (Beckman Coulter, Inc.) for 1 h at 42,000 rpm. The supernatant was passed at 2 mL/min over a Toyopearl SuperQ-650M anion exchange column (Tosoh Bioscience GmbH) that had been equilibrated with buffer A. The flow-through was concentrated to ~5 mL in a Vivaspin 20 10,000 MWCO PES spin concentrator (Sartorius Stedim Biotech). The protein (~2.5 mL per run) was exchanged into buffer B (50 mM HEPES, pH 6.2, 5% glycerol) by gravity using an ~100 mL Sephadex G-25 column. The protein was then applied at 0.5 mL/min to a Toyopearl CM-650M cation exchange column (Tosoh Bioscience GmbH) that had been equilibrated with buffer B. The column was washed at 0.5 mL/min with buffer B until the absorbance at 280 nm was steady. The protein was eluted with a NaCl gradient from 0% to 40% buffer C (50 mM HEPES, pH 6.2, 500 mM NaCl, 5% glycerol) over 90 mL while 2 mL fractions were collected. Fractions 25-40 were pooled and concentrated to less than 1 mL using a 10,000 MWCO spin concentrator. Finally, the concentrated protein underwent size-exclusion chromatography with a HiLoad 26/60 Superdex 75 column (GE Healthcare) that had been equilibrated with buffer A. The protein was separated with an isocratic flow of buffer A at 0.4 mL/min while 4 mL fractions were collected. Fractions 52-58 were pooled and concentrated with a 10,000 MWCO spin concentrator. Protein was stored at -

80 °C. The yield of Ru *Tt* H-NOX was ~5 mg/L of *E. coli* expression. Purity was assessed to be >90% by Coomassie stain following SDS-PAGE. ESI-MS Calcd. (Found): 22,012.4 (22,012).

For Ru Mb, all manipulations were carried out at 4 °C or on ice. Cell pellets (from 9 L of *E. coli* expression) were slowly thawed and re-suspended in ~100 mL of buffer D (50 mM sodium phosphate, pH 8.0, 200 mM NaCl, 1 mM benzamidine hydrochloride), which also contained 1 mM 4-(2-aminoethyl)-benzenesulfonylfluoride hydrochloride and DNase I. The resuspended cells underwent homogenization and centrifugation as described above. The supernatant was applied at 0.5 mL/min to a Ni-NTA Superflow column (Qiagen) that had been equilibrated with buffer D. The column was washed at 0.5 mL/min with buffer D containing 25 mM imidazole until the absorbance at 280 nm was constant. The protein was then eluted at 0.5 mL/min with buffer D containing 250 mM imidazole. The eluate was concentrated to ~ 3 mL using a Vivaspin 20 3,000 MWCO PES concentrator and loaded onto the size-exclusion column described above. The protein was separated with an isocratic flow of buffer E (100 mM HEPES, pH 7.5, 50 mM NaCl) at 0.4 mL/min and 4 mL fractions were collected. Fractions 53-57 were combined and diluted ~10-fold into buffer F (20 mM Tris, pH 8.0). The protein was then flowed at 5 mL/min over a POROS HQ/20 (10 x 100) anion exchange column (Applied Biosystems) equilibrated with buffer F. The eluate was concentrated and stored at -80 °C. The yield of Ru Mb was 0.5-1.0 mg/L of *E. coli* expression. Purity was assessed to be >90% by Coomassie stain following SDS-PAGE. ESI-MS Calcd. (Found): 17,892.5 (17,891).

Crystallization of Ru *Tt* H-NOX. All crystallization experiments for Ru *Tt* H-NOX were carried out in low light. Protein was exchanged into buffer G (20 mM TEA, pH 7.5) using a PD-10 desalting column (GE Healthcare) and then concentrated to ~50-60 mg/mL using a Vivaspin 500 5,000 MWCO PES spin concentrator. Crystals were grown using sitting drop vapor

diffusion in which 1 μL of the protein was mixed with 1 μL of reservoir solution and equilibrated against a 700 μL reservoir of 24% (w/v) PEG 3350 and 0.1 to 0.2 M lithium acetate at 20 °C. Crystals appeared within 24 h. Cryoprotection was achieved by titrating glycerol into the drop reservoir until a final concentration of 12.5% (v/v) was reached. The crystals were flash frozen in liquid N_2 for storage.

Physical measurements. All mass spectra were acquired by the QB3/Chemistry Mass Spectrometry Facility at the University of California, Berkeley. A mass spectrum of RuMP was obtained in negative ion mode with a quadrupole time-of-flight (Q-ToF) mass spectrometer equipped with an electrospray ionization (ESI) source (Q-ToF Premier, Waters). Protein mass spectra were acquired on an Agilent 1200 liquid chromatograph (LC) that was connected in-line with a LTQ Orbitrap XL mass spectrometer equipped with an ESI source (Thermo). The LC was equipped with a C8 guard (Poroshell 300SB-C8, 5 μm , 12.5 x 2.1 mm, Agilent) and analytical (75 x 0.5 mm) columns. Solvent A was 0.1% formic acid/99.9% water and solvent B was 0.1% formic acid/99.9% acetonitrile (v/v). Following sample injection, analyte trapping was performed for 5 min with 99.5% A at a flow rate of 90 $\mu\text{L}/\text{min}$. The elution program consisted of a linear gradient from 30% to 95% B over 24.5 min, isocratic conditions at 95% B for 5 min, a linear gradient to 0.5% B over 0.5 min, and finally isocratic conditions at 0.5% B for 9.5 min, at a flow rate of 90 $\mu\text{L}/\text{min}$. The column and sample compartments were maintained at 35 °C and 10 °C, respectively. Positive ion mass spectra were recorded over the range $m/z = 500$ to 2000. Measured charge state distributions were deconvoluted using ProMass software (version 2.5 SR-1, Novatia).

High performance liquid chromatography (HPLC) for determining the RuMP stoichiometry was carried out on a System Gold chromatograph (Beckman Coulter, Inc.). The LC was equipped with a 126 NMP Solvent Module, a diode array 168 NM Detector, and a Vydac C4 column (5 μ m, 4.6 mm x 250 mm). The RuMP-containing proteins were prepared in buffer H (50 mM HEPES, 7.4, 50 mM NaCl) and manually injected in 20 μ L volumes. Solvent A was 0.1% TFA/99.9% water. The elution profile consisted of a linear gradient from 0% to 100% solvent B (0.05% TFA/99.95% acetonitrile v/v) over 20 min, isocratic conditions at 100% B for 5 min, a linear gradient to 0% B over 5 min, and finally isocratic conditions at 0% B for 10 min at a flow rate of 1.0 mL/min. Peaks were integrated using 32 Karat software (version 7.0, Beckman Coulter, Inc.).

UV-vis absorption spectra were acquired on a Cary 3E, 300, or 5000 spectrophotometer (Varian). Steady-state emission spectra were recorded on an automated Photon Technology International (PTI) QM 4 fluorometer equipped with a 150-W Xe arc lamp and a Hamamatsu R928 photomultiplier tube. Sample excitation was carried out at 550 nm. Time-resolved emission measurements were made with pump light provided by the third harmonic (355 nm) of a Quanta-Ray Nd:YAG laser (Spectra-Physics) running at 10 Hz. The pump light was passed through a BBO crystal yielding a visible frequency that was tuned to 550 nm and employed to excite samples. All lifetime values were collected in triplicate. Anaerobic protein samples were obtained by exchanging the protein into anaerobic buffer H using a PD-10 column while inside a glove box (Coy Laboratory Products Inc.) maintained at 4 °C. Samples were brought into the glove box following 2 series of the following cycles: vacuum (20-25 psi), Ar, vacuum, Ar, vacuum, 90:10 high purity Ar:H₂ gas mixture. All gasses were purchased from Airgas. The proteins were kept anaerobic in a septum-sealed quartz cuvette. Aeration was achieved through

slow addition of air to the sample followed by equilibration through careful mixing. O₂ values were quantified using a fiber optic O₂ sensing system (Ocean Optics) equipped with a ruthenium-based probe (FOXY).

Relative quantum yields of samples, Φ_{sam} , were calculated using [Ru^{II}(bpy)₃](PF₆)₂ in water as the reference according to:

$$\phi_{sam} = \phi_{ref} \left(\frac{A_{ref}}{A_{sam}} \right) \left(\frac{I_{sam}}{I_{ref}} \right) \left(\frac{\eta_{sam}}{\eta_{ref}} \right)^2 \quad (2)$$

where A is the measured absorbance, η is the refractive index of the solvent, I is the integrated emission intensity, and Φ_{ref} is the emission quantum yield of the reference.⁶ Φ_{ref} was taken to be 0.053 for Ru(bpy)₃²⁺.⁷ All absorption and emission data were acquired at room temperature in buffer H.

X-ray diffraction data were collected for the Ru *Tt* H-NOX crystals using synchrotron radiation at Beamline 8.3.1 at the Advanced Light Source, Lawrence Berkeley National Laboratory (Berkeley, CA). Diffraction images were collected at 100 K with 1 s exposure times and 1° oscillation per frame. Data were processed using the HKL2000 suite⁸ and molecular replacement was performed using Phaser⁹ with PDB 1U55 as the search model. Model building was carried out using Coot¹⁰ and refined using Phenix.¹¹ The porphyrin ligand was refined using ruthenium mesoporphyrin as a model in the absence of any restraints. The final Ru *Tt* H-NOX structure was refined to a R_{work} of 21.0% (R_{free} of 23.3%) at 2.00 Å resolution.

5.7 References

1. Karow, D. S.; Pan, D.; Tran, R.; Pellicena, P.; Presley, A.; Mathies, R. A.; Marletta, M. A. *Biochemistry* **2004**, *43*, 10203-10211.
2. Khajehpour, M.; Rietveld, I.; Vinogradov, S. A.; Prabhu, N. V.; Sharp, K. A.; Vanderkooi, J. M. *Proteins: Structure, Function and Genetics* **2003**, *53*, 656-666.
3. Lakowicz, J. R.; Weber, G. *Biochemistry* **1973**, *12*, 4161-4170.
4. Barboy, N.; Feitelson, J. *Biochemistry* **1987**, *26*, 3240-3244.
5. Horie, T.; Vanderkooi, J. M.; Paul, K. –G. *Biochemistry* **1985**, *24*, 7931-7935
6. Beckham, S.; Cook, M. P.; Karki, L.; Luchsinger, M. M.; Whitlock, V. R.; Wu, Y.; Zhang, Q. F.; Schuh, M. D. *Arch. Biochem. Biophys.* **1994**, *310*, 440-447.
7. Vanderkooi, J. M.; Wright, W. W.; Erecinska, M. *Biochim. Biophys. Acta* **1994**, *1207*, 249-254.
8. Vanderkooi, J. M.; Wright, W. W.; Erecinska, M. *Biochemistry* **1990**, *29*, 5332-5338.
9. Teale, F. W. *Biochim. Biophys. Acta* **1959**, *35*, 543.
10. Schmidt, P.; Schramm, M.; Schröder, H.; Stasch, J. P. *Protein Expr. Purif.* **2003**, *31*, 42-46.
11. Woodward, J. J.; Martin, N. I.; Marletta, M. A. *Nat. Methods* **2007**, *4*, 43-45.
12. Dou, Y.; Maillett, D. H.; Eich, R. F.; Olson, J. S. *Biophys. Chem.* **2002**, *98*, 127-148.
13. Boon, E. M.; Marletta, M. A. *J. Am. Chem. Soc.* **2006**, *128*, 10022-10023
14. Helmlinger, G.; Yuan, F.; Dellian, M.; Jain, R. K. *Nat. Med.* **1997**, *3*, 177-182.
15. Srivastava, R. S. *Inorg. Chim. Acta* **1981**, *55*, L71-L74.

16. Paulson, D. R.; Addison, A. W.; Dolphin, D.; James, B. R. *J. Biol. Chem.* **1979**, *254*, 7002-7006.
17. Caspar, J. V. and Meyer, T. J. *J. Am. Chem. Soc.* **1983**, *105*, 5583-5590.

Table 5.2. Statistics of Crystallographic Data Collection and Refinement for the Ru *Tl* H-NOX structure.

Data Collection	
Space group	<i>P</i> 6 ₁ 22
Cell dimensions	
<i>a</i> , <i>b</i> , <i>c</i> (Å)	61.183, 61.183, 245.116
α , β , γ (°)	90, 90, 120
Resolution (Å)	50-2.00 (2.07- 2.00)
<i>R</i> _{merge} (%)	7.6 (30.7)
<i>I</i> / σ^a	26.7 (10.1)
Completeness ^a (%)	99.0 (96.0)
Redundancy	19.4 (19.4)
Refinement	
No. of reflections	19295
<i>R</i> _{work} / <i>R</i> _{free} ^b (%)	21.0/23.3
No. atoms	
Protein	1547
Porphyrin	43
CO molecules	1
Water molecules	98
<i>B</i> -factors	
Overall	37
Rms deviation	
Bond lengths (Å)	0.009
Bond angles (°)	1.020

^aThe values in parentheses relate to the highest resolution shells. ^b*R*_{free} is calculated for a randomly chosen 5% of reflections.

Conclusions and Future Directions

6.1 Preliminary Work on Pd *Tt* H-NOX

6.1.1 Motivation

Successful incorporation of RuMP into *Tt* H-NOX during protein expression opens the door for mixing and matching unnatural porphyrins and proteins with heme binding domains. The great stability of *Tt* H-NOX provides incentive to explore the protein properties upon incorporation of other unnatural porphyrins. Ru *Tt* H-NOX provided a good starting point for synthesis of a protein-based luminescent oxygen sensor in Chapter 5. However, the quantum yield of Ru *Tt* H-NOX was found to be 1.7×10^{-4} . The k_q value was also somewhat high at $1350 \text{ mmHg}^{-1} \text{ s}^{-1}$. Obtaining a protein sensor with improved quantum yield and a longer lifetime would provide sensitivity to lower oxygen levels as well as decreased measurement time, due to increased sensor brightness. Use of another metal center for the porphyrin generates a protein sensor with different photophysical properties, such as a longer excited state lifetime and higher quantum yield, as seen in Chapters 3 and 4.

Additionally, employing a FRET donor, such as a QD, as examined in Chapters 2 and 3, can also enhance the sensor brightness and possibly affect the oxygen sensitivity by changing the oxygen diffusion to the phosphor, as was seen with the QD-Os sensors in Chapter 2. Our knowledge of histidine/imidazole interactions with the chalcogenides, namely ZnS and CdS provides an alternative route for phosphor attachment to the QDs, which is especially useful with proteins, many of which contain histidine chains for purification.

This chapter investigates PdMP incorporated within *Tt* H-NOX as an oxygen sensor and as a FRET acceptor for increased multiphoton absorption. Methods of protein-QD binding and bioconjugation are also examined.

6.1.2 Background

Palladium porphyrins are characterized by long lived excited states with phosphorescence in the red or near-IR and thus have often been employed for phosphorescence quenching based oxygen sensing, including in biological systems. Investigations of Pd porphyrins in Chapters 3 and 4 found them to be excellent oxygen sensors because of their sensitivity and bright phosphorescence.

As discussed in Chapter 5, *Thermoanaerobacter tengcongensis* (*Tt* H-NOX) presents a H-NOX (Heme Nitric oxide / OXygen binding) domain that can be used as a scaffold for binding unnatural porphyrins.^{1,2} Incorporation of the luminescent porphyrin within the protein scaffold generates an optical oxygen sensitive protein. However, the quantum yield of Ru *Tt* H-NOX was less than 0.02%. Extension of the expression based unnatural porphyrin incorporation method used in Chapter 5 to PdMP yields a significantly brighter protein oxygen sensor.

QDs are known to have large two-photon absorption cross-sections³ and may transfer this useful photophysical property to molecules through energy transfer. Previous methods for sensor binding to QDs have employed amide or ester bond formation,^{4,5} click chemistry,⁶ charge interactions,⁷ and metal affinity coordination.^{8,9} Metal affinity coordination of histidines is well known. In fact, a Histidine-tag, consisting of 5 or more histidine residues, is often used to purify the proteins on columns composed of Cu^{2+} , Ni^{2+} , Co^{2+} or Zn^{2+} .¹⁰ Attachment of proteins to QDs using these his-tags has been previously explored.^{8,11} Extending this to Pd *Tt* H-NOX can generate a very powerful tool for oxygen sensing in biological systems.

6.1.3 Results and Discussion

6.1.4 Pd *Tt* H-NOX

Pd *Tt* H-NOX was prepared similarly to Ru *Tt* H-NOX, as described in Chapter 5. PdMP was incorporated into the protein during expression. Further details can be found in the experimental section.

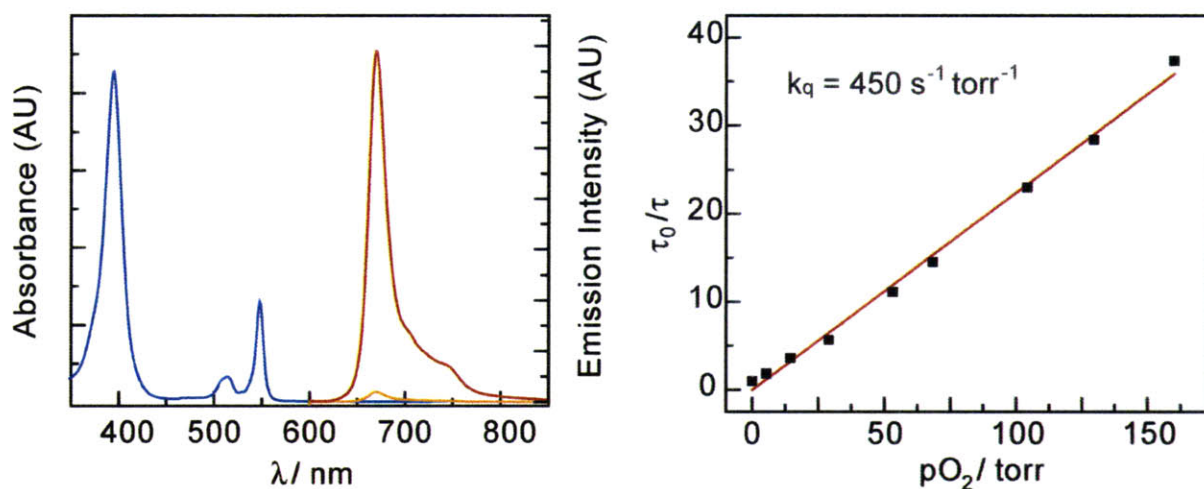


Figure 6.1. Absorption and emission spectra of Pd *Tt* H-NOX (left). Emission spectra are shown in the absence (red) and the presence (orange) of oxygen. Stern-Volmer plot of the oxygen sensitivity of Pd *Tt* H-NOX.

Spectroscopic characterization of Pd *Tt* H-NOX showed similar properties to Ru *Tt* H-NOX, but with a brighter, more strongly oxygen dependent emission in the red. Table 6.1 lists the photophysical properties of Pd *Tt* H-NOX and Ru *Tt* H-NOX. The absorption spectrum has a Soret band near the same wavelength as Ru *Tt* H-NOX, but a much stronger and sharper α band (Figure 6.1, left). The emission is also at approximately the same wavelength as that of Ru *Tt* H-NOX, but appears as a sharper band with a smaller shoulder. The quantum yield is 2.5%, more than two orders of magnitude larger than Ru *Tt* H-NOX and the excited state lifetime of 705 μs is significantly longer than that of Ru *Tt* H-NOX (7.7 μs). As a result of the longer lived excited

state, Pd *Tt* H-NOX was found to be more sensitive to oxygen. A Stern-Volmer plot (Figure 6.1, right) was generated using the SV equation:

$$\frac{\tau_0}{\tau} = 1 + k_q \tau_0 pO_2 \quad (1)$$

where τ_0 and τ are the excited state lifetimes in the absence and presence of quencher, respectively, k_q is the quenching constant, and pO_2 is the oxygen pressure. Pd *Tt* H-NOX displays linear oxygen sensitivity over the biological oxygen range and a bimolecular quenching constant of $450 \text{ mmHg}^{-1} \text{ s}^{-1}$

Table 6.1. Steady-state and Time-resolved Emission Properties of Ru *Tt* H-NOX and Pd *Tt* H-NOX.

Protein	$\lambda_{\text{abs}} / \text{nm}$	$\lambda_{\text{em}}^a / \text{nm}$	Φ_{em}^c	$\tau_{\text{em}}^d / \mu\text{s}$	$k_q (\text{mmHg}^{-1} \text{s}^{-1})$
Ru <i>Tt</i> H-NOX	400, 524, 555	668, ~734 ^b	1.7×10^{-4}	2.9, ^e 7.7 ^f	1350
Pd <i>Tt</i> H-NOX	394, 514, 548	670, ~745 ^b	2.5×10^{-2}	21.4, ^e 705 ^f	450

^a $\lambda_{\text{exc}} = 550 \text{ nm}$. ^b Shoulder. ^c $\lambda_{\text{exc}} = 550 \text{ nm}$, argon. ^d $\lambda_{\text{exc}} = 550 \text{ nm}$, $\lambda_{\text{det}} = 640 \text{ nm}$. ^e In air. ^f In argon.

6.1.5 QD-Pd *Tt* H-NOX

The QDs were prepared and water solubilized as previously described.^{12,13} Two types of QDs were generated: QDs with DHLA-PEG ligands¹² and QDs with DHLA ligands.¹³ The DHLA-PEG QDs are more stable than the DHLA QDs as the PEG groups better encapsulate the QD, are less labile, and prevent oxidation of the thiol groups. However, for protein coordination, some ligand dissociation from the QD is required.

Another concern is the large size of the protein as compared to small molecules. *Tt* H-NOX is comparable in size to the QDs (Figure 6.2) restricting the number of proteins that may coordinate

to the QD surface as well as increasing the FRET distance, r , eq (6). The distance from the heme domain in *Tt* H-NOX to the end of the protein, the point of QD coordination, is about 3 nm. Although this is a long distance, FRET is known to occur at distances up to 8 nm.¹⁴

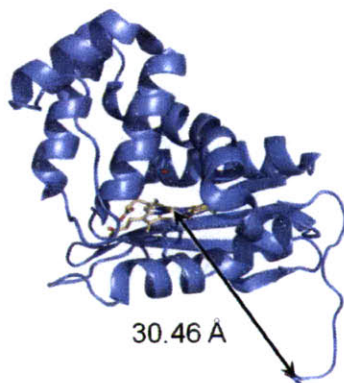


Figure 6.2. Structure of *Tt* H-NOX (left) and a close up of the distance from the heme to the terminal asparagine residue (right).

The first QD-Pd *Tt* H-NOX sample was prepared based on literature procedures. Briefly, Pd *Tt* H-NOX was added to the water solubilized DHLA-PEG QDs and incubated for 2 hours at room temperature in the absence of light. The sample was then purified using a desalting column. The steady state absorption and emission spectra of the sample are shown in Figure 6.3. The absorbance of the sample (blue) can be seen to be primarily QD. The sample was excited at 460 nm, where the porphyrin minimally absorbs, and the resulting emission in argon (red) shows a strong QD peak with very little Pd *Tt* H-NOX phosphorescence. In the presence of oxygen (air, orange), the QD emission remains unchanged, while the phosphorescence of the protein is quenched. The ratio of QD: Pd *Tt* H-NOX was calculated using the sum of the absorption spectra of the QD and the protein. There was less than one protein per QD (1:~0.1) indicating the QD emission is due mostly to QDs with no protein attached. Work by Dennis *et. al.* has shown there

is very little protein coordination when DHLA-PEG QDs are used, while DHLA QDs show higher amounts of protein coordination.⁸

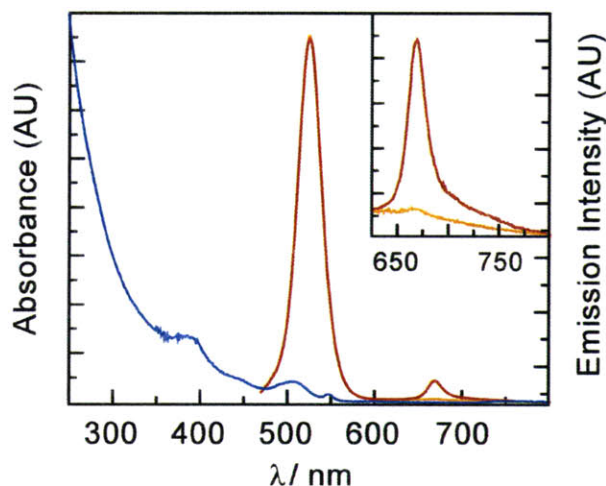


Figure 6.3. Absorption of the QD (blue) with the emission of the Pd *Tt* H-NOX in the absence (red) and presence (orange) of oxygen.

The smaller, more labile DHLA ligands offer the opportunity to ligate more protein to the QDs. To improve the stability of the DHLA-QDs, the samples were prepared just before use, as described in the experimental section. To examine the exchange interaction between the DHLA ligands and Pd *Tt* H-NOX, the steady-state emission of a mixture of the DHLA-QDs and Pd *Tt* H-NOX was monitored over time. Figure 6.4 shows the emission spectra of the sample over 150 minutes. The emission spectra were corrected for porphyrin emission not due to energy transfer because of the very high mixing ratio (1:62, QD: Pd *Tt* H-NOX). The spectra are separated into the first 60 minutes (left) and the following 90 minutes (right). Over the first hour, the QD emission peak decreases and the Pd *Tt* H-NOX emission increases, as expected. After the first hour, the sample was monitored for an additional 90 minutes. During this time, the emissions of both the QD and Pd *Tt* H-NOX decreased. The decrease in the QD emission is probably due to decomposition of the sample as opposed to energy transfer from the QD to Pd *Tt* H-NOX. Thus,

there is less energy transferred from the QD to Pd *Tt* H-NOX due to the darkening QD emission, and the emission of Pd *Tt* H-NOX decreases as well.

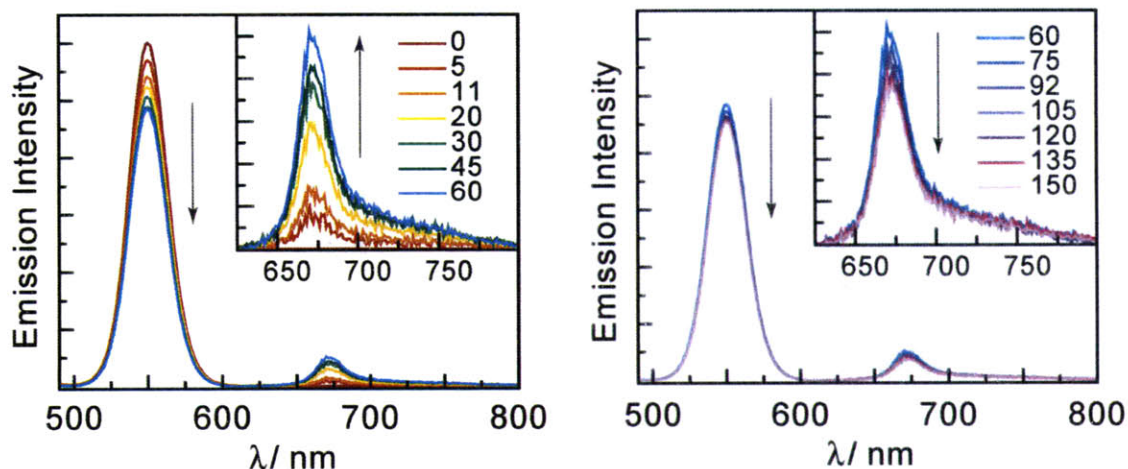


Figure 6.4. Emission spectra of a mixture of DHLA-QDs and Pd *Tt* H-NOX from 0 to 60 minutes (left) and from 60 to 150 minutes (right).

6.1.6 Conclusions

Work thus far with Pd *Tt* H-NOX has shown the protein to be stable, bright, and highly sensitive to oxygen. The 2.5% QY is significantly brighter than that of Ru *Tt* H-NOX, which was explored in Chapter 5. Pd *Tt* H-NOX is also significantly more sensitive to oxygen, which can be seen in the steady state emission quenching as well as in the bimolecular quenching constant, k_q .

6.2 Comparison of Selected Oxygen Sensors

To determine the feasibility of using oxygen sensors presented thus far for tumor imaging, comparison of them with other, well known optical oxygen sensors is required. Table 6.2 presents the optical properties of a variety of oxygen sensing molecules. In addition to intrinsic emission properties, such as quantum yields, the precision of lifetime-based O_2 sensors is governed by the instrument error associated with the lifetime measurement. Assuming an

instrument error of 2.5%, the precision for determining O₂ levels has been calculated and is shown for a variety of molecules listed in Table 6.2.

Table 6.2. Comparison of Various Optical O₂ Sensors in Aqueous Solution.

Complex	k_q (mmHg ⁻¹ s ⁻¹)	τ_0 (μ s)	Precision ^a (mmHg)	Φ_{em}
Oxyphor (R ₀) ¹⁵	259	711	0.28	0.06
Oxyphor (R ₂) ¹⁶	293	707	0.25	0.1
PtP-C343 ¹⁷	150	60	5.9	0.10
Ru ^{II} (bpy) ₃ ¹⁸	4300	0.58	21	0.053
QD-2	3000	0.163	105	0.23 ^b
QD1-R₀	750	36 ^c	2	ND
PolyPt3	870 ^d	57.3	1.0	ND
Ru <i>Tl</i> H-NOX	1350	7.7	5.0	0.00017
Pd <i>Tl</i> H-NOX	450	705	0.16	0.025

^a Determined assuming an error of 2.5% in τ_0 measurement. ^b Estimated from the enhancement factor (Figure 2.4). ^c Estimated from SV plot. ^d Estimated from τ_0 and τ_{air} . Oxyphor properties were determined in 2% BSA solutions. Φ_{em} for **QD1-R₀** and **PolyPt3** are estimated to be less than 0.01.

Using the Stern-Volmer equation and knowing the values of τ_0 and k_q , a precision can be estimated using the error in the τ_0 measurement (2.5%). The difference between τ_0 and 2.5% of τ_0 yields τ , as this is the smallest measurable difference. Using eq (11), the concentration of quencher can be estimated. As the error in measurement corresponds to uncertainty in both positive and negative directions, twice of this minimum represents the total precision of this measurement.

$$precision = \pm[Q] = \frac{1}{k_q} \left(\frac{1}{\tau} - \frac{1}{\tau_0} \right) \quad (1)$$

For example, Ru *Tt* H-NOX can be used to determine O₂ levels to within ± 2.5 mmHg, resulting in a precision of 5.0 mmHg, comparable to the precisions reported for commercial O₂ sensors (Table 6.2).

In addition to precision, the quantum yield of the optical sensor is an important factor in determining sensor performance. Quantum yields of phosphorescence are generally small as the transition from T₁ to S₀ is forbidden (Chapter 1). Table 6.2 exemplifies this as the highest performing optical O₂ sensors available are limited to quantum yields of about 10%. The higher the quantum yield, the brighter the sensor, resulting in decreased time required for measurements, a critical requirement for *in-vivo* experiments. Methods are available for circumventing these low quantum yields, such as QD FRET to a phosphorescent molecule, as outlined in Chapter 1. Additional consequences of the QD-phosphor attachment have also been seen to change the precision of the O₂ sensor (Chapter 2).

The popular commercial O₂ sensor Oxyphor R₀ presents good precision and quantum yield (0.28 and 0.06, respectively). The well-known low values of two-photon absorption (σ_2) for symmetric porphyrins inspired work in Chapter 3, in which QDs were used to increase the σ_2 of the porphyrin. The multifunctionality of the porphyrin proved problematic, so other, singly functionalized porphyrins were examined (Chapter 4). The resulting porphyrins obtained were only soluble in organic solvents. However, binding of platinum(II) 5-(4-carboxyphenyl)-10,15,20-triphenylporphyrin (PtTPPCOOH, Pt3) to a water soluble polymer engendered phosphor water solubility. The photophysical properties of this phosphorescent polymer, **PolyPt3**, are listed in Table 6.2, and a decent oxygen precision is observed. However, the quantum yield of the polymer is estimated at less than 1%, representing a severe limitation in its imaging utility. The recently investigated Pd *Tt* H-NOX is perhaps the most promising of the

molecular O₂ sensors in that it presents a good precision and quantum yield (0.16 and 0.025, respectively) in addition to promising energy transfer interactions with QDs, which may yield much larger two-photon phosphorescence.

6.3 Future Work

Two promising avenues are available for future work on QD-oxygen sensing systems. The first, the water soluble phosphorescent polymer (Pt bound imidazole polymer, **PolyPt3**), presents a molecule with good oxygen sensing precision. Although the quantum yield of the sensor is low, improvement of the quantum yield should be obtained upon integration of the polymer-porphyrin system with QDs. **PolyPt3** also enables an alternative route for synthesis of a QD-porphyrin conjugate as the porphyrin-polymer linkage may be obtained in organic solvents. Subsequent water solubilization of the QDs using this polymer may result in a brighter O₂ sensing system with possible improvements in O₂ sensitivity, as was seen with the Os-QD systems in Chapter 2.

Initial work in the second avenue, attaching Pd *Tt* H-NOX to QDs, has shown that despite the large size of the protein, energy transfer can occur, and an enhancement in emission of the protein is seen. However, the QD-Pd *Tt* H-NOX sensors made thus far show decomposition. Other types of QDs must be used to generate more stable, bright sensors. Future work will explore covalent attachment of the protein to the imidazole polymer QDs described in Chapter 4. Genetic modification of Pd *Tt* H-NOX gives the protein a cysteine functionality, which can be used for bioconjugation to maleimides. The imidazole QDs may be given maleimide functionality through amide bond formation to a maleimide linking molecule and further steps could yield Pd *Tt* H-NOX covalently bound to a QD through this linker.

6.4 Experimental Section

Materials. The following chemicals were used as received: cadmium oxide (CdO), decylamine, anhydrous N,N-dimethylformamide (DMF, 99%), D-(+)-glucose, triethanolamine hydrochloride (TEA), deoxyribonuclease I (DNase I), sodium phosphate (Na₂HPO₄), benzamidine hydrochloride, imidazole, tris base, and rhodamine 6G from Sigma-Aldrich; tri-n-octylphosphine (TOP, 97%), palladium(II) chloride, and dimethylcadmium from Strem; Selenium shot and 1-tetradecylphosphonic acid (98%, TDPA) (Alfa Aesar); trifluoroacetic acid (TFA, 99.9%) (J. T. Baker). Diethyl zinc (ZnEt₂) bis(trimethylsilyl)sulfide [(TMS)₂S] (Fluka); hemin and mesoporphyrin IX dihydrochloride from Frontier Scientific; ampicillin, terrific broth (TB), isopropyl-β-D-thiogalactopyranoside (IPTG), and N-2-hydroxyethyl piperazine-N'-ethanesulfonic acid (HEPES) from Research Products International Corp.; glacial acetic acid and dimethylsulfoxide (DMSO) from EMD Chemicals, Inc.; sodium chloride (NaCl) and glycerol from Fisher Scientific; 4-(2-aminoethyl)-benzenesulfonylfluoride hydrochloride from Biosynth International, Inc.; Bio-Rad Protein Assay from Bio-Rad Laboratories, Inc. DNA primers for PCR amplification and site-directed mutagenesis were synthesized by Elim Biopharmaceuticals, Inc. and Integrated DNA Technologies, respectively. Tri-n-octylphosphine oxide (TOPO) and hexadecylamine were distilled from 90% reagent grade materials (Sigma-Aldrich). Trioctylphosphine Selenide (TOPSe) was prepared by dissolving 5.92 g selenium shot in 50 mL TOP. Dihydro lipoic acid, amino-PEG and hydroxyl-PEG were prepared as previously described.^{12,13}

Pd^{II} mesoporphyrin IX. Synthesis and all subsequent manipulations of PdMP were carried out in low light. PdMP was prepared through modification of known methods.¹⁹ Mesoporphyrin

IX (100 mg) was refluxed with excess PdCl₂ (100 mg) in DMF (10 mL) in the dark for 8 hours. Reaction progress was monitored with UV-vis spectroscopy. The reaction product was cooled in an ice bath, precipitated through the drop wise addition of chilled ddH₂O, and collected on Whatman grade 42 filter paper (55 mm, Whatman International Ltd.), yielding a deep red-purple solid, which was formed quantitatively, as judged by UV-vis spectroscopy. The product was washed with several volumes of chilled ddH₂O and dried overnight under house vacuum. ESI-MS Calcd. (Found): [M – H]¹⁻ 698.5 (698.5).

Plasmids for protein expression. The gene for *Tt* H-NOX (residues 1-188 of *Tt*Tar4H from *Thermoanaerobacter tengcongensis*) was PCR amplified from an expression plasmid for insertion into the pCW vector. The 5' oligo, GGA ATT CCA TAT GAA GGG GAC AAT CGT CGG, was used to introduce a NdeI restriction endonuclease site. The 3' oligo, GCT CTA GAT CAG TGG TGG TGG TGG TGG TG, was used to introduce a XbaI restriction endonuclease site. The PCR product was double digested with XbaI and NdeI and ligated into the pCW plasmid. A stop codon was subsequently introduced at the 3' end of the *Tt* H-NOX gene using site-directed mutagenesis following the Quikchange protocol (Stratagene). The 5' oligo was GTT TTT GAG TAT AAG AAA AAT TGA GAG CAC CAC CAC CAC CAC, and the 3' oligo was GTG GTG GTG GTG GTG GTG CTC TCA ATT TTT CTT ATA CTC AAA AAC. Sequencing of the final *Tt* H-NOX construct was carried out by Elim Biopharmaceuticals, Inc.

Protein expression and incorporation of Pd^{II} mesoporphyrin IX. A modified method for unnatural porphyrin incorporation was used to express *Tt* H-NOX containing PdMP.⁴ Overnight cultures of RP523 *E. coli* cells were grown anaerobically in Hungate tubes (Bellco Glass, Inc.) as described,⁴ except antibiotic selection was carried out with 75 µg/mL ampicillin. TB media (9

L) containing 75 µg/mL ampicillin was sparged overnight in a 10 L fermentor vessel with house N₂ that had been passed through a 0.22 µm filter (Millipore). Sterile 0.2% D-(+)-glucose was added to the media immediately prior to inoculation with the overnight culture. The expression culture was grown at 37 °C to an OD₆₀₀ of 0.8-1.0 in the fermentor vessel while being continuously sparged with N₂. The media was then cooled to 25 °C and the fermentor was covered in aluminum foil before the addition of 3-6 µg/mL RuMP (from an ~200X stock in DMSO). Expression was induced with 1 mM IPTG and induction was allowed to occur for 18-22 h at room temperature while the culture was continuously sparged with N₂. *E. coli* pellets were harvested in the dark and stored at -80 °C following centrifugation.

Purification of *Tt* H-NOX containing Pd^{II} mesoporphyrin IX. Purification of *Tt* H-NOX⁵ was carried out as described previously but with some modifications. All manipulations of Pd *Tt* H-NOX during the purification were performed in the dark and/or behind aluminum foil.

Cell pellets (from 9 L of *E. coli* expression) were slowly thawed using warm water and re-suspended in ~100 mL of buffer A (50 mM TEA, pH 7.5, 50 mM NaCl), which also contained 1 mM 4-(2-aminoethyl)-benzenesulfonylfluoride hydrochloride and DNase I. The resuspended cells were lysed 3 times with an EmulsiFlex-C5 homogenizer (Avestin, Inc.) at 4 °C between 50,000 and 150,000 psi. The lysate was then heat-denatured at 70 °C for 30 minutes using a water bath. All further manipulations were carried out at 4 °C. The lysate underwent centrifugation with an Optima XL-100K ultracentrifuge (Beckman Coulter, Inc.) for 1 h at 42,000 rpm. The supernatant was applied at 0.5 mL/min to a Co column that had been equilibrated with buffer D. The column was washed at 0.5 mL/min with buffer D (50 mM sodium phosphate, pH 8.0, 200 mM NaCl, 1 mM benzamidine hydrochloride) containing 25 mM

imidazole until the absorbance at 280 nm was constant. The protein was then eluted at 0.5 mL/min with buffer D containing 250 mM imidazole. The eluate was concentrated to ~ 3 mL using a Vivaspin 20 3,000 MWCO PES concentrator and underwent size-exclusion chromatography with a HiLoad 26/60 Superdex 75 column (GE Healthcare) that had been equilibrated with buffer A. The protein was separated with an isocratic flow of buffer A at 0.4 mL/min while 4 mL fractions were collected. Protein was stored at -80 °C. Purity was assessed to be >90% by Coomassie stain following SDS-PAGE. ESI-MS Calcd. (Found): 23,180.7 (23,180).

CdSe/CdZnS Nanocrystals (TOPO-QD1s). CdSe QDs overcoated with alloyed CdZnS were prepared by modified literature methods.^{20,21} Briefly, CdO (0.128 g, 1.0 mmol), TDPA (0.418 g, 1.5 mmol) and TOPO (6 g, 15.5 mmol) were degassed at 320 °C for 1 hour. The resulting clear, colorless solution was cooled to 270 °C under N₂ and 1.5 M TOPSe (5 mL, 7.5 mmol) was rapidly injected into the flask. The resulting solution was heated at 220 °C until the first absorption feature of the core CdSe QDs was 470 nm. The bare CdSe NCs were precipitated twice with butanol and methanol and dispersed in 4 mL hexanes. The QDs were subsequently overcoated by injecting a hexane solution of the bare CdSe into a degassed solvent of TOPO (10 g, 25.9 mmol) and HPA (0.4 g, 2.4 mmol.). The hexane was removed in vacuo at 80 °C from the CdSe cores. Decylamine (0.25 mL, 1.3 mmol) was added to the solution, which was then stirred for 2 hours. Using a syringe pump, two separate solutions of (TMS)₂S in 5 mL TOP and a 90:10 molar ratio of ZnEt₂ and CdMe₂ in 5 mL TOP were added to the CdSe solution at 130 °C over the course of two hours. Amounts of (TMS)₂S, ZnEt₂ and CdMe₂ were chosen to yield a ~3 monolayer coating of ZnS on the bare CdSe QDs, using the methods of Dabboussi et al.⁸ yielding the QDs (FWHM = 32 nm Φ = 58%).

Water-soluble nanocrystals (DHLAPEG-QDs). The **TOPO-QDs** were isolated by repeated precipitation from hexanes with a mixture of n-butanol and methanol and re-dissolved in a minimal amount of CHCl_3 . In a separate vial, DHLA-hydroxyPEG (100 mg) and DHLA-aminoPEG (125 μL , 20% methanolic solution) were stirred and the solvent evaporated. Under N_2 , the chloroform QD solution was injected into the ligand mixture and stirred vigorously. The solvent of the QD-ligand mixture was removed and the reaction was stirred at 60 °C for three hours. Upon removing the reaction from heat, ethanol (0.5 mL) and chloroform (0.1 mL) were added. The QDs were precipitated from solution with hexanes (1 mL). The solution was then centrifuged (3900 rpm \times 5 min), decanted, and dialyzed (with 50 kDa MW cutoff spin concentrators, Millipore) to furnish aqueous QDs ($\lambda_{\text{PLmax}} = 526 \text{ nm}$, $\Phi = 16\%$).

Water-soluble nanocrystals (DHLA-QDs). The **TOPO-QDs** were isolated by repeated precipitation from hexanes with a mixture of n-butanol and methanol and re-dissolved in a minimal amount of CHCl_3 . An excess of freshly prepared DHLA was added to the QD solution. This mixture was heated at 60 °C under nitrogen for three hours. After cooling, the QDs were precipitated from solution with hexanes, isolated, and redissolved in aqueous solution.

DHLA-PEG QD-Protein Conjugates. **DHLAPEG-QDs** were filtered through a 200 nm syringe filter to remove aggregates. A concentrated solution of Pd *Ti* H-NOX was added to the QD solution, so the pink color of the protein could be seen. The mixture was incubated for two hours at room temperature in the absence of light. The sample was then purified on a desalting column with PBS. One fraction was collected and used in subsequent experiments.

DHLA-QD-Protein Study. A small amount of **DHLA-QDs** were added to a solution of the protein in a cuvette. The sample was not purified or stirred. Emission spectra were taken over two-and-a-half hours without disturbing the cuvette.

Physical measurements. All mass spectra were acquired by the QB3/Chemistry Mass Spectrometry Facility at the University of California, Berkeley. A mass spectrum of PdMP was obtained in negative ion mode with a quadrupole time-of-flight (Q-ToF) mass spectrometer equipped with an electrospray ionization (ESI) source (Q-ToF Premier, Waters). Protein mass spectra were acquired on an Agilent 1200 liquid chromatograph (LC) that was connected in-line with a LTQ Orbitrap XL mass spectrometer equipped with an ESI source (Thermo). The LC was equipped with a C8 guard (Poroshell 300SB-C8, 5 μm , 12.5 x 2.1 mm, Agilent) and analytical (75 x 0.5 mm) columns. Solvent A was 0.1% formic acid/99.9% water and solvent B was 0.1% formic acid/99.9% acetonitrile (v/v). Following sample injection, analyte trapping was performed for 5 min with 99.5% A at a flow rate of 90 $\mu\text{L}/\text{min}$. The elution program consisted of a linear gradient from 30% to 95% B over 24.5 min, isocratic conditions at 95% B for 5 min, a linear gradient to 0.5% B over 0.5 min, and finally isocratic conditions at 0.5% B for 9.5 min, at a flow rate of 90 $\mu\text{L}/\text{min}$. The column and sample compartments were maintained at 35 $^{\circ}\text{C}$ and 10 $^{\circ}\text{C}$, respectively. Positive ion mass spectra were recorded over the range $m/z = 500$ to 2000. Measured charge state distributions were deconvoluted using ProMass software (version 2.5 SR-1, Novatia).

UV-vis absorption spectra were acquired on a Spectral Instruments (SI) CCD array UV-vis spectrophotometer or a Cary 3E, 300, or 5000 spectrophotometer (Varian). Steady-state emission spectra were recorded on an automated Photon Technology International (PTI) QM 4 fluorometer equipped with a 150-W Xe arc lamp and a Hamamatsu R928 photomultiplier tube.

Sample excitation was carried out at 550 nm. Time-resolved emission measurements were made with pump light provided by the third harmonic (355 nm) of a Quanta-Ray Nd:YAG laser (Spectra-Physics) running at 10 Hz. The pump light was passed through a BBO crystal yielding a visible frequency that was tuned to 550 nm and employed to excite samples. All lifetime values were collected in triplicate. Anaerobic protein samples were obtained by exchanging the protein into anaerobic buffer H using a PD-10 column while inside a glove box (Coy Laboratory Products Inc.) maintained at 4 °C. Samples were brought into the glove box following 2 series of the following cycles: vacuum (20-25 psi), Ar, vacuum, Ar, vacuum, 90:10 high purity Ar:H₂ gas mixture. All gasses were purchased from Airgas. The proteins were kept anaerobic in a septum-sealed quartz cuvette. Aeration was achieved through slow addition of air to the sample followed by equilibration through careful mixing. O₂ values were quantified using a fiber optic O₂ sensing system (Ocean Optics) equipped with a ruthenium-based probe (FOXY) as described in Chapter 3.

Time-resolved emission data for Pd *Tt* H-NOX were analyzed according to the Stern-Volmer equation for O₂ quenching:

$$\frac{\tau_0}{\tau} = 1 + k_q \tau_0 [Q] \quad (2)$$

where τ_0 is the excited state lifetime in the absence of O₂, τ is the excited state lifetime at a certain O₂ concentration, and k_q is the bimolecular quenching constant.⁶

Relative quantum yields of samples, Φ_{sam} , were calculated using rhodamine 6G (R6G) or Rhodamine 101 (R101) in water as the reference according to:

$$\phi_{sam} = \phi_{ref} \left(\frac{A_{ref}}{A_{sam}} \right) \left(\frac{I_{sam}}{I_{ref}} \right) \left(\frac{\eta_{sam}}{\eta_{ref}} \right)^2 \quad (3)$$

where A is the measured absorbance, η is the refractive index of the solvent, I is the integrated emission intensity, and Φ_{ref} is the emission quantum yield of the reference.⁶ Φ_{ref} was taken to be 0.90 for R6G in water and 1.0 for R101 in water.^{22,23,24} All absorption and emission data were acquired at room temperature in buffer H.

Energy transfer analysis. The efficiency of energy transfer from the QD to Pd *Tt* H-NOX was evaluated using Förster analysis:

$$E = \frac{mk_{D-A}}{mk_{D-A} + \tau_D^{-1}} = \frac{mR_0^6}{mR_0^6 + r^6} \quad (4)$$

where k_{D-A} is the rate of energy transfer, r is the distance between the donor and acceptor, R_0 is the critical transfer distance or the distance at which half of the donor molecules decay by energy transfer, and m is the number of acceptor molecules per donor. Experimentally, E can be obtained as:

$$E = 1 - \frac{\tau_{D-A}}{\tau_D} \quad (5)$$

where τ_D is the lifetime of the QD donor alone and τ_{D-A} is the lifetime of the bound donor (**QD-Pd *Tt* H-NOX**).

While E may be experimentally determined from the excited state lifetime quenching, additional information is needed to quantify R_0 , r , and m :

$$R_0 = \frac{9000 \ln 10 \kappa^2 \Phi_D J}{128 \pi^5 n^4 N} \quad (6)$$

$$J = \int_0^{\infty} dv \frac{f_D(v)e_A(v)}{v^4} \quad (7)$$

where κ^2 is the relative orientation factor of the dipoles, taken to be $2/3$, Φ_D is the quantum efficiency of the donor, N is Avogadro's number, and n is the index of refraction of the medium, which is taken to be 1.4 in aqueous solution. The constants may be incorporated into one value, which is simply multiplied by Φ_D . Similarly, the latter half of the equation may be represented as J , the overlap integral, where $F_D(\lambda)$ is the normalized intensity of the donor and $\epsilon_A(\lambda)$ is the extinction coefficient of the acceptor at λ .^{14,25} R_o may thus be calculated for the overlap of the experimentally determined spectra.

The average number proteins attached to the donor, m , can be determined from the optical cross-sections of the donor and acceptor as well as the absorption spectra of the conjugated **QD-Pd Tr H-NOX** system. The absorption spectra of the conjugates may be taken as a sum of the absorption of the donor and acceptor. The donor:acceptor ratio and the concentrations of the conjugates may be calculated using the individual donor and acceptor absorption spectra, their known ϵ values, and Beer's law.

6.5 References

1. Dou, Y.; Maillett, D. H.; Eich, R. F.; Olson, J. S. *Biophys. Chem.* **2002**, *98*, 127-148.
2. Boon, E. M.; Marletta, M. A. *J. Am. Chem. Soc.* **2006**, *128*, 10022-10023
3. Larson, D. R.; Zipfel, W. R.; Williams, R. M.; Clark, S. W.; Bruchez, M. P.; Wise, F. W.; Webb, W. W. *Science* **2003**, *300*, 1434-1436.
4. Snee, P. T.; Somers, R. C.; Nair, G.; Zimmer, J. P.; Bawendi, M. G.; Nocera, D. G. *J. Am. Chem. Soc.* **2006**, *128*, 13320-13321.
5. Medintz, I. L.; Clapp, A. R.; Brunel, F. M.; Tiefenbrunn, T.; Tetsuo Uyeda, H.; Chang, E. L.; Deschamps, J. R.; Dawson, P. E.; Mattoussi, H. *Nat. Mater.* **2006**, *5*, 581-589.
6. Bernardin, A.; Cazet, A.; Guyon, L.; Delannoy, P.; Vinet, F.; Bonnaffe, D.; Texier, I. *Bioconj. Chem.* **2010**, *21*, 583-588.
7. Shi, L. X.; Hernandez, B.; Selke, M. *J. Am. Chem. Soc.* **2006**, *128*, 6278-6279.
8. Dennis, A. M.; Sotto, D. C.; Mei, B. C.; Medintz, I. L.; Mattoussi, H.; Bao, G. *Bionconj. Chem.* **2010**, *21*, 1160-1170.
9. Somers, R. C.; Bawendi, M. G.; Nocera, D. G. *Chem. Soc. Rev.* **2007**, *36*, 579-591.
10. Hochuli, E.; Bannwarth, W.; Döbeli, H.; Gentz, R.; Stüber, D. *Nature Biotech.* **1998**, *6*, 1321-1325.
11. Goldman, E. R.; Medintz, I. L.; Whitley, J. L.; Hayhurst, A.; Clapp, A. R.; Uyeda, H. T.; Deschamps, J. R.; Lassman, m. E.; Mattoussi, H. *J. Am. Chem. Soc.* **2005**, *127*, 6744-6751.
12. Liu, W.; Howarth, M.; Greytak, A. B.; Nocera, D. G.; Ting, A. Y.; Bawendi, M. B. *J. Am. Chem. Soc.* **2008**, *130*, 1274-1284.

13. Mattoussi, H.; Mauro, J. M.; Goldman, E. R.; Anderson, G. P.; Sundar, V. C.; Mikulec, F. V.; Bawendi, M. G. *J. Am. Chem. Soc.* **2000**, *122*, 12142-12150.
14. Lakowicz, J. R., *Principles of Fluorescence Spectroscopy*, 3rd ed.; Springer: New York, 2006.
15. Lo, L. W.; Koch, C. J.; Wilson, D. F. *Anal. Biochem.* **1996**, *236*, 153-160.
16. Dunphy, I.; Vinogradov, S. A.; Wilson, D. F. *Anal. Biochem.* **2002**, *310*, 191-198.
17. Finikova, O. S.; Lebedev, A. Y.; Aprelev, A.; Troxler, T.; Gao, F.; Garnacho, C.; Muro, S.; Hochstrasser, R. M.; Vinogradov, S. A. *Chem. Phys. Chem.* **2008**, *9*, 1673-1679.
18. Oter, O.; Ribou, A. C. *J. Fluoresc.* **2009**, *19*, 389-397.
19. Cowan, J. A.; Gray, H. B. *Inorg. Chem.* **1989**, *28*, 2074-2078.
20. Dabbousi, B. O.; Rodriguez-Viejo, J.; Mikulec, F. V.; Heine, J. R.; Mattoussi, H.; Ober, R.; Jensen, K. F.; Bawendi, M. G. *J. Phys. Chem. B* **1997**, *101*, 9463-9475.
21. Aldana, J.; Wang, Y. A.; Peng, X. *J. Am. Chem. Soc.* **2001**, *123*, 8844-8850.
22. Henderson, L. J. Jr.; Cherry, W. R. *J. Photochem.* **1985**, *28*, 143-151.
23. Magde, D.; Wong, R.; Seybold, P. G. *Photochem. Photobiol.* **2002**, *75*, 327-334.
24. Karstens, T.; Kobs, K. *J. Phys. Chem.* **1980**, *84*, 1871-1872.
25. Förster, T. *Ann. Phys.* **1948**, *2*, 55-75.

Acknowledgements

The longer you stay in graduate school, the more people you have to thank.

Let me start with Cliff Kubiak, and his wonderful wife Pam, for encouraging me to pursue chemistry at a graduate level and convincing me to apply to MIT, a place I never thought I was good enough to get into. Thankfully, you did Cliff. The Kubiaks have also continued to support me throughout my time at MIT, spending time with me at conferences and welcoming me during my visits back to UCSD.

Karen, Nathaniel, and Ethan Nocera have always been welcoming during the winter and summer events held at the Nocera household. It's been awesome to see Nathaniel and Ethan grow up. Nathaniel, you're a total Californian now. Karen is one of the most wonderful people I know and I feel lucky to have her as a part of my life.

Dan, you have molded me. I realize more and more each day just how much you taught me. I'll miss our days at the Muddy and the Miracle. I am glad you gave me a chance to join your lab and work with you and the other talented people you attract. You've always been able to see things how they are, to have an uncanny ability to read people and give them what they need in order to learn and grow as scientists. I appreciate you being patient with me and allowing me the time I needed to figure things out.

I couldn't ask for a better thesis chair than Moungi. His personality is so opposite Dan's, but that only made them more complimentary as far as advisors go. He is a resource I wish I had used more while I was at MIT. I appreciate more and more the quality of work that has come out of his lab and the small but critical details he taught me during the times we met. He was always

free with his time and very understanding of graduate students. He also made a fantastic faculty REF.

Allison, I am so indebted to you, especially with this whole thesis thing. I am glad we had time to hang out and I got to get to know you. I'm sorry I never made it to one of your BBQs, maybe this summer. You really hold the lab together these days. I have so many favorite Allison moments it's been hard to pick the best. It might be when we were at Noir and they were trying to get us to leave, even though it wasn't closing time yet, and you insisted on sitting and finishing our drinks, rightly so. You gave me your lip gloss that night. That was nice. I think my best memories might be from the ACS meeting in SF last March and getting into fights with that Scottish guy, as well as the other fun stuff we did then.

My labmates, both senior and junior, have taught me loads over the years. Becky welcomed me into the lab and did her best to help me get my project together and steer me in the right direction along the way. You always worked hard and were a good role model for me. I only worked with Preston briefly, but it was an experience. I didn't have a chance to appreciate how well you understood the art of quantum dot synthesis until after you were gone, but I won't ever forget it now. I feel very lucky to have worked so closely with Andrew Greytak while at MIT. He was always patient, a good teacher, and ridiculously intelligent. I'm sure he'll do well at USC. I wish him, his wife Sarah and his two little boys the best of luck. I still tear up a bit every time I think about Peter Curtin. You were so smart and so good at science Pete, I wish I could have worked and hung out with you more. The huge amount of work you achieved in your short time at MIT is only a small testament to how much you loved science. And finally for the sensing project, Chris Lemon, who was brave enough to join the project with so little time left

for overlap with the people currently on it. Chris, you work too hard, remember to go to Characters and have fun. There will always be more columns.

I've had many other friends and mentors in the lab over the years. The oldest students when I joined, Julien, Justin, Jenny, and Joel all taught me different things. Julien helped me learn calculations and the computer cluster, Justin helped me with spectroscopy and getting to know Cambridge, Joel taught me how to get along with Dan and that porphyrin synthesis is hard. Finally, Jenny is one of my best friends still. She taught me everything from how to run columns better to how to get along with all the different personalities in lab as well as how to hang out with the hockey team, since sadly I never learned to play hockey. I'm excited to be in the same state as her again.

Arthur and Streece were the next most senior in lab when I joined. They both helped me out in so many ways and are still good friends. Arthur helped me with the glove box when I was making dimolybdenum compounds. He also helped me with the high vac line and any other random questions I had. He was always there to help in addition to being a great friend, sharing his friends with me as well. And he has fantastic taste in food and drinks. Streece, you know I could write a novel about all the ways you helped me, but apparently google is indexing our theses now so that might be too much information. It has been frustrating at times to get advice from you, because it's not what I want to do, but you are always right, dammit. I appreciate you continuing to give me advice, listen to me, and ultimately be a great friend. I hope we get to work together again soon.

Mike Winter is the most awesome scientist I know. He has made me like biochemistry, which I was pretty adverse to before we started working together, and I think I may have imprinted a

little inorganic/physical chemistry on him as well. I miss cowboying experiments with you and I hope we can work together again too, maybe with Streece...

Ted Betley and Dr. Kanan (said in Ted's high pitched sexy voice) were my first postdocs, and as a postdoc now I try to be as helpful as you both were to me to the grad students I work with. Ted I'm glad you are a professor and teaching others. I still think of advice you gave me. My favorite pieces of advice are "don't do anything your advisor asks you to until they've asked for it three times" and when you told me there were three things I could do "waste time, figure it out, or start over". Matt I hope we can hang out in Palo Alto. You have one of my favorite senses of humor, ever. You have a way of understanding chemistry that I admire, okay, I'm jealous of it, but it gives me something to strive for. And Dino, thanks for those late Saturday nights helping me make that ridiculous molybdenum compound. I still remember when you showed me the blue color change. I never would have figured that out on my own.

"Big" Emily was my WIC mentor to begin with. You said so many things to me that were spot on when I was just starting at MIT, and you continued to be friendly and willing to talk throughout your time there. Liz is still a force to be reckoned with. Both a lover of kittens and hockey her personality was characterized by a soft side as well as her "angry" side. Good luck at Amherst, I'm sure you'll do well and inspire many young women. Glen, vitamin G, Glennis, I will always miss you. You were so quiet but understood things so well. You made up the trio that was the most welcoming to me at MIT. I'm glad you're still doing science. The other members of the trio, Arfox and maNiS (I can never get the spelling right), also helped me adjust and understand the environment I was in. I still miss the nights we'd hang out at the miracle after hours. I'll see you in the Midwest Chris, and Alex, well, I saw you Sunday, I'm sure I'll see you again soon. Quit twitching.

Thanks to JB for letting us hang out at the Miracle late and then Dennis for taking over after JB left. You'll always be my bartender Dennis. Nate, I miss you, I hope we can play video games together sometime. You are awesome for letting me DJ at the Middlesex. Sully, thanks for always being a sweetheart to me. I'll miss your Boston/Cape Cod accent. And your poker tattoos. Annie I'll miss hanging out with you. At least I have pictures of a snowman to remember you by. Justin you're an awesome guy and maybe I'll run into one of these days when you're traveling. Let me know if you need help with organic chemistry. 'shuta I'm glad I was still in Cambridge when you started bartending. You're too nice to be a bartender there. There are bigger and better things in store for you. Thanks also to all the other Miracle and Middlesex employees I've importuned over the years.

I have to give a shout out to JP at Cambridge Common. Although I didn't know him for that long, he was always welcoming and as far as Sunday mornings go, he was the most pleasant person I have ever known.

Bryan and Joel are awesome because they can love chemistry and hip-hop at the same time. And they're both better at mixing than I am. I hope you guys get some gigs and your PhDs. Thanks also to WMBR especially Frank who trained me and Jimizz who was a great mentor. Becky was a great station manager as well as a good friend. I enjoyed having a non-chemistry outlet and I got to meet a lot of awesome people in the process.

Then there were my classmates, Tim, Montana, and Changhoon. We were lucky we all wanted to work on different things. I think that made it easier for us to get along and help each other out. You all were a good class to be a part of. I'll never forget your sense of humor, or pizza, Tim. Montana, thanks for being a good friend and drinking buddy. I hope you get to live in Ithaca

soon. Changhoon, I think you are the friendliest person in lab. It was nice to work next to you.

You are a meticulous scientist and I'm sure you'll do well wherever you end up next.

My other classmates, Lindsey, Annie, Keith, and Evan especially, were also good friends.

Lindsey it was great to have you as a sensing buddy and also a great girlfriend. Annie and Evan I wish you both all the best. I hope you stay in Boston so I can see you. Keith, good luck with science. I know it's something you love. You and Natalie are two of my favorite Midwesterners.

Marshak, you've always been a great friend, and I think our similar personalities bode well for being friends forever. Treat Casandra right dammit. I'll do my best with Gabe too. Yogi, don't do any reactions in vials on the stir plate, stick to being the fantastic electrochemist you are. I'm excited you're joining the dark side (nano science). Hannah, I wish you had stayed at MIT, but I think you made the right decision. Maybe I'll get to work with you again some day. Jay, of all the cold people I've met, they still wouldn't have worn a sweater in August in Boston when it was in the 80s and humid out. I hope you find your way into politics.

Tom, you're one of the easiest people to work with I know. Good luck conveying to others your criticism without offending people. Just remember, they need to take it less personally. Dorothy, Dan said after my defense I had always kind of been glue for his lab. I got less good at it over time, but you've definitely stepped in and I'm sure you will help hold the Nocera ship together. Keep rocking at hockey. I hope I can see you play again. Arturo, I always had fun with you. I know I chewed you out a few times, and I still feel bad for that, but I knew you could take it. I couldn't be happier you took on the RNR project and I hope you get to do the fun experiments you have planned with your pulsed EPR.

Casandra, I miss you tons and I hope you come visit me. You have learned so much since you came to MIT and although it might be painful I hope you know it'll be worth it in the end. Call

me whenever. That goes for you too Christina. Good luck with your kitty and binding constants. And remember you're the best dancer in lab, by far. Andrew Uhlman, I wish I had understood your sense of humor better earlier on. I also wish we had gotten to hang out more often. Lisa, I'm glad you came to further represent UCSD in Dan's lab. I also wish we had gotten to hang out more often, you just live so far away! Kwabena, I still remember you during visiting weekend. You were excited about science and joining Dan's lab then and I know you still are. You're a great person to continue Yogi's work. Play good music in the lab.

Rick, you joined the lab just as Streece was leaving. You were willing to work with me and always patient and helpful when I couldn't get the laser to work just right. I value our chats and I hope you and Audrey are happy. Danny, you had all the pressure of stepping in right where Streece left off. You were thrown into things quickly and only with a 2nd/3rd year graduate student to try to help you. You were able to master the nanosecond TA system anyway and have gone on to be a role model and resource in our lab. Good luck teaching graduate students in the future.

Jon and I met at the B-side sometime before he joined the lab. You've always been a relaxed guy who is interested in science and research but unwilling to let it control his life. It's something I always admired. Alex, I still remember your first day in the lab, our welcome dinner you attended knowing nothing about the group. You took your introduction in stride and the same could be said for all the following hits the members of the lab took at you, although I think they were all in good fun. That sounded bad, I just mean to say you've got a great sense of humor and I'm sad we never went to the races. I'm not at MIT anymore though so I can't help you get papers. And don't call Tom on the lab phone late at night to talk trash about Lebron. That's mean.

Dilek, you are such a kind, patient person. I appreciate all the help you gave me with synthesis and I hope we can hang out again soon. You are so much the lab mother, make sure to take care of yourself too. Danna, I'm glad we got to work together for a bit. I've always considered myself a physical inorganic chemist, but your understanding of magnetism puts me to shame. Bob, it was nice to have another Mic in the lab. You've been a great labmate and drinking buddy. Good luck with real jobs and take care of Meaghan (I don't know the spelling). Stas, we're very lucky you joined our lab and got some oxo chemistry going. You obviously are able to take initiative and do well, but you are patient enough to help and teach others too. The two don't often go hand-in-hand, and I'm glad I got to know someone who could do both. Costi, I wish we had been able to talk about science more often. You were a resource I barely began to use before I left. I am sure you'll be a resource to others in the lab.

Pat you are one of the great postdocs I have known. You're helpful, smart, and extremely competent. I only wish I could have learned more from you while I had the chance. I hope you become a professor so you can teach others because you're really good at it. Mircea I feel the same about you. I'm glad you became a professor because I know you'll do a good job and continue helping out us helpless graduate students. Here's to hanging out at a conference in California again soon.

I owe so much to many members of the Bawendi lab. Gautham was willing to help me look at QD lifetimes or two-photon spectra and come hang out and spin records and talk about death metal. Wen was always upbeat despite the fact he worked so hard and really developed a lot of QD technology that helped me through my PhD. Peter Allen and I commiserated for a while, moping about being away from California, but it all worked out in the end for both of us. See

you on the West coast. Hee-sun is another person I owe a lot to. She's always been helpful and knows way more about QD synthesis and bioconjugation than I do.

The ChemREFS were a fantastic group to have been a part of. Brian, you always took initiative to do things and more of us might have stepped in if you hadn't been so good at it. Alicia and Kevin were great fellow classmates to be REFS with. I'm excited for the new REFS too. I think it's a great program to have at MIT and I hope people can continue improving it as time goes on.

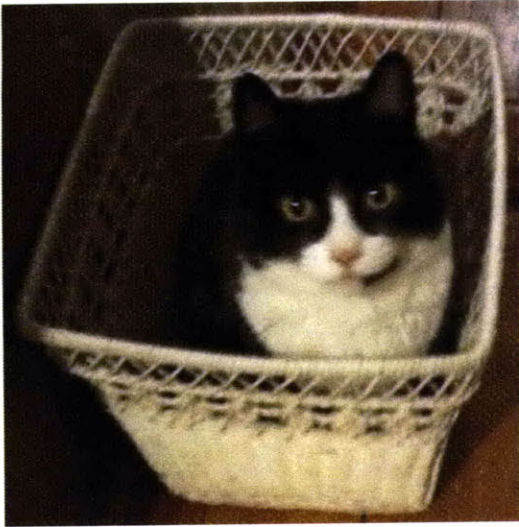
Markus and I only worked together for six months or so, and the fact that we became so close in that short of a time says a lot. He's always been laid back but able to get work done, that magical trait so many Europeans have, and having his more relaxed presence in lab was a blessing. You've made me excited about every German I get to work with now, although of course they're not you.

My family has always supported me. Even when we didn't talk for months at a time my mother was patient and waited for me to call her back without taking it personally or retaliating in some form or other. She gave me research skills from a very young age, refusing to tell me how to spell words when I asked, suggesting rather that I look them up in a dictionary. Although it was annoying at the time, it's benefited my patience and understanding of the English vocabulary. She has patience and understanding for scientists I'm not sure I'll ever have, knowing when to ask questions and just sooth through talking and when to be quiet to get me to finally talk. My father brought me up as a scientist. His passion for learning was imprinted on me at a young age and I doubt I would have become a chemist if I hadn't experienced the wonders of swimming pool pH and bromine testing. After all, who doesn't love color changes. My brother was never bitter about his overachieving older sister. It helped that our parents did our best not to compare us, but there are always people who will. He has always been interested in

my life and willing to chat on the phone more so than any other man I've known. I know I've frustrated him, and the rest of my family over the years, but he hasn't held a grudge against me. Then there's Lucy. It's strange for me to look at you and see myself so much, but you're so different. I think we might be most alike in appearance after all. I admire your interest in physics, although I can't say I understand it at all. Well, that's not exactly true. I imagine it parallels my interest in chemistry, which stems from a desire to better understand our physical world. Studying physics is probably a better way to do that though. Remember to have fun while you're working though. I've never regretted going to a baseball game or away for a weekend. I have regretted missing out on activities because I was working though.

Nancy and Nicole have continued to be roommates although we haven't been living in the same city. Nancy I always enjoyed your visits. You were much more brave about visiting me in the cold than I would have been. Nicole I had fun meeting up with you in So Cal. I'll see you more often now that I'm back on the west side, I'm sure. Lee you'll always be my best friend. It was nice to see you a couple times in Boston. It was more fun to see you in San Francisco. You're such a city girl now. Here's to hanging out at your employer's base every month or so. Paul I'm so happy we've kept in touch over the years. I'm sorry for every New Year's Eve party I've missed and I hope you keep having them. I still think about you whenever I see a corrosive 8 sticker (which is often).

Kiley has been a great friend over the past 6 years. Her calm, friendly personality has balanced my edginess and helped keep things in perspective for me. I'm excited to hang out on the beach with you in Hull. You are so mature to be able to buy a house and deal with all the responsibilities that go along with that. I'm sorry for every time I took out my stress on you. I owe you big time.



Last but not least, Gabriel Volpicelli, who, like Kiley, has endured much of my stress throughout my years of grad school. I will keep this short because he is waiting to print out my thesis for me now. That in itself exemplifies the level of support he has shown me over the years and continues to show. I can't wait to start our new life in Seattle.

There are many others, but I have to leave you to know I thank you without dropping you a line. I'm sorry, I'm just out of time.

Curriculum Vitae

Dr. Emily J. McLaurin

77 Massachusetts Avenue, 2-301, Cambridge, MA 02139

Education Ph.D. in Inorganic Chemistry 2011
Massachusetts Institute of Technology, Cambridge, MA
Dissertation: "Phosphorescent Semiconductor Nanocrystals and Proteins for Biological Oxygen Sensing"

B.S. Degree in Chemistry 2005
University of California, San Diego, La Jolla, CA
Honors Thesis: "UV-Vis and IR Studies of Charge-Transfer Complexes of Methyl-Substituted Benzenes with Tetracyanoethylene"
Graduated magna cum laude with highest distinction

Research Experience

Massachusetts Institute of Technology, Cambridge, MA 2005-2011
Graduate Research Assistant
Advisor: Professor Daniel G. Nocera

- Designed and synthesized O₂ sensors composed of either osmium polypyridyl complexes or asymmetric Pt and Pd porphyrins conjugated to group II/VI quantum dots
- Developed, maintained, and operated one- and two-photon laser spectroscopy systems for characterizing photophysical properties of nanocrystal-phosphor oxygen sensors
- Managed and used a nanosecond transient absorption spectroscopy system to study electron transfer in ruthenium and rhenium polypyridyl systems

University of California, San Diego, La Jolla, CA 2004-2005
Undergraduate Research Assistant
Advisor: Professor Clifford P. Kubiak

- Formulated various organic charge-transfer complexes in solution and on gold surfaces
- Studied and quantified charge-transfer in complexes using IR and UV-Vis spectroscopies
- Correlated experimental charge-transfer data to Mulliken theory

University of California, Santa Cruz, Santa Cruz, CA 2004
Summer Undergraduate Research Fellow
Advisor: Professor Jin Z. Zhang

- Synthesized Mn²⁺:ZnSe and ZnSe quantum dots for use in biological labeling
- Characterized nanocrystals using UV-vis absorption and steady-state emission
- Improved and developed nanocrystal syntheses and water-solubilization methods

Publications & Presentations

Winter, M. B.; McLaurin, E. J.; Reece, S. Y.; Olea, C.; Nocera, D. G.; Marletta, M. A. "Ru-Porphyrin Scaffolds for Sensing O₂" *J. Am. Chem. Soc.* **2010**, *132*, 5582-5583.

McLaurin, E. J.; Greytak, A. B.; Bawendi, M. G.; Nocera, D. G. "Two-Photon Absorbing Nanocrystal Sensors for Ratiometric Detection of Oxygen" *J. Am. Chem. Soc.*, 2009, *131*, 12994-13001.

Stires, J. C.; McLaurin, E. J.; Kubiak, C. P. "Infrared spectroscopic determination of the degree of charge transfer in complexes of TCNE with methyl-substituted benzenes" *Chem. Comm.*, 2005, *28*, 3532-3534.

Teaching & Leadership Experience

- Resources for Easing Friction and Stress (REFS) 2007-present
Chemistry Department, MIT
- Trained and certified as a mediator in Massachusetts
 - Assisted the chemistry community with a wide variety of problems, especially those affecting graduate students
 - Presented issues of concern to the faculty
 - Brainstormed and implemented ideas for improving the quality of life for chemistry department members
- Curriculum Development 2006
URIECA, with Professors Bawendi, Ceyer, and Nocera, MIT
- Extended advances in scientific literature to the undergraduate laboratory
 - Adapted the synthesis of semiconductor nanocrystals to utilize safer methods
 - Tailored the challenging synthesis of air-sensitive compounds to undergraduates
- Teaching Assistant 2005
Chemistry 5.310: Laboratory Chemistry, MIT
- Prepared laboratory materials for individual student experiments
 - Lectured to and wrote quizzes for students
 - Tutored individuals and small groups during bi-weekly office hours
 - Graded exams, lab reports, and quizzes

Awards & Honors

- Corning Fellowship 2006-2007
Joseph E. Mayer Award for outstanding research in chemistry 2005
Summer Undergraduate Research Fellowship 2004
U. C. San Diego Leadership Program Award 2002

Memberships & Affiliations

- American Chemical Society
WMBR, MIT radio station
Women in Chemistry (WIC), MIT
Chemistry Graduate Student Committee (CGSE), MIT